SELECTIVE MOLECULAR RECOGNITION CONJUGATED NANOPARTICLES FOR BIOLOGICAL APPLICATIONS

By

JOSHUA E. SMITH

A DISSERTATION PRESENTED TO THE GRADUATE SCHOOL
OF THE UNIVERSITY OF FLORIDA IN PARTIAL FULFILLMENT
OF THE REQUIREMENTS FOR THE DEGREE OF
DOCTOR OF PHILOSOPHY

UNIVERSITY OF FLORIDA

2007

To my family and friends

ACKNOWLEDGMENTS

Joshua is extremely grateful to everyone that was involved in this work. Their suggestions, efforts, and ideas were invaluable. He especially thanks his research advisor Dr. Weihong Tan for providing guidance, support, and continuous encouragement throughout his graduate studies. Dr. Tan made performing this research possible, and Josh is appreciative for the opportunities that were available and provided to him as a member of the Tan research group.

Josh thanks Dr. Charles Martin, Dr. Ben Smith, Dr. Tom Lyons, and Dr. Steve Pearton for agreeing to be members of his graduate committee. Josh thanks Dr. Frances Ligler for allowing him the opportunity to perform research with her group in Washington D. C. She and the rest of the research group had a profound and very positive impact on me. That experience really helped me to develop as a scientist and more importantly as a person.

The work presented here would not have been possible without the help of many scientists. First, Josh acknowledges Dr. Tim Drake for introducing him to research with nanomaterials and guiding him in the early stages of this research. Josh gives special thanks to Colin Medley for being such a reliable resource and for all his help with everything over the last few years. Josh recognizes Josh Herr for all his hard work and help while he was in the group. Joshua Smith gives thanks to Dr. Kim Sapsford for taking the time to work with him while he was at the Naval Research Laboratory and all the helpful discussions they had. Josh recognizes Dr. Jeremiah Tipton for his dedication and continuous assistance.

Smith's time at graduate school was an enjoyable and a joyful experience thanks to his family, friends, and lab mates that helped keep everything in perspective. Without his parents, John and Jean, none of this would have been possible, so he thanks them for their continuous love, endless support, and constant encouragement. Josh thanks his brother and sisters and their families for being there for him when he needed them and for always just being themselves and

making life more interesting. For the ones that he knew before graduate school, he thanks you for being there for him, particularly Rish, Laila, Seyb, Ganoe, and Scott. Smith gives thanks to his friends that he made while in graduate school, especially EJ, Brent, Lisa, Alex, and Jeremiah. You really helped him to become who he is, and he will remember you always.

Finally, Joshua thanks all the members of the Tan group, past and present for all the great times we spent together. It has been a privilege being a member of the Tan group. To James, Marie, Alina, Karen, Tim, Shelly, and Colin you made Josh's time at the University of Florida enjoyable and pleasant. He also acknowledges Santra, Steve, Lisa, and Charles for all their help and support. There was a lot of fun both inside and outside the lab. Keep up the newly established traditions.

TABLE OF CONTENTS

page

LIST OF TABLES

LIST OF FIGURES

Abstract of Dissertation Presented to the Graduate School
of the University of Florida in Partial Fulfillment of the
Requirements for the Degree of Doctor of Philosophy

SELECTIVE MOLECULAR RECOGNITION CONJUGATED NANOPARTICLES FOR BIOLOGICAL APPLICATIONS

By

Joshua E. Smith

August 2007

Chair: Weihong Tan
Major: Chemistry

The collection and enrichment of biomolecules from complex biological samples is critical for disease diagnostics, environmental analysis, and biotechnological applications. Current separation methods suffer from numerous limitations that include time consuming procedures, difficulties with handling complex samples, and lack of selective molecular isolation. The objective of my research is to create nanodevices for the selective separation and isolation of biological molecules and to evaluate their applications for biological studies.

First, nanoharvesting agents (NHAs) were developed for the selective collection, separation, and detection of DNA and peptide targets. The NHAs are composed of silica coated magnetic nanoparticles bioconjugated with DNA probes on the nanoparticle surfaces. For peptide recognition, a DNA aptamer was used for the selective binding of the analytes. The NHA were demonstrated to have excellent specificity and sensitivity in both artificial buffer and complex biological samples for subsequent analysis by either fluorescence or mass spectroscopy.

Additionally, the NHAs were functionalized with antibody molecules, and used in a high-throughput protein microarray to improve the detection limit. The NHAs were used as a tracer device, where the antibody on the particle surface was labeled with fluorescent dye molecules for

signaling. Prior to analyses by the microarray device, the NHAs were extracted from large volume samples, concentrated to small volumes, and used directly for the detection of proteins.

Furthermore, a novel method was developed for the rapid collection and detection of whole cancer cells using a two silica-based nanoparticle approach. Magnetic nanoparticles were used for target cell extraction, and fluorescent nanoparticles were employed for sensitive cell detection. The nanoparticles were conjugated with DNA aptamers for target recognition. This system was used for the multiple extraction and detection of cancer cells.

These newly developed techniques will be useful in biotechnology, biomedical science, and disease diagnostics for the selective extraction and isolation of biological targets from complex samples. Future investigations will include the improvement and exploration of biological applications for nanoparticle based techniques.

CHAPTER 1
INTRODUCTION

Impact of Selective Recognition Nanoparticles for Biological Applications

The development of novel bioassays with sensitive and multiplexing capabilities that have simple detection and sample preparation protocols are critical for high throughput evaluations of samples designed for clinical diagnosis, biomedical science, and other biotechnological fields. Such analyses rely immensely on the recognition of individual molecules based on physical and chemical interactions. Common biological analytes include oligonucleotides, peptides, proteins, and even cells that often exist in low abundance in complex biological matrices. In addition, these analyte molecule types exist on a small size range, and it is this size scale that makes nanomaterials attractive for the development of new technologies involving selective recognition molecular probes for the analysis of biomaterials leading to crucial advancements in biological diagnostics.[1,2]

Selectivity and sensitivity of bioassays is directly related to the critical interactions of molecular recognition elements with target molecules. The interactions involved with these devices use the selective recognition of receptor-ligand associations, antibody-antigen, and oligonucleotide hybridization. Additionally, designing bioanalysis techniques require the linking of the target binding action with an induced signaling event. Consequently, signal transduction is what affects the overall sensitivity of these devices with optical and electrical methods being the most often used.[3,4] However for complex biological samples, before bioanalysis procedure can be performed a great deal of sample preparation is needed. Typical sample clean-up and purification techniques involve a variety of centrifugation, electrophoresis, and chromatographic protocols. These techniques are often criticized because of the multiple steps and time

consuming procedures that are often inadequate for proper purification. New materials or procedures capable of overcoming these issues are of great interest to performing bioanalysis.

Typical pathogenic or clinical diagnosis requires the screening for multiple target molecules from a single sample as a means to detect the presence of these marker molecules. This multiplexed analysis can provided crucial information to clinicians and scientists with the added understanding and ability to identify small differences in disease states.[5] The difficulty with using the mentioned standard separation techniques is that with complex biological sample markers often occur in low abundance and an enrichment step prior to analysis is necessary. In addition, the chance for sample loss as a result of complex sample preparation procedures is a major concern. These factors greatly limit the performance of current bioassays.

The heart of this dissertation is the development of selective nanoparticles for the collection and subsequent detection of biological samples to overcome the challenges of the present sample preparation methods. The materials that follow highlight conventional biological sample treatment methods, recently developed nanomaterials with their respective applications, as well as the synthesis and characterization of silica-based nanoparticles. A brief discussion of the systematic evolution of ligands by exponential enrichment (SELEX) will follow, and the principles involved with selecting oligonucleotide ligands for biological targets. Finally, a summary of the overall focus of this dissertation will be provided.

Standard Sample Treatment for Biological Analysis

Oligonucleotide Sample Preparation

Oligonucleotide samples, which include DNA or RNA molecules, are obtained from whole cells. To acquire these samples from intact cells, a popular approach involves lysing the cell to release the genes from the interior of the cell. In general, the extraction and purification of oligonucleotides requires isolation of the genes from cellular debris by a number of

centrifugation based techniques often from a kit. Oligonucleotide molecules are used with a variety of methods for analysis, such as gel electrophoresis, southern blot (for DNA) and northern blot (for RNA), polymerase chain reaction (PCR), and real time PCR (RT-PCR) for sequence identification.[6]

Oligonucleotide gel separations, such as gel electrophoresis are most often carried out using either polyacrylamide or agarose polymeric material depending on sequence size. The gel material forms different sized pores that act as a molecular sieve isolating oligonucleotides as a function of their size (mass) and shape when an electric field is applied to the system. Although this technique does not have the ability to provide sequence identification of complex unknown samples containing thousands of gene fragments, it is a powerful tool for separating oligonucleotide samples.[7]

To obtain sequence recognition, an additional sample work up is necessary. One of the original and probably most famous techniques for obtaining sequence identification is called blotting. Once the oligonucleotides are isolated from cells using the above mentioned process, the isolated oligonucleotides are transferred to a membrane and treated with probe sequences. Labels on the probe sequence are often radioactive or fluorescent molecules, which allow for easy detection. Unfortunately when low amounts of viable cellular material are available, this method is not sensitive enough to provide the necessary sequence determination.[8,9]

In situations where low oligonucleotide copy numbers are available, a technique termed polymerase chain reaction (PCR) is used to exponentially increase the amount of sequences that are available for detection. [10,11] PCR involves short predetermined synthetic sequences (primers), the four individual nucleotides, and an enzyme (polymerase) to create the oligonucleotide copies. After amplification, a more sensitive sequence determination is made by the blotting technique

described previously. However to complete this entire process, a lengthy and time consuming procedure is needed.

A more recently developed procedure for the identification and amplification of gene material is an extension of PCR, called real-time PCR (RT-PCR). RT-PCR involves the same amplification scheme as PCR. However, the major difference between the two techniques is in the sequence determination. With PCR, sequence determination can only be achieved at the end-point, or plateau region, of the PCR reaction, but obtaining the quantity of the original sample is not accurate. In the case of RT-PCR, the amplicon, amplified sequence, is monitored throughout the amplification process, and the quantity determined during the PCR reaction. The process by which these copies are detected is via a reporter probe molecule added to the PCR sample. Commonly, these probe molecules are based on fluorescent signal transduction, where the signal increases as more target molecules are created.[12,13]

Protein Sample Preparation

Protein samples are obtained from intact cells. These molecules are acquired by lysing the cell to release the proteins from the cellular matrix. Proteins are isolated by centrifugation from cellular debris, and the protein fraction of interest is isolated using centrifugation based on their relative solubility. The protein samples from the cellular matrix are further separated sodium dodecyl sulfate polyacrylamide gel electrophoresis (SDS-PAGE). SDS-PAGE has two main categories, one-dimensional and two-dimensional electrophoresis (2DE). One-dimensional PAGE is similar to gel electrophoresis described above in the oligonucleotide section. Two-dimensional SDS-PAGE separates the samples using the isoelectric point (pI) and electric potential in orthogonal directions, which separates by pH and size respectively.[14,15] Separation is achieved with smaller polypeptides migrating faster and larger ones more slowly.[7]

Electrophoresis is a powerful separation tool for proteins, but is not a reliable technique for identifying and quantifying complex samples containing multiple proteins.

Traditionally, western blot is used methods for determining the identity and even quantifying proteins from cellular lysates. Similarly to the oligonucleotide blotting, the samples separated by electrophoresis are transferred from the gel to a membrane material by blotting. Once transfer is completed, the membrane is treated with labeled antibody probes that bind to proteins of interest. Labels used for antibody probes include radioactive or fluorescent molecules.[16] This process uses a lengthy and complex procedure.

Another method conventionally used for analyzing protein extracts separated by gel electrophoresis is mass spectroscopy (MS). In general, the gel with the protein of interest is excised and treated with a protease to digest the protein. The resultant peptides are analyzed by MS. MS has the ability to provide the identification and the quantity of the proteins in most cases.[17,18] The sample preparation procedure has numerous steps and is time consuming.

Cellular Sample Preparation

There is a limited number of ways for harvesting cells from a live source. The first is through biopsy, where tissue cells are surgically removed. The second is by gradient density separation from biological fluids. For biopsy, there are three major classes. Incisional biopsies remove a small portion of tissues or organs for medical testing, excisional biopsies remove entire masses of cells for diagnosing medical conditions, and needle aspiration biopsies collect tissue or fluid with a needle and are often used to avoid performing major surgical biopsies.[19] For density gradient separation, a gradient of solution densities are layered in a centrifuge tube, and the cells are localized in the tube based on their densities after centrifugation. The two categories of density gradient separation are discontinuous and continuous. The difference between the two is that continuous density gradient separation has a continuous flow of the density solutions during

centrifugation.[20,21] Changing the centrifugation speed, centrifugation time, sample volume and solution composition has a dramatic effect on the separation performance.[21]

After cell harvesting, one of the original analysis techniques for cells involves determination of the morphology, such as the shape, structure, and pattern using an optical microscopy. However, further sample handling and preparation is required before the cells morphology can be determined. The cells are solidified, sliced, and placed on a microscope slide. Finally, the specimen is stained to reveal structural anomalies that can be microscopically observed for scientific and diagnostic purposes.[22] Selective cell staining methods use antibodies to specifically visualize and recognize proteins, carbohydrates, and lipids, called immunohistochemistry (IHC). These antibody molecules are labeled with fluorophores, radiolabels, or other molecules that produce a color response upon binding, and analyzed by the appropriate instrumentation. IHC is widely used for the diagnosis and treatment of diseases, such as leukemia. Leukemia is a cancer of the blood and detection entails a sophisticated version of IHC known as immunophenotyping. This process uses a panel of antibodies that recognize cell membrane antigens, and a pattern develops that specifically identifies the leukemia disease type.[23,24]

Recent Growth and Development of Nanoparticles

Fluorescent Semiconductor Nanocrystals

Quantum dots (QDs or qdots), fluorescent semiconductor nanostructures, have aided in the advancement of biological research. QDs are constructed in a core-shell structure, and with no further surface coating these materials range in size from 1 to 10nm in diameter. The shell coating provides protection and stability for the light emitting core component from environmental degradation. QDs have been found to be superior to traditional dyes by being brighter, more photostable, and having longer fluorescence emission times.[25] One of the more

unique qualities of semiconductor nanocrystals is their size-dependent absorption and emission properties, where larger qdots emit light more in the red wavelengths compared to smaller ones. The result of all the extraordinary characteristics of qdots proves the attractiveness of these structures for biological applications.

One such biological application involves oligonucleotide detection, a number of sensing platforms have been used in the development of these technologies.[26] DNA modified QDs are used as fluorescent tracer agents for the analysis of target molecules on a slide surface or in a chip format.[27] Simply, two short-complementary DNA sequences one attached to the QDs and the other to the slide surface selectively recognize the target resulting in detection. More recently, quantum dot fluorescence resonance energy transfer (FRET) has been taken advantage of in oligonucleotide analysis.[28,29] In this format two fluorescent species, an energy donor and acceptor, provide detection of the target DNA upon binding. The two fluorescent agents are each modified with complementary sequences. When target hybridization occurs, the donor and acceptor species are brought into close proximity to one another, during which the donor is excited at its excitation wavelength and transfers its emitted light to the acceptor inducing fluorescence emission from the acceptor. Utilizing FRET, researchers have used QDs as both the donor and acceptor species and as the donor with a fluorophore acting as the acceptor species.

Additional bioconjugated qdots have been developed for the detection and study of a number of other biomaterials and even for the study of cells and cellular processes. For the majority of these detection schemes, the dots are labeled with antibody and other protein molecules for target recognition.[30,31] In cellular staining approaches, QDs have been used to process mammalian and pathogenic cell samples.[31,32,34] In these studies, qdots provide a level of observation not possible with conventional dyes by providing long term, as much as several

hours, observation times as a result of the dots resistance to photobleaching. Also, biofunctionalized dots have been used to selectively label both liberated and cell surface proteins.[35,36] Antibody conjugated QDs were employed to study receptor-mediated signals to identify cancer markers on cells, and for the detection of proteins harvested from lysed cells by western blot.

QDs have been shown to be advanced versions of fluorescent labels for biological detection compared to dye molecules, but limitations exist. Synthesizing these structures is difficult to reproducibly perform, and the surface chemistries are not well understood. QDs are notorious for their observable intermittent fluorescence or uncontrollable blinking effect, which can make obtaining reliable quantifiable data challenging. Perhaps the biggest hindrance to employing these dots in vivo is the uncertainty of the toxicity these materials.[26] Researchers are currently investigating ways to overcome these issues.

Noble Metal Nanoparticles

Metallic materials such as gold, silver, and platinum have been used to create nanoparticles. However, due to the reactivity of silver and the expensive nature of platinum, gold (gold colloids) is the attractive choice for extensive investigations.[37] Numerous studies have demonstrated the abundance of unique physical and chemical properties associated with these metallic nanoparticles. Focusing on the optical properties, gold nanoparticles have size dependent spectral character with the response being red shifted as particle size increases. In addition, this result is affected by particle shape, particle-particle interaction, and environmental conditions. These superior spectral properties are the result of light energy being transferred to surface electromagnetic waves and propagate along the metal interface. This phenomenon is called surface plasmon resonance. This process is associated with metal colloids, which allow them to be controllable scatters and absorbers of light.[38]

One bioassay developed using gold nanoparticles utilizes colorimetric detection of DNA. A set of thiol modified oligonucleotide molecules complementary to the DNA target were attached to 10-15 nm gold nanoparticles.[39] In the absence of the target DNA, the colloid solution appears red in color with a narrow absorption maxima occurring around 520nm depending on the particle size. With addition of target DNA, the particles are forced into close proximity to one another increasing the extinction coefficient producing a blue color change in the solution. Spectrally, the sample has a red shift that occurs as a result of binding obtained by absorbance measurements.[40] This detection event has been observed in the analysis of other targets, which include proteins and small organic compounds. In these instances, target recognition is achieved using DNA probes, called aptamers.[41] In simple terms, an aptamer is an oligonucleotide sequence that forms a complex three-dimensional structure to selectively bind to a variety of targets, which will be discussed in more detail in a later section.

Noble metal particles have also been used in detection scheme that involve more complex data acquisition methodologies than that for the colorimetric approach, namely surface enhanced Raman scattering (SERS). The normal Raman process is the result of a small fraction of light scattered at frequencies different from that of the incident light, most often at lower frequencies. However, Raman produces extremely weak signals making it difficult to use in practical applications. On the other hand, SERS is one of the most sensitive techniques available for molecular analysis with enhancements as high as 10^{14} over the background. SERS takes advantage of the inelastic scattering process of the Raman effect, but in this instance the substance being detected is adsorbed directly on or is within a few Angstroms of a metal surface.[42] Commonly used metal surfaces include gold and silver with silver having the strongest observable Raman scatter.[43,44] The surface enhanced effect is the result of incident light energy

being transferred to electronic energy by the metal surface, often as surface plasmon resonance. This electronic energy is then transferred to the substance associated to the metal surface producing enhanced Raman scattering.

A number of bioassays have been developed using SERS as the signaling motif.[45-48] One of the more attractive features of SERS is that molecules with different chemical structures form characteristic spectra, much like a fingerprint, based on that materials chemical makeup. For instance, unlabeled oligonucleotides have been detected by SERS using gold nanoparticles. Unfortunately difficulties arise when sequence identification is required because of the structural similarities from one oligonucleotide to the next, which result in similar spectra.[49,50] In addition, Raman-active molecules have been employed to selectively recognize analyte molecules to distinguish different targets from one another, such as proteins and oligonucleotides.[45,51,52] In both circumstances, gold nanoparticles have been used as the SERS surface.

Magnetic Nanoparticles

Magnetic materials have been the subject of research interest for several decades. The interest in magnetic materials has been to gain an understanding of magnetic properties and to synthesize materials with specific magnetic properties. Until more recently magnetic materials have been studied as bulk substances.[53] These materials are often divided into two categories of magnetism. Those that have no unpaired electrons repulsed by an external magnetic field (diamagnetic), and those with unpaired electrons attracted to an external magnetic field (paramagnetic). For paramagnetic materials, no magnetization is retained by the substance in the absence of a magnetic field.

Additional classes of magnetism include ferromagnetic and ferrimagnetic substances. Ferromagnetic materials are attracted to a magnetic field, and retain magnetization after removing the magnetic field. Additionally, ferromagnetic substances contain equal and opposite

unpaired electrons on each of the atoms within the metal complex structure. Alternatively for ferrimagnetic compounds, the opposing magnetic moments associated with the atoms within the metal complex structure are unequal resulting in a retained magnetism after removal of an induced magnetic field. Since ferrimagnetic materials have unequal opposing magnetic moments within the metal complex structure, these compounds are attracted to a magnetic field.

As bulk substance, ferrimagnetic materials are divided into magnetic domains that have regions of aligned electron spins and a net magnetic moment.[54] When demagnetized, the magnetic moments of the domains are randomly oriented, and the magnetic moments cancel each other resulting in no net magnetism. With the reduction of the size of the material or particle, there is a point when a single-domain is reached.[55,56] Further reducing the size of the single-domain magnetic material creates a particle that can no longer sustain an induced magnetic moment for an extended amount of time (Figure 1-1). However, in the presence of a magnetic field the particles become magnetized. This phenomenon is known as superparamagnetism because there is no magnetic hysteresis. The material does not become magnetized by an external field and returns to its original state in the absence of the field, just like with paramagnetism.[54]

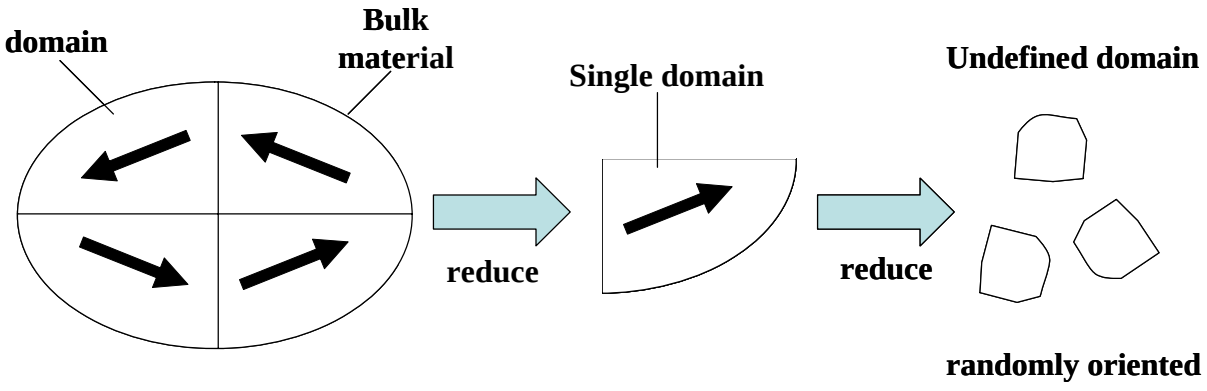

Figure 1-1. The scheme representing the effect size has on magnetic materials in the absence of a magnetic field.

Countless superparamagnetic materials have been synthesized using transition metals of iron containing compounds, such as magnetite (Fe_3O_4). These substances have become extremely attractive for biological applications. This is due to the superparamagnetic characteristic, which is essential for avoiding particle aggregation. Magnetite particles have been used in biology for numerous applications, which include MRI contrasting agents, magnetic separations, and as drug delivery vehicles.[57-59] For MRI contrast, iron oxide particles darken the image acting as a negative contrasting agent. Typically, these particles have a reduced uptake by tumor tissue, and therefore appear brighter than the surrounding health tissue.[60] In drug delivery, drugs are chemically or physically bound to the magnetic particles and a magnetic field is applied to direct the particles to the target tissue or organ.[44] As in a magnetic separation, a targeting molecule is chemically bound to the magnetic materials to provide attachment to the biomolecules or cells of interest.[58] These and other advancements in magnetic technology have provided powerful tools to a variety of biology and biotechnology related fields, but further research and improvements are still necessary to realize the full potential of these materials.

Silica Nanoparticle Fundamentals

Synthesis of Silica Nanoparticles

Silica nanoparticles have been prepared by two common processes, microemulsion method and the Stöber (sol-gel) approach. The Stöber method involves an ethanol and ammonium hydroxide solution that hydrolyzes silane molecules, such as tetraethylorthosilicate (TEOS), to form amorphous silica nanoparticles (Figure 1-2). The Stöber process is relatively simple to perform and can be carried out in as little as a few hours. This method has been modified to form organic dye nanoparticles by covalently attaching the fluorophore to the silica matrix.[67-69] Additionally, magnetic nanoparticles Fe_3O_4 and Fe_2O_3 have been incorporated in the silica

particles using this method.[65] However, the nanoparticles formed via this method are often large and have non-uniform shapes.[66]

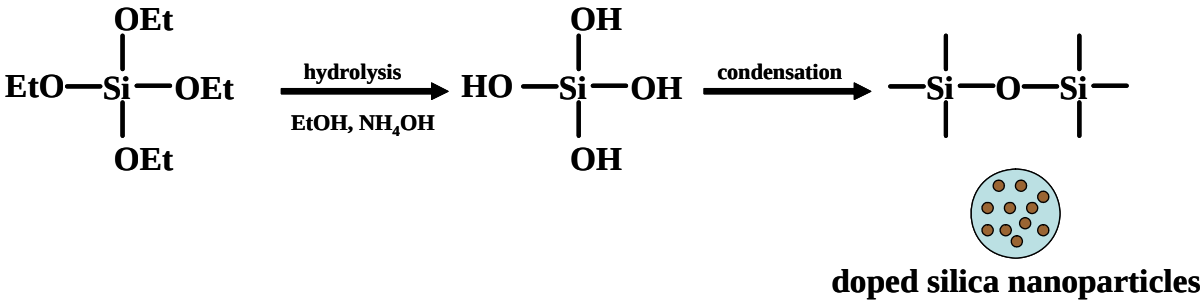

Figure 1-2. The scheme representing the Stöber process used to create silica nanoparticles.

An alternative synthesis of silica particles is to use the reverse-micelle approach, also known as water-in-oil microemulsion (w/o) method. This method consists of three primary components: water, oil, and a surfactant.[67-69] These components form a single-phase microemulsion system which is both isotropic and thermodynamically stable (Figure 1-3).

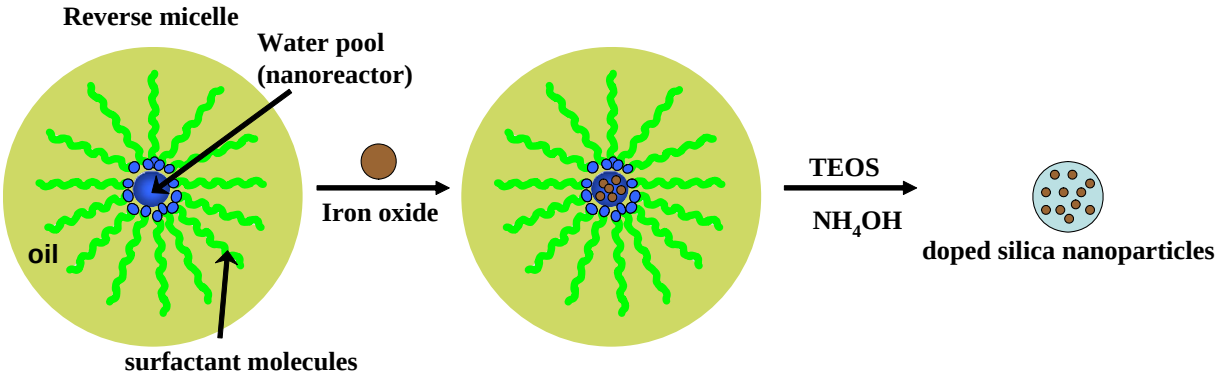

Figure 1-3. The scheme representing the water-in-oil microemulsion system used to create silica nanoparticles.

Nanodroplets of water form in the bulk oil phase, which act as a confined medium (nanoreactors) for discrete particle formation. Again, silica particles form by the hydrolysis of silane molecules. The nanoparticles size can be controlled by altering the water -to-surfactant molar ratio (Wo).

The microemulsion yields monodispersed and highly uniform nanoparticles taking anywhere from 24-48 hours to complete. The water-in-oil microemulsion synthesized silica nanoparticles have been doped with various inorganic and modified organic dye molecules.[70-73] In addition to the dye-doped particles, the same doping procedure has been used to incorporate Fe_3O_4 and Fe_2O_3 nanoparticles in the silica matrix.[74,75]

Silica Nanoparticle Modification and Conjugation

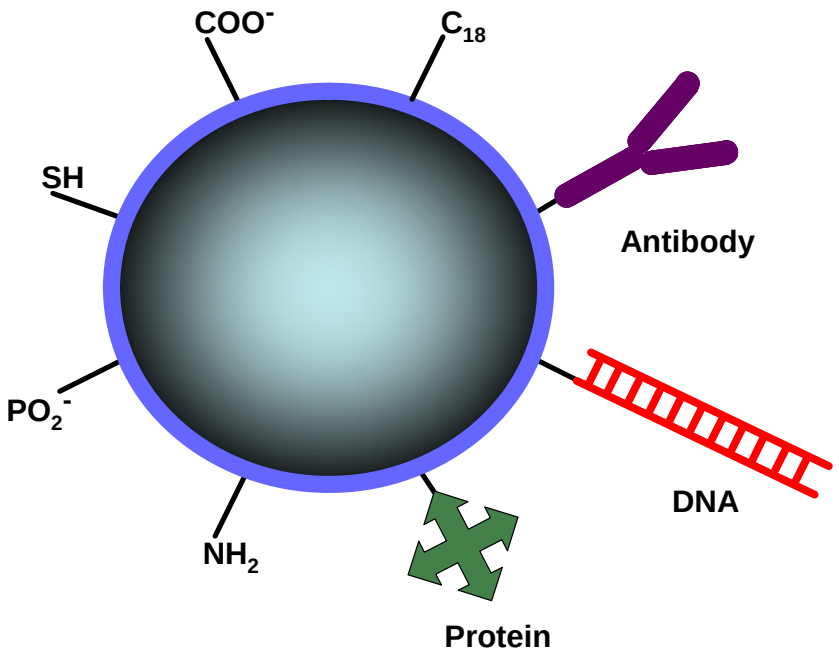

Figure 1-4. Organosilane functionalized and biomolecule conjugated silica nanoparticles used for biological applications.

For biological applications, the nanoparticle surface is often modified with recognition elements, such as antibodies and oligonucleotides that selectively bind target molecules. This modification has been accomplished by both physical adsorption and covalent attachment. Physical adsorption uses electrostatic, van der Waals, hydrophobic and hydrophilic interactions to associate biomolecules to the particle surface. Where as, covalent attachment requires the modification of nanoparticles with organosilane molecules that contain chemically reactive

functional groups such as thiols, amines, and carboxyls (Figure 1-4).[76,77] These groups are applied to the surface either after synthesis by postcoating with an organosilane or by postcoating during synthesis via cohydrolysis with TEOS.[78]

Another role of functionalization is to provide solubility and stability to nanoparticles in solution. When particles are modified with amine groups as well as with biomolecules at physiological pH, the net surface charge of the complex is typically reduced. This causes the particle to be less stable in aqueous solutions resulting in particle aggregation. To overcome this issue, additional chemical groups are added to the particle surface to restore the colloidal stability. For example, during postcoating charged-unreactive organosilane compounds or polymer-based stabilizing reagents have been used to improve their dispersibility.[79,80] Polymeric reagents, such as polyethylene glycol (PEG), have been used to block the adsorption of unwanted molecules to the particle surface and reduce adsorption of the particles to detection surfaces. When using the unreactive charged silane groups, the desired charge needed to disperse the particles is reestablish.[81,82]

To covalently label functionalized particles with the preferred biological recognition molecules, chemical attachments are often used such as peptide and disulfide bonds along with numerous amine reactive linking reagents (Figure 1-4). For carboxylic acid functionalized nanoparticles, amine containing biomolecules have been attached through peptide coupling by way of activating the carboxyl group with carbodiimide reagents.[83] Additional conjugations have been executed through the disulfide linkage, where nanoparticles coordinated with sulfide groups can react with sulfur containing biomolecules to fix them to the particle surface.[78] Succinimidyl esters and isothiocyanates are commonly used as cross linking reagents for attachment of a variety of molecules to amine labeled particle surfaces.[84] A popular surface attachment method

uses the natural interaction between biotin and avidin. In many instances, avidin protein molecules are physically adsorbed or covalently bound to a surface. The biorecognition molecule is modifying with biotin, and immobilization of the biotinylated molecule is made possible via the biotin-avidin interaction. The decision as to which bioconjugation strategy to use depends on the application and expected function of prepared materials.

Characterization of Prepared Nanoparticles

Determining the physical and chemical properties of nanomaterials is essential. Since many of the characteristics are based on physical size, one of the leading categories of techniques used to determine particle size has been electron microscopy (EM). Nanoparticles have been imaged using transmission electron microscopy (TEM), scanning electron microscopy (SEM), and atomic force microscopy (AFM).[62-64,85-87] The limitation with EM techniques is that the images are obtained from a surface, which provides little indication as to the dispersive nature of nanoparticles in solution. To solve this problem, light scattering can be used to measure both particle size and dispersion of samples in solution.[88]

Another important characteristic of nanoparticles is the overall surface charge or zeta potential (ζ), which is effected by the particle environment. The magnitude of the ζ indicates the repulsive force that is present on the particle sample, and is used to determine the solution stability and dispersion of the particle sample. Some of the factors that effect particle stability are pH, salt content, and particle concentration. Particles of high positive or negative ζ values, 30mV or larger, repel each other and have a lower propensity for aggregation. In addition, ζ measurements can be used to verify whether bioconjugation reactions or surface modifications have taken place. Throughout the synthesis and modification process the nanoparticle surface charge can be monitored after each step. Based on the materials coordinated to the particles the ζ

will change with the addition of a charged species or by screening of the surface charge by these additional molecules, like charged organosilanes and oligonucleotides or polymers and proteins respectively.[85]

Other characterizations of nanoparticles are dependent on the type of particles that are being analyzed. For dye-doped silica nanoparticles, the optical properties are of significant interest. Dyes incorporated in silica nanoparticles have no significant changes to the absorption and emission properties with the exception of Rubpy nanoparticles, where a slight red shift in the emission is observed. The photostability of the dyes trapped in the silica matrix was improved compared to free dye molecules. The dye-doped nanoparticles did not suffer from photobleaching after long periods of continuous-intense light exposure and have high signal intensities compared to free dye molecules.[74,89] For magnetic nanoparticles (Fe_3O_4), the magnetic properties are of particular interest. These properties are measured using a superconducting quantum interference device (SQUID) magnetometer and is accomplished by varying the magnetic field applied to the sample and monitoring the magnetic response of the magnetic material.[75]

Selective Biorecognition Component

The essential component when developing tools for bioanalysis deal with molecular interactions and using those interactions for recognition of disease states. Diseases have been known to have specific markers associated with them. These biomarkers have aided researchers and scientists in diagnosing and treating diseases. The limitation for the development of diagnostic devices has been with the lack of known markers for these applications. The discovery of selective biomolecules as markers involves separating and identifying these molecules from complex biological samples. This requires a great deal of time and effort to

avoid ascertaining a nonselective or even an incorrect molecule. Two classes of molecules used for biorecognition are antibodies and aptamers.

The most studied recognition molecules are antibodies, which are large protein molecules produced by the body to identify and neutralize foreign materials like diseases. The two classes of antibodies are polyclonal and monoclonal. Polyclonal antibodies are mixtures of these proteins that recognize different epitopes of the antigen. Polyclonal antibodies are produced by many different cells by injecting the antigen into an animal and isolating the antibody from the animal's blood. Monoclonal antibodies are homogeneous proteins that recognize the same epitope of an antigen and are isolated from a population of identical cells rather than from different cells. Since antibodies are produced as a biological response to antigens they are difficult to reproduce, difficult to chemically modify, sensitive to environmental conditions, and have limited shelf lives.

A more recent development in molecular recognition has been with aptamers, which are single-stranded DNA, RNA, or peptides that selectively bind to target molecules ranging from small organic compounds to proteins.[90-92] Aptamer molecules have binding affinities and target recognition that is comparable to antibodies, and are able to discriminate between protein targets that are highly homologous.[93,94] This is due to the complex three-dimensional structures, which provide the basis for target recognition.[95,96] Oligonucleotide aptamers are selected by a process called the Systematic Evolution of Ligands by Exponential enrichment (SELEX). Aptamers are selected from a library of around $10^{12\text{-}15}$ random sequences of synthetic oligonucleotides by repeatedly binding these molecules to the target of interest.[90, 97-99]

More recently, a cell-based aptamer process was developed to obtain molecular probes for profiling diseases, such as cancer. In cell-SELEX, whole cells are used to identify DNA

aptamers that distinguish target cells from control or nontarget cells (Figure 1-5). Through the cell-SELEX approach a panel of cell-selective aptamers is screened. This is accomplished by using a subtraction strategy where aptamer candidates that interact with nontarget cells are removed. The aptamers that are screened are determined without knowing the biomarkers that are present on the cell's surfaces.[100] The attractive features of DNA aptamers over antibodies are that they have low molecular weights allowing for fast tissue penetration, and are simple to synthesis and modify as a result of well established oligonucleotide chemistries.[101] Aptamers can also be used as tools for identifying new biomarkers expressed in other disease states.

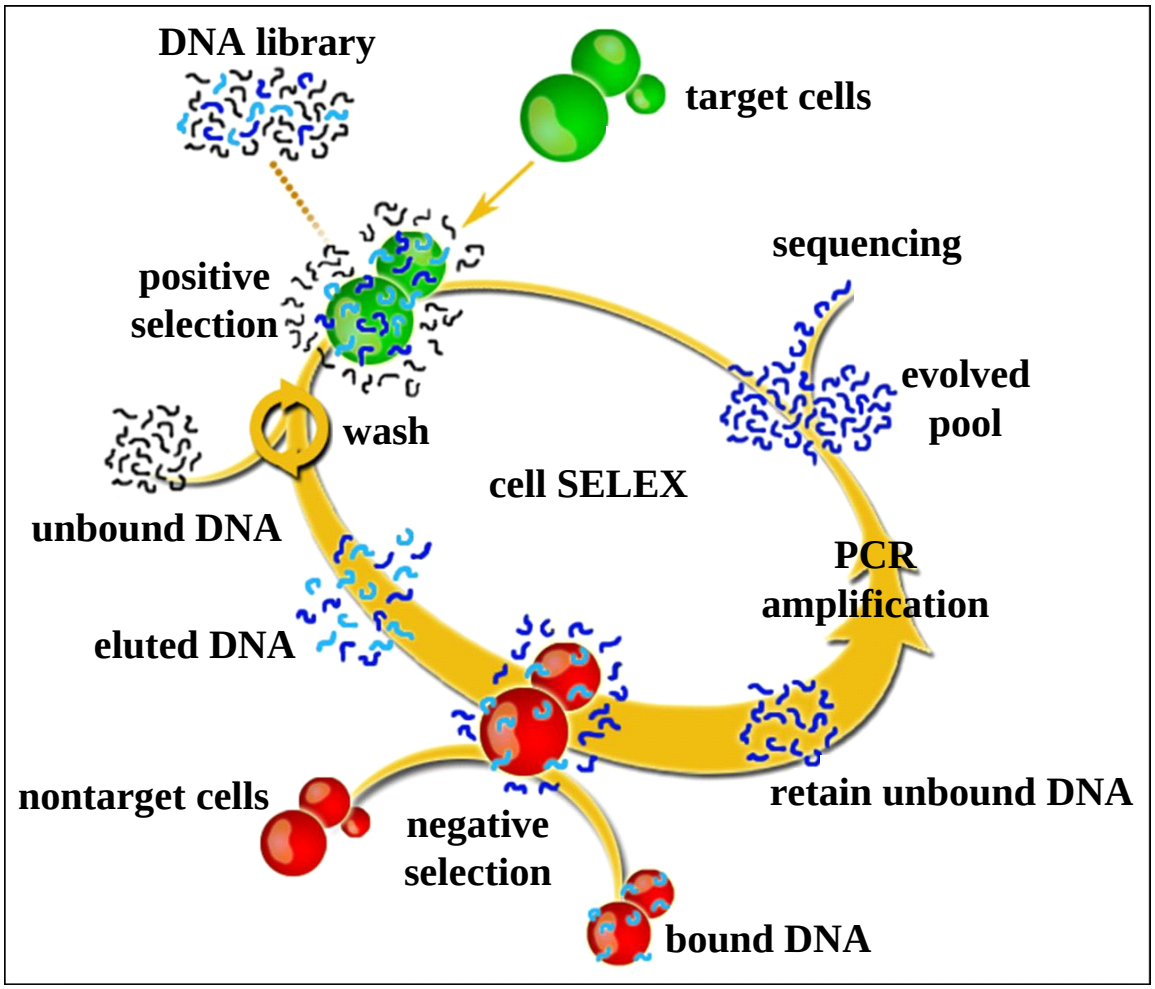

Figure 1-5. Schematic representation of the selection process used to generate cell binding aptamers (cell-SELEX).

Research Scope

The research in this dissertation describes the development of selective recognition conjugated nanoparticles for biotechnological, biomedical, and clinical applications. Silica coated magnetic nanoparticles were used to collect and isolate oligonucleotides, peptides, proteins, and intact cells from complex biological matrices. The collected oligonucleotide and peptide samples were analyzed by both optical and mass spectroscopic devices. Fluorescently labeled antibodies modified to silica nanoparticles were used to improve the detection limit of protein microarray devices. A two particle, one fluorescent and one magnetic, approach was investigated for the multiplexed detection of cancer cells using a flow system, fluorescent imaging, and simple optical methods.

CHAPTER 2
PREPARATION OF SILICA COATED MAGNETIC NANOPARTICLES

Introduction

Magnetic materials have been created from numerous metallic elements, and until the past few decades these substances have been developed and studied in bulk. Researchers have spent a large amount of time and effort employing metallic elements to construct magnetic nanoparticles and molecules. One of the metals commonly used to produce these items has been iron, particularly as iron oxide. Some synthesis protocols used to make iron oxide nanoparticles include coprecipitate of Fe^{2+} and Fe^{3+} in alkaline or microemulsion systems, the oxidation-reduction of suitable valence iron ions, and the utilization of copolymer gels or other templates.[54,57,102] The research that follows uses the coprecipitation procedure. However, bare iron oxide objects are difficult to take advantage of as is because the ability to chemically modify the nanoparticle surfaces with reactive groups is not possible.

To provide magnetic nanoparticles the ability to be chemically treated, one of the standard approaches has been to encapsulate these compounds with modifiable surface coatings. Iron oxide nanoparticles have been coated with a number of synthetic and biological polymers, some of which are commercially available, and with silica. The focus of this work was on coating these magnetic particles with a silica surface. Iron oxide particles have been coated with silica using the microemulsion protocol for biological functionalizations and applications.[75] Silica nanoparticles have been created using a process called the Stöber method.[66] The magnetic particles in this work were coated using this procedure, and additional surface modifications were explored for covalently and physically attaching biomolecules to the particle.

Experimental

Materials and Methods

All materials were purchased from Sigma-Aldrich (St. Louis, MO) unless other noted. Ammonium hydroxide (NH_4OH), ethanol (EtOH), and hydrochloric acid (HCl) was purchased from Fisher Scientific (Fair Lawn, NJ, USA). The biotinylated DNA and fluorescein labeled sequences were obtained from GenoMechanix (Gainesville, FL). Other DNA molecules were synthesized in-house. A neodymium iron boron magnet purchased from Edmund Optics (12,200 gauss, Barrington, NJ). Carboxylethylsilanetriol sodium salt (carboxyl or COOH) was purchased from Gelest, Inc. (Morrisville, PA). 1-Ethyl-3-[3-dimethylaminopropyl] carbodiimide hydrochloride (EDC) was purchased from Pierce Biotechnology, Inc. (Rockford, IL). Avidin was obtained from Molecular Probes (Eugene, OR). All other chemicals were of analytical grade.

Instruments

A Hitachi H-7000 transmission electron microscope (TEM) was used to obtain the size and shape of the formed nanoparticles from dried samples. Light scattering and zeta potential (ζ) measurements were made on a series 1270 Brookhaven Zeta Plus instrument to gain solution size and surface charge information, respectively. A Perkin-Elmer PHI 5100 ESCA X-ray Photoelectron Spectroscopy (XPS) and a JEOL JSM 6335F SEM with Energy Dispersive X-ray Spectroscopy (EDS) instruments were used to demonstrate the chemical composition of the surface and interior of the synthesized silica nanoparticles. Additional sizing measurements were obtained on a Veeco Multimode with a Nanoscope IIIa controller atomic force microscope (AFM) of a dried sample. Fluorescence and absorbance measurements were obtained using a TECAN Safire microplate reader (Research Triangle Park, NC, USA).

Nanoparticle Synthesis, Surface Modification, and Bioconjugation

The iron oxide core magnetic nanoparticles were prepared by coprecipitation of iron oxide salts.[54] The procedure was slightly modified from the source materials. Solutions of ammonium hydroxide (2.5%) and iron chlorides were added together under nitrogen, and continuously stirred at 350 RPM using a mechanical stirrer for 10 minutes with a final volume of around 255 mL. The iron chloride solution was made from ferric chloride hexahydrate (0.5 M), ferrous chloride tetrahydrate (0.25 M), and HCl (0.33 M) at a final volume of approximately 100 mL. The ammonium hydroxide solution was diluted in a 500 mL beaker at a volume of about 155 mL. The bulk solution of the formed iron oxide nanoparticles was stored as is at room temperature until needed for further experiments.

The iron nanoparticles were coated with silica using the Stöber process, similar to the sol-gel approach.[66] To begin, a 6 mL aliquot of the magnetic particle solution was magnetically extracted and washed three times with water and once with ethanol, and the washed samples were suspended in an ethanol solution containing ~1.2 % ammonium hydroxide. The final concentration of the washed particles was around ~7.5 mg/mL, which contained 60 mg of iron oxide in 6 mL of solvent. To this sample, 210 μL of tetraethoxyorthosilicate (TEOS) was added and then sonicated for 90 minutes to complete the hydrolysis process to form the silica coating. A postcoating layer of pure silica was created by adding an additional 10 μL aliquot of TEOS, and the sample was sonicated for an additional 90 minutes. The resulting silica nanoparticles were magnetically extracted and washed three times with a 6 mL aliquot of ethanol to remove excess reactants.

Avidin physical adsorption

For avidin protein coating by physical adsorption, a 0.1 mg/mL silica coated magnetic nanoparticle solution washed three times with 1 mL aliquots of 10 mM phosphate buffered saline (PBS) pH 7.4 and suspended in 12 mL of the buffer. A 10 mL solution at a concentration of 5 mg/mL avidin was added to the nanoparticle solution and sonicated for 5 minutes. This solution was incubated at 4° C overnight. The particles were magnetically extracted and washed three times with 5 mL aliquots of 100 mM phosphate buffered saline (PBS) pH 7.4. The sample was dispersed in a 30 mL solution of 1% glutaraldehyde diluted by 100 mM PBS and continuously mixed for 1 hour at 25º C to stabilize the avidin layer by cross-linking. After stabilization, the particles were magnetically extracted and washed three times with 5 mL aliquots of 1M Tris-HCl buffer pH 7.0, and the samples dispersed in 5 mL of the buffer then incubated for 3 hours at 4º C. Finally, the avidin coated particles were washed three times with 5 mL aliquots of 20 mM Tris-HCl, 5 mM $MgCl_2$, pH 8.0 and suspended in 4 mL of this buffer at a concentration of ~0.2 mg/mL.

Biotin-avidin oligonucleotide attachment

DNA modification was performed by adding 6 nmols of biotinylated DNA (5'-biotin-TTT AAA TCT AAA TCG CTA TGG TCG C-3') to 500 μL of the avidin nanoparticles. This reaction was completed by incubating the sample at 4° C overnight. Three final washings of the particles were performed using 500 μL aliquots of 20 mM Tris-HCl, 5 mM $MgCl_2$ buffer and suspended in 500 μL of this buffer. The final concentration of the DNA labeled particles was ~0.2 mg/mL and stored at 4° C until used.

Carboxyl modification

For covalently attachment after postcoating the iron oxide particles with silica and washing with ethanol and 10 mM PBS, 80 μL of the carboxyethylsilanetriol sodium salt was added to 1 mL of 10 mg/mL silica-coated magnetic nanoparticles (MNP) in 10 mM PBS, pH 7.4 and continuously mixed for four hours. Finally, the particles were washed three times with 10 mM PBS and stored at room temperature until used.

Direct oligonucleotide attachment

To attach DNA, a 250 μL solution of 4 mg/mL of the carboxyl-modified MNPs were washed three times with 250 μL aliquots of a 0.5 mM MES, pH 5.0 buffer. To these particles, 50 μL of a 20 mg/mL EDC solution to the washed particles and incubated for fifteen minutes. A 10 μL volume of amine modified DNA (5'-amine-TTT AAA TCT AAA TCG CTA TGG TCG C-3') at a concentration of 100 μM was added to the activated particles. The solution was allowed to react for four hours with continuous mixing. The MNPs were magnetically extracted and washed three times with 500 μL aliquots of the 10mM PBS buffer. The final concentration of the MNPs was 2 mg/mL in the 10mM PBS, and the samples were stored at 4 ˚C until used.

Avidin Modification Determination

To confirm the presence and activity of the avidin layer on the nanoparticle surface, 50 μL of 0.5 mg/mL biotin labeled with fluorescein isothiocyanate (FITC) dissolved in deionized water was added to 100 μL of 0.2 mg/mL avidin modified magnetic nanoparticles (MNP) into two separate particle samples incubated at different times, 24 and 4 hours respectively. Simultaneously, two samples of 100 μL at 0.2 mg/mL silica magnetic nanoparticles were treated with 50 μL of the biotin-FITC and one was incubated for 24 hours and the other for 4 hours. After incubation, the samples were magnetically extracted and washed three with 100 μL of 20

mM Tris-HCl, 5 mM $MgCl_2$, pH 8.0. These samples were analyzed by the microplate reader to obtain the fluorescence data. The zeta potential of the avidin modified MNP was measured to confirm the presence of the avidin coating.

Investigation of DNA Modification

To verify the presence of DNA and that the DNA was functional, the zeta potential of biotin-DNA treated avidin nanoparticles were measured, and the biotin-DNA treated nanoparticles (NPs) were treated with FITC labeled DNA, which were a target (5'-FITC-GCG ACC ATA GCG ATT TAG A-3') and control (5'-FITC-AAT CAA CTG GGA GAA TGT AAC TG-3') sequences. To 180 μL of 0.2 mg/mL DNA modified magnetic nanoparticles called nanoharvesting agent (NHA), were treated with FITC-DNA to make a 100 nM final concentration of dye labeled DNA in a final volume of 200 μL. These samples were typically incubated at room temperature for 1 hour, however shorter times have been used. These samples were magnetically extracted and washed three with 200 μL aliquots of 20 mM Tris-HCl, 5 mM $MgCl_2$, pH 8.0 buffer, and the extracted samples were heated to 70 ˚C for 10 minutes to release the captured DNA from the NHA. The NHA materials were magnetically removed from the sample while the sample was heated. The released DNA sample was allowed to cool to room temperature and then analyzed by microplate reader.

Optimization of DNA Functionalization

For determining the optimum amount of biotin-DNA attached to the nanoparticle surface, this was accomplished by performing a dose-response or saturation study of prepared DNA labeled magnetic nanoparticles. Two different factors were controlled and monitored to demonstrate the optimized DNA functionalization to the nanoparticle surface. The concentrations of DNA per nanoparticle were controlled by increasing the biotin-DNA amount

from 1 μM to 71 μM (~330, 2000, 5100, 10300, and 23800 molecules). To determine the number of functional DNA molecules per particle, target DNA-FITC was added to seven aliquots of 180 μL of the NHA at concentrations of 100, 250, 400, 550, 700, 850, and 1000 nM in a final volume of 200 μL. These samples were incubated at room temperature for 1 hour, and the samples washed and heated as described previously. The DNA samples were analyzed by a microplate reader.

Results and Discussion

Iron Oxide Formation and Silica Coating

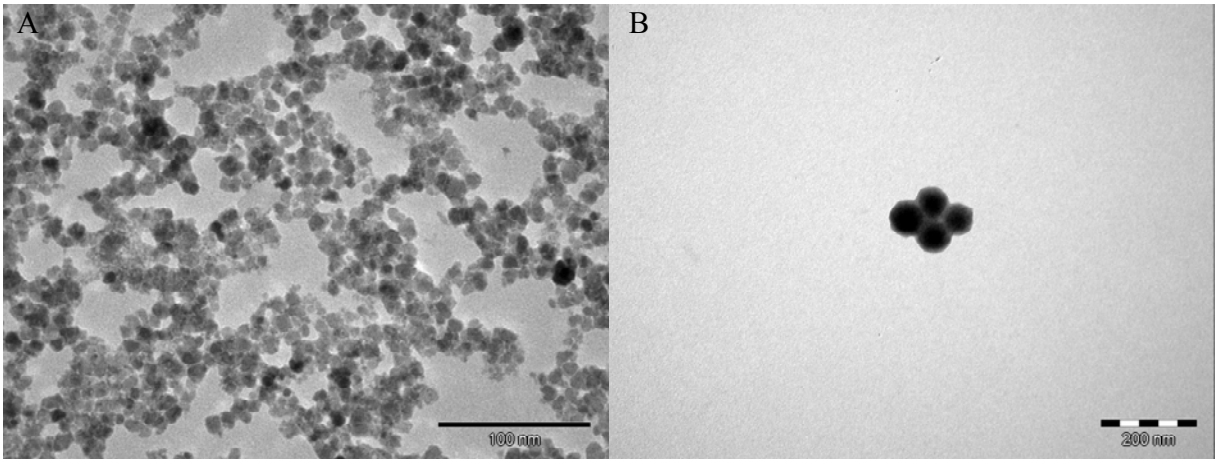

Figure 2-1. The transmission electron microscope images of synthesized nanoparticles. A) Iron oxide nanoparticle images. B) Silica coated iron oxide nanoparticle images.

The uncoated iron oxide, magnetite (Fe_3O_4), and silica coated nanoparticle size and shape were by transmission electron microscopy (TEM). The uncoated magnetite particle (Figure 2-1 A) size was found to be 10 ± 2 nm in diameter and these particles had a variable shape. The representative image for silica coated magnetite particles (Figure 2-1 B) determined the diameter to be 65 nm, and these particles were spherical in shape. However, the size of silica coated iron oxide particles was more variable. The smallest silica coated particles were found to be

approximately 30 nm and some of the largest were 90 nm in diameter. This is caused by the Stöber synthesis procedure because of the lack of control over nucleation of the silica nanoparticle formation. In addition to obtaining the particle size, the TEM images showed that the iron oxide nanoparticles were encapsulated with the silica layer. This was seen by the differences in size and shape of the materials observed in the TEM images. Additional techniques were used to further demonstrate the particle size and that the magnetic nanoparticles were coated with silica.

The silica coated magnetic nanoparticles (MNP) were analyzed using atomic force microscopy (AFM). The size of the particles obtained by this method showed diameters of approximately 30 ± 5 nm with uniform spherical shapes (image not shown). This technique again provided evidence that the magnetite nanomaterials were coated with silica. Both nanoparticle types were further characterized by light scattering and zeta potential measurements. The light scattering data indicated the hydrodynamic particle sizes in solution of approximately 27 ± 3 nm and 90 ± 10 nm for the bare magnetic and silica coated nanoparticles, respectively. These larger sizes of the analyzed samples were possibly the result of larger or aggregated particles dominating the samples.

Table 2-1. The zeta potential measurements obtained from various nanoparticle surfaces and coatings.

Nanoparticle surface	Zeta potential* (mV)
Magnetite	-30.09
Silica	-19.59
Avidin-silica	-4.37
Biotin-DNA (biotin-avidin)	-14.56
Carboxyl-silica	-43.27
Amine-DNA (peptide bond)	-33.31

* All measurement variations were within 1-3 mV in all samples.

Zeta potential (ζ) measurements (Table 2-1) taken of the bare iron oxide and silica coated particles indicated surface charges of -30.09 mV and -19.59 mV, respectively. This study

indicates that uncoated particles have a better colloidal stability as a result of the ζ, and seen by the settling of the silica coated samples out-of-solution after several hours. Both the light scattering and zeta potential data provide evidence for successful coating of the iron oxide with a silica layer as seen by the differences in the measured particle size and surface charge.

X-ray Photoelectron Spectroscopy (XPS) and Energy Dispersive X-ray Spectroscopy (EDS) measurements were acquired to ensure the elemental composition of the silica-magnetite nanoparticles. The atomic ratios obtained from the XPS plot (Figure2-2) indicated that the surface of these particles consist of 96.9% Si and 3.1% Fe, and atomic ratios attained from EDS measurements illustrate that the overall composition of the silica coated particle was 62.3% Si and 37.7% Fe. Based on these results, the synthesized nanoparticles had a higher Si to Fe ratio. The XPS and EDS analysis demonstrate a layered composite structure with a successful silica coating of the iron oxide.

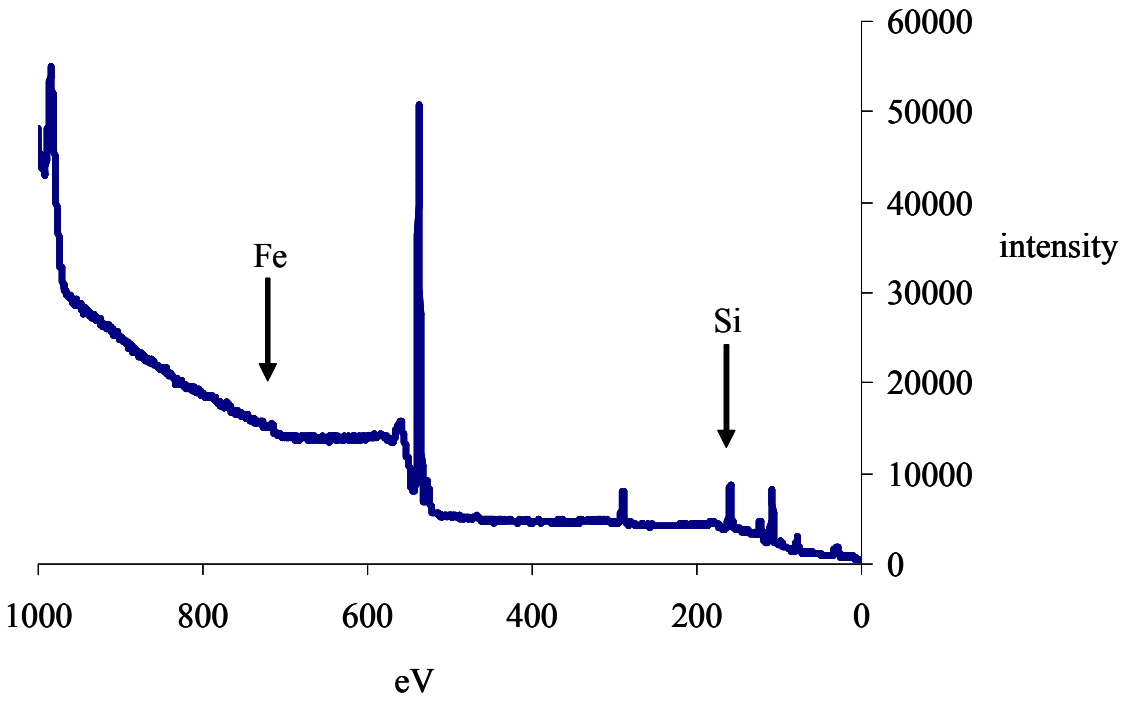

Figure 2-2. The X-ray Photoelectron Spectroscopy data collected from silica coated magnetite nanoparticles.

Avidin Surface Modification

After completing the avidin coating process, the particles were analyzed by zeta potential. The surface charge of avidin coated magnetic nanoparticles (MNP) was determined to be -4.37 mV (Table 2-1). With such a low zeta potential, these particles were prone to aggregation. Comparing the silica coated nanoparticles to the avidin modified samples; the zeta potential measurements indicated a decrease of more than 15 mV with immobilization of avidin to the silica surface. The decrease in the overall surface charge is explained by the introduction of positively charged avidin protein molecules to the negatively charged silica surface. This change in surface charge provides evidence that the silica particles were covered with an avidin layer.

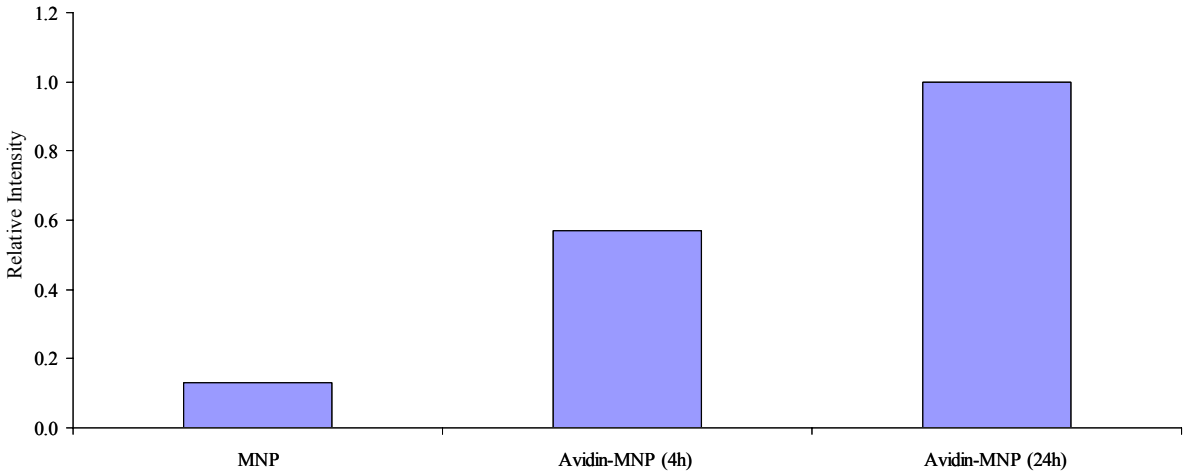

Figure 2-3. The fluorescence data obtained from avidin modified silica magnetic nanoparticles (MNP) treated with biotin-FITC.

The avidin coated particles were treated with biotin-FITC to further determine whether the avidin layer was added to the silica surface, and the fluorescence data obtained (Figure 2-3). The information indicated that these nanoparticles have been modified with avidin molecules as evidence of the increased fluorescence intensity observed in both of the biotin treated samples. The fluorescence analysis showed that the particle bound avidin molecules remained active upon

being immobilized to the particle surface. Additionally, this experiment indicated that longer incubation times provide increased biotin-avidin hybridization. The zeta potential and fluorescence analysis provide confirmation of the presence and activity of avidin on the nanoparticle surface.

DNA Labeled Nanoparticles

Creating DNA functional nanoparticles using biotin-avidin linkage was assessed by first performing zeta potential measurements. The surface charge of the DNA modified nanoparticles was -14.56 mV, which were 10 mV higher then the avidin only nanoparticles (Table 2-1). The increase of the surface charge can be explained by adding negatively charged DNA molecules, which improves the overall charge of the particle. The DNA labeled nanoparticles had a lower propensity for aggregation than the avidin modified particles, but aggregated after a longer period of time. However, the sample was suspended by simply shaking or vortexing. The change in the particle charge provides evidence that the sample was labeled with DNA through the biotin-avidin interaction.

DNA functionalized magnetic nanoparticles were treated with complementary DNA labeled with FITC (target). A random biotin-DNA sequence was modified to the particles and, these particles were treated with the FITC-DNA (control). This experiment was performed to confirm that the particles were modified with DNA and if the immobilized DNA remained functional (Figure 2-4). Based on the target sample, these nanoparticles have been labeled with DNA and the DNA collected the target DNA as seen by the fluorescence signal. Furthermore, this experiment showed that the DNA nanoparticles were selective for the target as determined from the lack of signal in the control sample and the intensity of signal in the target sample. At these experimental conditions, the collection efficiency was determined to be 95 ± 3 %. The zeta

potential and fluorescence data confirm the presence and binding activity of the immobilized DNA.

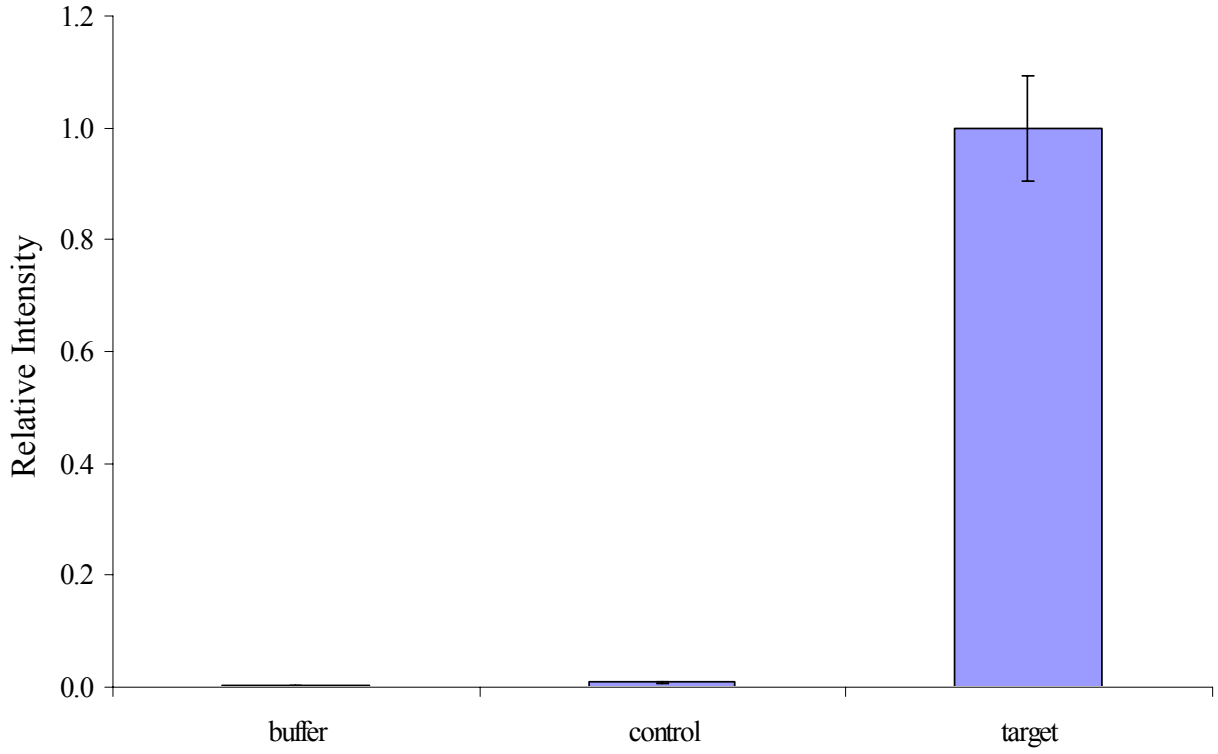

Figure 2-4. The microplate reader fluorescence intensity data collected for FITC labeled DNA molecules.

Nanoparticle Characterization and Optimization

The density of the silica coated magnetic nanoparticles was determined to be approximately 2.87 g/mL by measuring the mass and acquiring the volume of those particles. From this data and the measured size of a single nanoparticle (~65 nm), the molecular weight of this material was calculated to be 2.44×10^7 g/mole. Using this molecular weight, the number of DNA molecules attached to the nanoparticle surface was determined by calculating the number of nanoparticles in 180 μL at 0.2 mg/mL, and the number of biotin-DNA reacted with each avidin coated silica particle (Biotin-DNA) was calculated based on the particle number.

These prepared samples were treated with FITC labeled DNA described in the experimental section. The DNA-FITC left in the sample after hybridization and extraction of the DNA modified nanoparticles (Remaining), the DNA-FITC extracted and removed from these particles by heating (Collected) was monitored by microplate reader fluorescence (Table 2-2). Saturation of the DNA conjugated nanoparticle was determined to be at ~1300 DNA molecules per particle by both methods, which were ~71 μM and ~ 6 μM by the remaining and collected procedures respectively. However, the point at which the samples become saturated differs depending on the method used to monitor the amount of DNA collected. In this instance, the values obtained from the collected samples provide a direct determination, and therefore more dependable versus the indirect sample determination (Remaining).

Table 2-2. The determined amount of DNA molecules modified to the nanoparticle surface.

Biotin-DNA (molecules)	DNA-FITC remaining (molecules)	DNA-FITC collected (molecules)
330	259	296
2000	614	1106
5100	769	1098
10300	890	1246
23800	1289	1347

The particle stability and reproducibility of the prepared nanoparticles were next examined. For the particle stability, both DNA conjugated and avidin coated samples were prepared in bulk, where the avidin samples were treated with biotin-DNA when needed. These samples were stored at 4 ˚C until used. Once a week 180 μL of the DNA modified magnetic nanoparticles (NHA) were obtained, and these samples were treated the same as the previously described DNA-FITC samples. For both prepared particle types, all samples resulted in similar signal responses for up to three months at which time no more sample remained to continue the investigation (data not shown). Therefore, the NHA and avidin modified nanoparticle have good stability.

Particle batch-to-batch (Figure 2-5 A) and sample-to-sample within a single batch (Figure 2-5 B) reproducibility was investigated. As determined from Figure 2-5 the NHA collection ability of DNA-FITC target samples from one sample to the next within a batch and from one

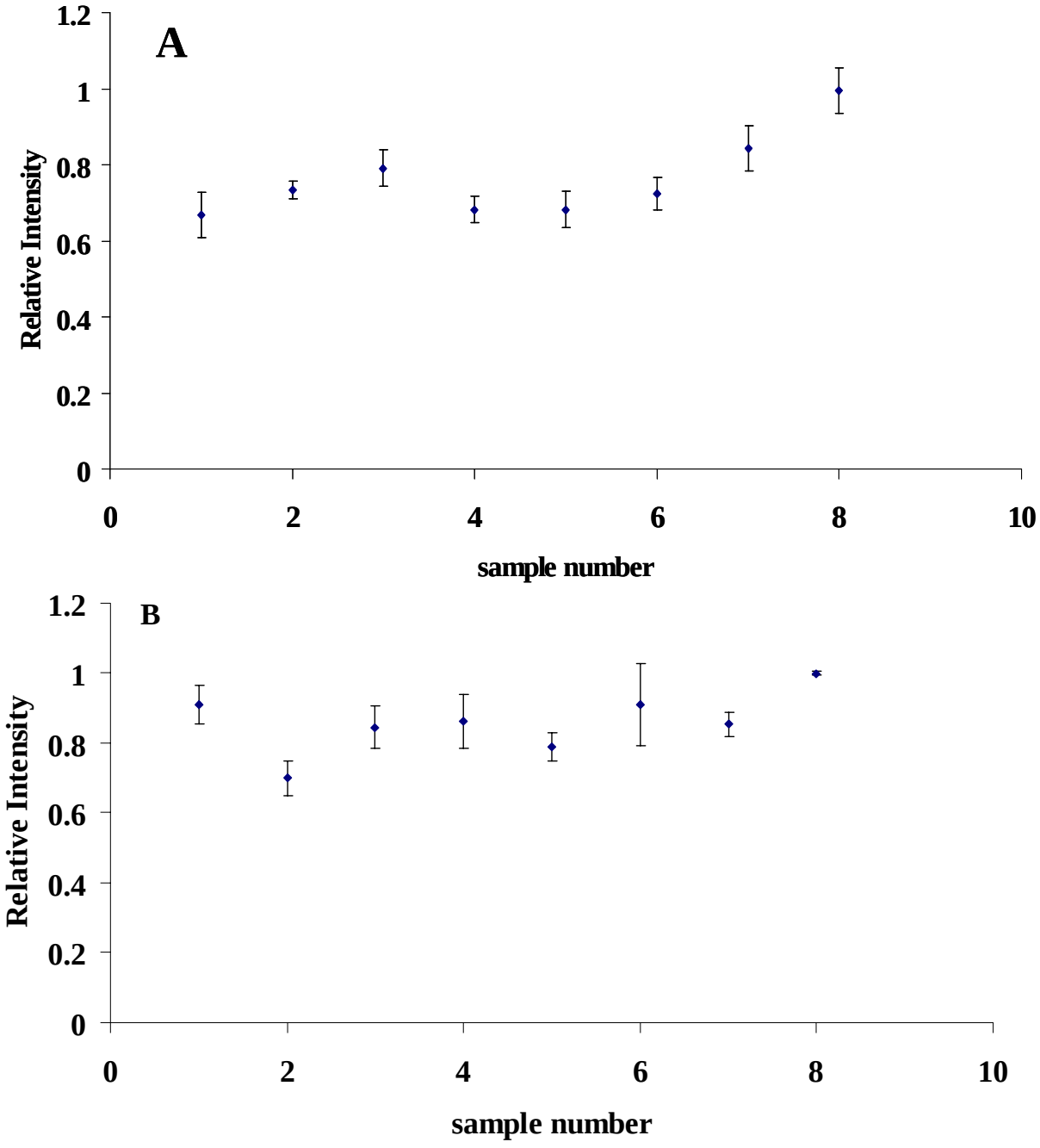

Figure 2-5. The fluorescent data obtained from batch-to-batch and sample-to-samples reproducibility studies. A) Testing the batch-to-batch reproducibility. B) Testing the sample-to-sample reproducibility within a single nanoparticle batch.

batch to the next, the results were highly consistent between samples. In both studies, the fluorescence signals collected from all samples produced nearly linear responses with some sample variability. The explanation for this irregularity is that the avidin coating procedure for these samples was accomplished through physical adsorption, and there is some difficulty in controlling the amount and the efficiency of adsorbing materials to the particle surface.

Carboxyl Modified Nanoparticles

As with the avidin treated and biotin-DNA conjugated particles, the carboxyl modified nanoparticles with covalently attached capture DNA samples were characterized by zeta potential measurements (Table 2-1) and monitoring collection of DNA-FITC by fluorescence (data not shown). Comparing the particle surfaces analyzed by zeta potential, recall that the silica coated particles had an overall charge of -19.59 mV, carboxyl modified nanoparticles had a surface charge of -43.27 mV, and covalently conjugated amine-DNA to the particle produced an overall charge of -33.31 mV. This translates to confirmation of the carboxyl surface modification, and these nanoparticles had an improved dispersion compared to the silica only surface. The carboxyl surface has an increased charge because at neutral pH these functional groups are inherently negatively charged. Upon conjugation with amine-DNA, the surface charge has a slightly lower surface charge, which means that the particles are more prone to aggregation. However, the charge was large enough to avoid severe settling of the particles, but settling was observed after several hours. The zeta potential measurements for the DNA conjugated particles provide evidence that the particles were modified. The decrease in the magnitude of the surface charge when labeled with amine-DNA is explained as the result of the reaction of the amine (NH_2) and carboxyl (COO-) forming a peptide bond and removing or reducing the presence of the added negative charge. Furthermore, DNA molecules have an

inherent negative charge, which should increase the overall charge of the particle. However, the charge added to the particles by DNA is not associated directly to the particle surface, but instead is spread across the DNA molecule, which is not compounded as a single charge point on the particle surface.

When the covalently modified DNA magnetic nanoparticles (NHA) were treated with target and control DNA-FITC, similar results were obtained for this experiment (data not shown) as with the biotin-DNA prepared particles in Figure 2-4. The covalent conjugated magnetic particles had similar characterizations of the particles as the biotin-avidin conjugation. The biggest difference between the conjugation processes was the covalently modified particles had lower DNA molecular densities by around an order of magnitude, and therefore, these particles saturate at lower target concentrations with the same amount of nanoparticles used in each sample.

Conclusions

Silica coated magnetite nanoparticles were successfully prepared using the Stöber process, and the biotin-avidin DNA conjugation was demonstrated. The DNA modified nanoparticles were characterized as these samples were constructed layer-by-layer using TEM, X-ray, zeta potential, and fluorescence analysis. The iron oxide particles were determined to have a full and complete silica coating with avidin and carboxyl functionalizations, which lends them to conjugations with target recognition molecules that are biotin and amine labeled, respectively. The conjugated nanoparticles proved to be exploitable for selectively binding and isolating target molecules in this particular instance was DNA.

CHAPTER 3
EXTRACTION OF OLIGONUCLEOTIDES USING SILICA COATED MAGNETIC NANOPARTICLES

Introduction

The selective separation of biomolecules from biological fluids is of distinct interest for disease diagnosis, biomedical studies, and biotechnology development. However, there is a lack of efficient biotechnology available to gather a single target molecule, such as DNA, mRNA, peptides, and proteins, at low concentrations and in large volumes of complex sample solutions. To date, routine separation techniques used for DNA purifications have included HPLC and gel electrophoresis.[103-105] These methods are used for the separation of high target capacity bulk samples.[106] HPLC purifications separate DNA based on length and hydrophobic interactions and not by the oligonucleotide sequence.[107] Gel separation has the same fundamental problem. When dealing with low-abundance target molecules in living cells, this separation issue becomes amplified. Thus, the selective extraction of oligonucleotide molecules from complex samples has been a difficult challenge for investigators that require innovative solutions.

Nanomaterials have quickly become an excellent medium to act as a molecular carrying device for many biological applications. This is the result of their large surface-to-volume ratio and extremely small size.[108] Nanoparticles have demonstrated unique advantages when combined with biomolecules as analyte recognition elements for bioanalysis.[72,110] In one instance, magnetic nanoparticles have been developed as a molecular carrying device for separating genes because of their controllable response to a magnetic field.[111-113] Separation and detection of DNA molecules has been accomplished by using avidin-coated magnetic nanomaterials,[114] and this type of approach has been used for the collection and separation of single-base mismatched DNA using fluorescence based detection scheme.[75] However,

fluorescence detection does not provide the ability to distinguish with any certainty the presence of the full complement or mismatch sequences.

An alternative method for the detection of separated DNA samples that has the ability to provide sequence identification is mass spectrometry (MS). One area that MS detection of DNA has gained notoriety was in the characterization of polymerase chain reaction (PCR) products. MS analysis compared to the traditional PCR detection methods has the potential advantages of speed, sensitivity, and mass accuracy.[115-119] MS has been shown to detect single-nucleotide polymorphisms (SNP), essentially single-base mismatch, and has emerged at the core of several SNP projects.[120,121] Prepared PCR samples present a challenge, the efficient and rapid removal of the reaction components was necessary for MS analysis. The current limitations on MS analysis of PCR exist with the time required for sample clean-up.[122]

In this work, the development of a nanoharvesting agent (NHA) using silica coated magnetite nanoparticles functionalized with avidin and conjugated with biotinylated DNA to the particles surface. DNA hybridization provided sequence selectivity, and combined that with the exceptional separation capability of magnetic nanoparticles extracted target molecules with little sample clean-up required. Target DNA was separated, collected, and analyzed from pure and mixed samples. To demonstrate the extraction properties of NHAs, single and multiple oligonucleotide targets in both buffer and complex samples, single target extractions in large volume from buffer and complex samples, and mismatch DNA experiments in buffer were investigated. The separated and collected targets were monitored by fluorescence and mass spectrometry techniques.

Experimental

Materials and Methods

The materials for these experiments were purchased from Sigma-Aldrich (St. Louis, MO) unless otherwise indicted. Ammonium hydroxide (NH_4OH), ethanol (EtOH), and hydrochloric acid (HCl) were obtained from Fisher Scientific (Fair Lawn, NJ). All the DNA molecules were synthesized in-house. The neodymium iron boron magnet used for extractions was purchased from Edmund Optics (12,200 gauss, Barrington, NJ). Clean resin used for desalting DNA samples was purchased from Sequenome (Newton, MA). The avidin protein was bought from Molecular Probes (Eugene, OR). AnchorChip matrix assisted laser desorption-ionization (MALDI) plate was obtained from Bruker Daltonics (Billerica, MA). All the chemicals used were of analytical grade.

Instruments

All fluorescence measurements were obtained using a TECAN Safire microplate reader (Research Triangle Park, NC, USA). The mass spectra were collected with a Bruker Microflex (Billerica, MA) MALDI time-of-flight (TOF) operated in negative ion reflectron mode.

DNA Conjugated Magnetic Nanoparticles

The DNA modified silica coated magnetic nanoparticle, referred to as nanoharvesting agent (NHA), synthesis was described in detail in Chapter 2. Briefly, a solution of ammonium hydroxide (2.5%) and a solution containing ferric chloride hexahydrate (0.5 M), ferrous chloride tetrahydrate (0.25 M), and HCl (0.33 M) were mixed. The sample was stirred at 350 RPM using a mechanical stirrer for 10 minutes. Silica coating was made by washing the iron oxide sample and suspending them in ethanol containing ~1.2 % ammonium hydroxide with 210 μL of tetraethoxyorthosilicate (TEOS) and sonicating for 90 minutes. Next, the sample was treated

with an additional 10 μL of TEOS with sonication for 90 minutes. The silica coated nanoparticles were washed with ethanol then 10 mM phosphate buffer saline (PBS) pH 7.4.

Avidin coating was completed by taking 1.2 mg of the silica coated magnetic nanoparticles with 5 mg of avidin and incubated at 4° C overnight. The particles were washed with 100 mM PBS pH 7.4, and suspended in a 1% glutaraldehyde solution diluted in 100 mM PBS for 1 hour with continuous mixing at room temperature. The sample was washed and dispersed in 1M Tris-HCl pH 7.0 for 3 hours at 4º C. These particles were washed with 20 mM Tris-HCl, 5 mM $MgCl_2$ pH 8.0 and suspended at a concentration of ~0.2 mg/mL. Biotin modified DNA, complementary to nonhuman (5'-biotin-TTT AAA TCT AAA TCG CTA TGG TCG C-3'), MnSOD (5'-biotin-TTT AAA CAG TTA CAT TCT CCC AGT TGA TT-3'), or β-actin (5'-biotin-TTT AAA AGG AAG GAA GGC TGG AAG AG-3') truncated genes, was attached adding 6 nmols of DNA to 500 μL of the avidin nanoparticles at 4° C overnight. Finally, the NHA were washed with 20 mM Tris-HCl, 5 mM $MgCl_2$ buffer and suspended at a concentration of ~0.2 mg/mL.

Extraction of DNA Targets

Pure oligonucleotide extractions

To 180 μL of 0.2 mg/mL of the NHA, 20 μL of each of the individual target DNA sequences, which were a nonhuman truncated gene (5'-FITC-GCG ACC ATA GCG ATT TAG A-3') labeled with fluorescein isothiocyanate (FITC), the MnSOD truncated gene (5'-cy3-AAT CAA CTG GGA GAA TGT AAC TG-3') labeled with cy3, and truncated β-actin gene (5'-Tx Red-CTC TTC CAG CCT TCC TTC CT-3') labeled with Texas Red (Tx Red) producing a final concentration of 50 nM. The prepared samples were incubated at room temperature for 1 hour. The samples were magnetically extracted and washed three with 200 μL aliquots of 20 mM Tris-

HCl, 5 mM $MgCl_2$, pH 8.0 buffer. These samples were heated to 70 ˚C for 10 minutes to release the captured DNA from the NHA. While the samples were still hot, NHA were magnetically removed from the supernatant. The released DNA sample was allowed to cool to room temperature and then analyzed by the microplate reader. Additionally, this experiment was performed in a more complex matrix, where 36 μg of the NHA was suspended in a final volume of 200 μL fetal bovine serum (FBS) containing the target DNA. After incubation, the samples were washed three times with 200 μL of the 20 mM Tris-HCl, 5 mM $MgCl_2$ buffer. These samples were then treated the same as the buffer incubated samples.

Large volume extractions

Large volume extraction experiments were investigated as well. The large volume buffer extractions were evaluated at final volumes of 10, 5, 1, and 0.2 mL. These samples were spiked with 20 μL of target DNA at 500 nM, and contained 0.2 mg of the NHA, which is 1 mL at 0.2 mg/mL. The samples were incubated for 1 hour at room temperature. After target binding, the samples were magnetically extracted and washed sequentially with 1 mL, 0.5 mL, and 0.2 mL of the 20 mM Tris-HCl, 5 mM $MgCl_2$ buffer. As described above, the isolated DNA was removed from the NHA by heating to 70 ˚C for 10 minutes, and the particles removed from the supernatant while the sample was still hot. The collected DNA sample was analyzed using the microplate reader. This experiment was repeated using 10 mL of FBS as the matrix, and the target DNA extracted.

DNA mismatch targets

The NHA ability to bind and extract one (5'-FITC-GCG ACC ATA TCG ATT TAG A-3') and two-base (5'-FITC-GGG ACT ATA GCG ATT TAG A-3') mismatch DNA sequences versus the full complementary target was explored using FITC labels based on the truncated

nonhuman gene. Individual samples containing the 50 nM full complement, one-base mismatch, and two-base mismatch DNA in a final volume of 200 μL with DNA labeled magnetic nanoparticles using the biotin-DNA sequences described above. These samples were extracted, collected, and isolated as described in previous sections. Each of the prepared samples was analyzed using the microplate reader.

Multiple target extraction

Using the sample extraction protocol presented previously, samples containing one, two, and three target DNA sequences using combinations of the nonhuman, MnSOD, and β-actin. These samples were treated with 36 μg, 180 μL at 0.2 mg/mL, of each of the three prepared NHA types simultaneously. When extracted, the one, two, and three target containing samples were heated to release the captured DNA targets from the nanoparticle, and the isolated materials were analyzed by fluorescence using the microplate reader.

Sample Preparation for Mass Spectrometry

The DNA extraction experiments were performed in the 20mM Tris-HCl, 5mM $MgCl_2$ buffer as described previously and analyzed by MALDI-TOF. The samples analyzed were single sequence type extractions of the nonhuman target (5836.9 g/mol) and one-base mismatch (5811.9 g/mol) followed by mixtures of full complementary and one-base mismatch at various ratios (1:1, 2:1, and 5:1 respectively). The multiple target extraction experiments were executed as previously described. The average mass ions for the truncated nonhuman gene were 5836.9 g/mol, MnSOD truncated gene was 7120.7 g/mol, and β-actin 5905.9 g/mol. After extraction and washes with the 20mM Tris-HCl, 5mM $MgCl_2$, the samples were dispersed in 20 μL deionized water. These samples were heated to 70 ˚C for 10 minutes in the deionized water. Desalting was performed prior to mass spectrometry analysis by using a weak anion exchange resin at half the

total volume of the sample in a 0.5 mL centrifuge tubes. The samples were then mixed with 1:1 with 1 μL of 10 mg/mL 3-hydroxypicolinic acid (50/50 H_2O/acetonitrile) and spotted (0.5 μL) onto a dry pre-spotted (1μL) anchor-chip.

Results and Discussion

Fluorescence Detection of Extracted Samples

Single oligonucleotide extraction

Individual target extractions of three different oligonucleotide sequences were performed in buffer and serum using DNA modified nanoparticles (NHA) labeled with capture sequences complementary to their respective targets, which include nonhuman, MnSOD, and β-actin. These collected samples were analyzed by the microplate reader and repeated 10 times. The control sequences for each of the nanoparticle types was one of the other DNA sequences used in this study, for example MnSOD and β-actin for the nonhuman capture NHA.

Figure 3-1 displays representative 20 μL aliquots of fluorescently labeled DNA targets extracted from buffer (solid bars) and serum (striped bars). The nonhuman DNA target was represented in blue, MnSOD DNA was represented in green, β-actin was represented in red, and the control experiments in black. The control data shown here was the nonhuman NHA treated with the dye labeled MnSOD oligonucleotide. The serum control experiment produced a slightly higher background signal than the buffer control. This increased background signal was most likely a result of the extraction being performed in a biological fluid, and after the wash steps some of the biomaterial remained in the sample.

As seen in the figure, each of the NHAs selectively extracted their respective targets, and a significant intensity difference was observed between the target and control samples for all NHAs. For all the control samples investigated, there was little to no signals observed. Due to

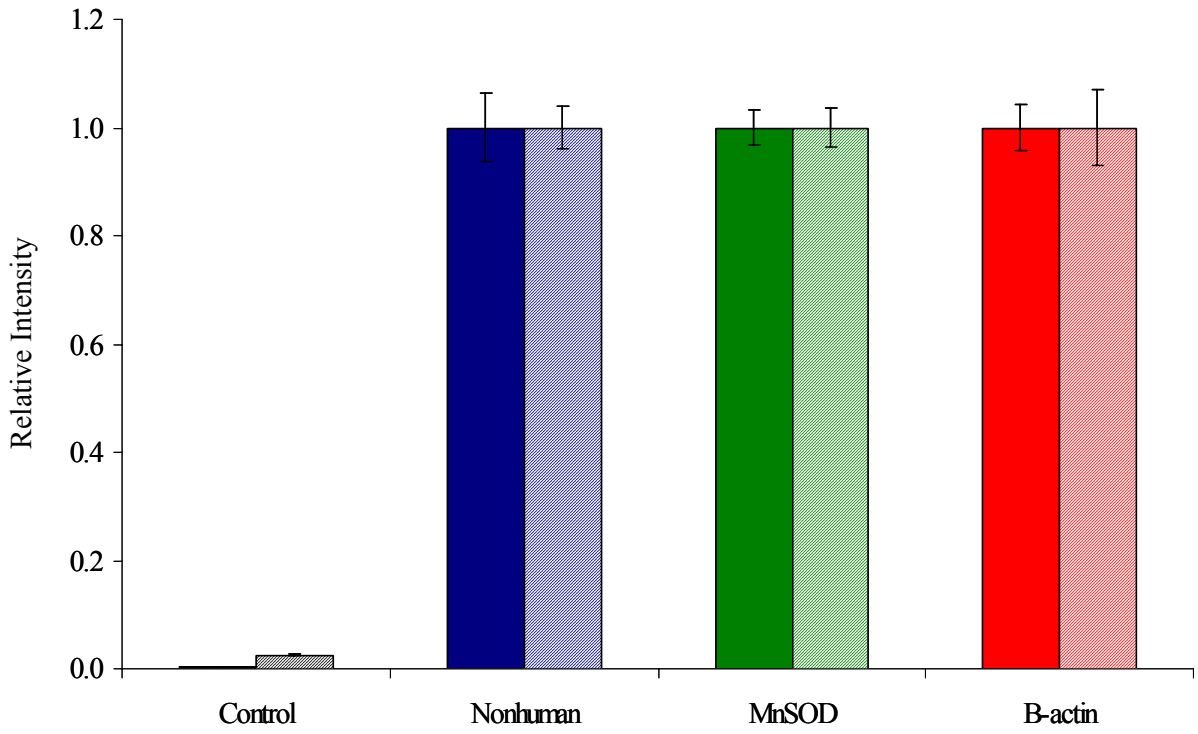

Figure 3-1. Fluorescence intensity data representing individually extracted DNA targets from buffer (solid bars) and serum (striped bars) samples.

the signals obtained, the target samples are easily distinguishable from the control sample. The samples extracted from buffer had signal enhancements of nearly 300-fold over the control samples, and for the serum extracted samples the enhancements were at least 40-fold over the control samples. The difference in signal enhancements was that the set performed in the serum media resulted in higher background signals most likely due to residual serum materials. At these experimental conditions of 0.2 mL sample volumes with 36 μg of NHA using 50 nM of target DNA, the collection efficiency from the buffer samples were determined to be more than 95% and the serum samples were estimated to be around 90% or higher (data not shown). For determining these collection efficiencies, the fluorescence signals for the DNA samples were

obtained prior to and after extraction for both the buffer and serum samples, and the percent recovered was calculated from these obtained values.

Sample enrichment and mismatch oligonucleotide extraction

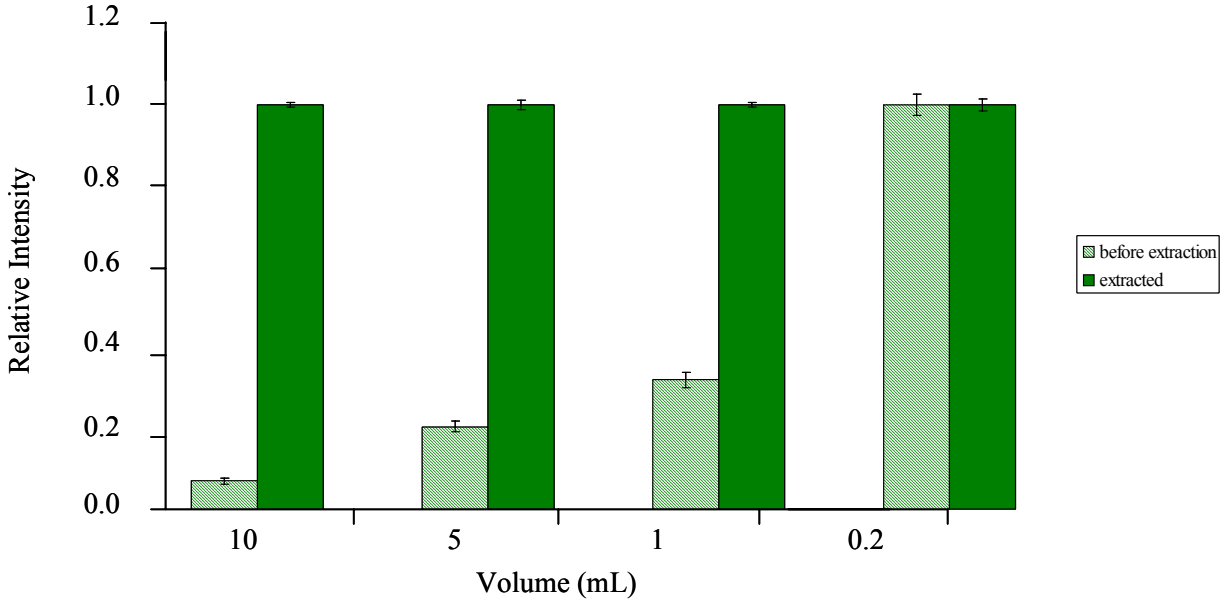

Figure 3-2. Enrichment study of extracting MnSOD fluorescent dye labeled DNA target from several different buffer volumes.

The NHAs were used to extract and concentrate 10 pmols of target DNA from various sample volumes, which were 10, 5, 1, and the standard 0.2 mL. The enriched samples were removed from the particles by heating into 0.2 mL sample volumes as described previously, and 20 μL aliquots were analyzed by the microplate reader. Each of the target DNA samples was tested. Figure 3-2 shows the representative fluorescence data obtained for the MnSOD enriched samples extracted from buffer, where the fluorescence intensities were obtained before extraction (striped bars) and after extraction (solid bars). The first set of samples is the 10 mL, the second set of samples is the 5 mL, the third set of samples is the 1 mL, and the last set of samples is the 0.2 mL sample volumes. The NHAs proportionally enriched the target molecules from the various sample volumes, as indicated in Figure 3-2. The samples were concentrated with a linear

response with respect to the signals observed prior to extraction, and the fluorescence intensities of the enriched samples were measured to be the same for all NHA treated samples.

The amount of the NHAs used in these studies was increased to 0.2 mg. This was done to ensure that sufficient collection of the target was obtained in the large volume samples. When the standard 36 μg were used, the collection efficiency of the target DNA from the 10 mL sample decreased by more than ½ that of the standard 0.2 mL volume. The amount of NHAs used was not optimized. The target DNA was enriched from 10 mL of serum, and similar results were obtained (data not shown).

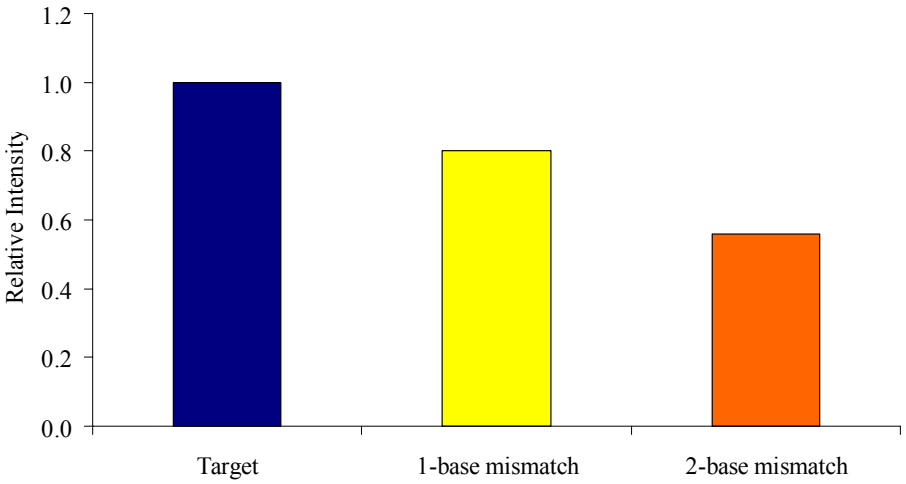

Figure 3-3. Fluorescence data obtained testing the ability of the nanoharvesting agent to collect and isolate mismatched DNA sequences.

For the mismatch extraction study, 50 nM concentration of the full complementary, one-base mismatched, and two-base mismatched DNA sequences labeled with a FITC fluorophore were added to three different NHA samples. The set of sequences represented in Figure 3-3 were the nonhuman oligonucleotides. The fluorescence of each sample solution was determined after collection and removal of the extracted sequence from the particle into 200 μL of buffer sample, and 20 μL aliquots of the samples were analyzed by the microplate reader. The first intensity

peak represents the full complementary nonhuman oligonucleotide (target), the second peak is the one-base mismatch oligonucleotide (1-base mismatch), and the third peak is the two-base mismatch oligonucleotide (2-base mismatch). As expected, the NHAs extracted each of the DNA sequences, but with different efficiencies. The target was removed with the highest efficiency followed by the 1-base and 2-base mismatch sequences, respectively. Additionally, this presents a problem for fluorescence analysis when mismatch sequences are present in a sample with a target sequence. There is no way to determine the identity of the sample extracted by fluorescence techniques.

Multiple oligonucleotide extraction

The multiple extraction and detection experiments were evaluated by creating mixtures of one, two, and three DNA targets at 50 nM final concentrations of each analyte used and adding 36 μg of all three of the NHAs. These samples were prepared in either buffer or serum media. For the single target samples, the sample contained the MnSOD target. Additionally, double and triple target samples were evaluated, which were composed of the MnSOD and nonhuman sequences and all three targets respectively. All combinations of the one, two, and three target mixed samples were evaluated (data not shown). Each sample was analyzed using 20 μL of the isolated materials by the microplate reader, and every sample was measured three times to check for the presence of each of the three dye-labeled oligonucleotides (Table 3-1). The first column represents the DNA samples that were analyzed, the second column indicates the presence or absence of the nonhuman sequence, the third indicates the MnSOD sequence, and the fourth represents the β-actin sequence. The rows of the table display the different DNA samples that were investigated.

The buffer extracted samples produced signal enhancements that were 200-fold and higher above the background signal, and the serum extracted samples had enhancements of at least 35-fold. In samples that contained the MnSOD but not the β-actin targets, a small signal was measured. This was the result of the cy 3 fluorophore on the MnSOD having a slight excitation overlap with the excitation wavelength used for the Texas Red dye. The determined standard deviations for these extractions were 8-12%. This data indicated that the NHAs were selective for the target DNA and reproducible in all evaluated samples.

Table 3-1. Representative normalized fluorescence intensities obtained from buffer and serum multiple target extraction.

Sample type	Nonhuman	MnSOD	β-actin
Buffer			
one target	0.0	1.0	0.1
two target	1.0	1.0	0.1
three target	1.0	1.0	1.0
Serum			
one target	0.0	1.0	0.1
two target	1.0	1.0	0.1
three target	1.0	1.0	1.0

Analysis by Mass Spectroscopy

The mismatch samples were further investigated by mass spectrometry. In this study, the sequences examined were the nonhuman target (m/z = 5836.9 g/mol) and its one-base mismatcl (m/z = 5811.9 g/mol) sequence, where these samples were not fluorescently labeled. The oligonucleotide sequences were extracted from 200 μL volumes of a 50 nM sample concentration. The extracted samples were released from the NHA into 20 μL of deionized water. This was performed to reduce the amount of salt present in the isolated samples for analysis. The DNA sequences were extracted from samples of the nonhuman (target), the one-base mismatch, and a mixture of the two sequences. For the mixed samples, three ratios of the target and mismatch sequences were investigated, which were 1:1, 2:1, and 5:1 target-to-

mismatch respectively. The target concentration was kept at 50 nM, and the mismatch concentration was varied according to the ratios indicated.

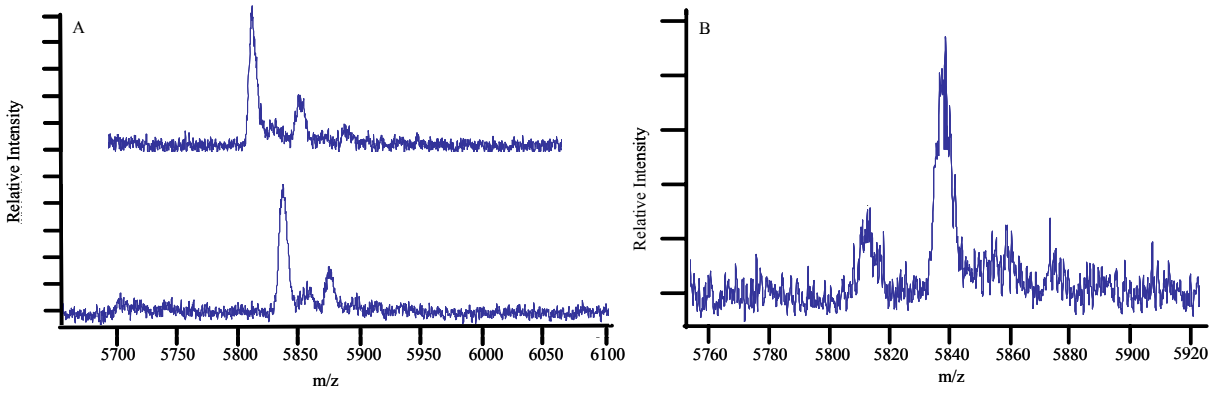

Figure 3-4. Mass spectra demonstrating the extraction of the nonhuman mismatched DNA using the nanoharvesting agents. A) The full complement DNA target is the bottom spectrum and the 1-base mismatched DNA is the top spectrum. B) Mixed samples of the full complement and mismatched DNA extracted using the nanoharvesting agent.

Figure 3-4 A contains the mass spectra obtained from the target sample (bottom) and one-base mismatch sample (top). These results indicated that the NHA extracts both the target and mismatch sequences which confirms the fluorescence intensity data. However, Figure 3-4 B displays the mass spectrum obtained when both sequences were mixed into the sample at the 5:1 ratio. This spectrum provides the ability to differentiate between the two sequences, which were not possible with the fluorescence measurements. The other ratios confirmed this conclusion as well. However, these ratios demonstrated that the mismatch sequence ionized better than the target DNA. Additional studies using this MALDI-TOF and the instrumental conditions indicated, this MS instrument can discriminate between sequences with mass differences around 9-10 mass units. The smallest possible mass difference obtainable between two nucleotide bases is 9-10 mass units.

The multiple DNA extraction study was further investigated by MS. The sequences examined were the nonhuman (m/z = 5836.9 g/mol), MnSOD (m/z = 7120.7 g/mol), and β-actin

(m/z = 5905.9 g/mol) sequence, where these samples were not fluorescently labeled. The oligonucleotide sequences were extracted from 200 μL volumes of a 50 nM sample concentration. The extracted samples were released from the NHA into 20 μL of deionized water. This was performed to reduce the amount of salt present in the isolated samples for analysis. Individual extractions were performed for each of the DNA sequences and analyzed by MS. Mixed samples of the three DNA targets were extracted by treatment with one, two, or all three of the NHA as described above. The extracted samples were analyzed by MS.

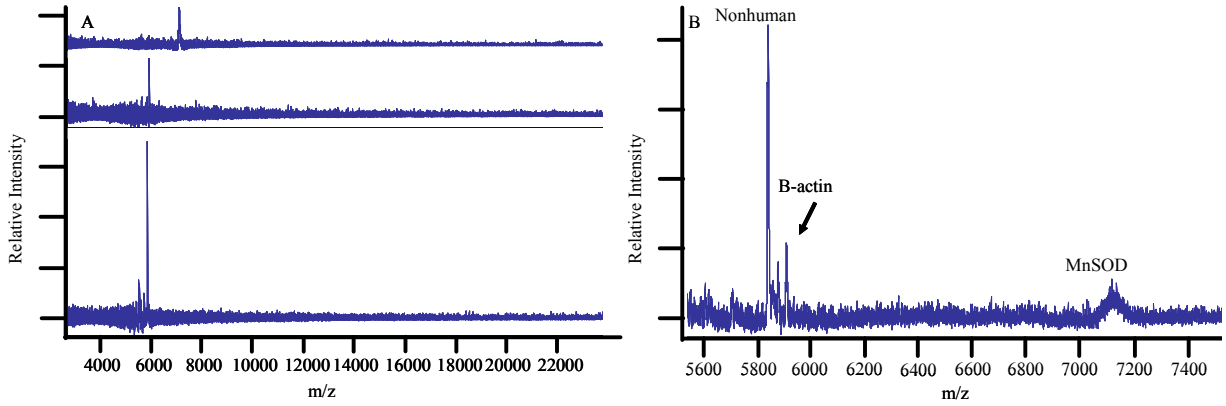

Figure 3-5. Mass spectra demonstrating the extraction of multiple DNA sequences using the nanoharvesting agents. A) The nonhuman sequence is the bottom spectrum, MnSOD sequence is the middle spectrum, and β-actin is the top spectrum obtained from extracted samples containing individual targets. B) Multiple DNA extraction from a sample containing all three target sequences using the nanoharvesting agents.

Figure 3-5 A contains the mass spectra obtained from the individual target samples treated with their corresponding NHA. The bottom spectrum is of the nonhuman oligonucleotide that was extracted, the middle spectrum displays the extracted MnSOD sequence, and the top spectrum is the extracted β-actin sequence. These results indicated that the NHA extract the target sequences, and confirm the fluorescence data. Figure 3-5 B displays the mass spectrum obtained from the multiple extraction samples when treated with all the NHAs simultaneously. MS provides the ability to differentiate between all the multiple extracted target sequences. This

data confirms the experiments performed by fluorescence. However, MS has the ability for increased multiplexed analysis of targets compared to fluorescence.

Conclusions

The selective and multiple extraction capability of the DNA conjugated silica coated magnetic nanoparticles (NHA) were demonstrated by analysis by both fluorescence and mass spectroscopy. These isolation experiments were demonstrated in buffer and serum for the fluorescence based analysis. Also compared to the fluorescence based detection method, MS has the capability for multiplexed analysis beyond that of fluorescence. Fluorescence techniques detect no more than 5-6 DNA target molecules simultaneously, where MALDI at these experimental conditions has the ability to detect dozens of DNA molecules. The limit to the number of DNA molecules to be detected by MALDI depends highly on the ionization capability of the targets. However, fluorescence analysis served well for characterizing the extraction characteristics of the NHA. The NHA was determined to extract mismatch DNA from samples containing these sequences. This data was collected by both fluorescence and mass spectrometry techniques. However, MS has the ability to discriminate with certainty the presence of mismatched DNA in samples, which is nearly impossible for fluorescence-based detection. Efficient extraction of DNA targets from large volume samples for enriching the DNA analytes for analysis were demonstrated fluorescently in both buffer and serum sample matrices. The extra dispersion into deionized water and desalting steps were added to the sample preparation to improve the ionization of the DNA molecule. The NHAs have been established as a powerful sample clean-up and preparation tool for oligonucleotide analytes.

CHAPTER 4
FUNCTIONALIZED NANOPARTICLES FOR PEPTIDE EXTRACTION

Introduction

With the recent advancements in mass spectrometry, it has become a routine technique for the analysis of biological molecules. However, for complex biological samples the analysis time is limited more by sample separation and clean-up processes than by mass analysis. In addition, as sample matrices become more complex and the analytes of interest are in lower and lower abundance, methods for selective extraction and concentration must be developed. This work describes the use of silica nanoparticles for target isolation and analysis by mass spectroscopy.

To date, a number of separation procedures have been developed for mass spectrometry analysis. Solid phase extraction (SPE) tools are a popular tool for the removal of background materials from biological samples, such as Ziptips®.[122] SPE procedure involve multiple step procedures for analyte isolation. This method provides sample clean-up and concentration, but SPE does not have the ability to selectively remove target molecules.

Another approach related to SPE called surface enhanced laser/desorption ionization (SELDI), where a MALDI plate is functionalized to selectively retain the analyte molecules. After the sample is treated to the SELDI surface, the plate is washed prior to MS analysis. This technique provides increased throughput for biological applications in profiling studies. However, SELDI requires bringing the sample to the surface for extraction increases the risk of sample loss.[123]

Alternatively, microparticles have been used for the collection of analytes prior to MALDI analysis with a choice of functionalization chemistries and particle recovery processes.[124-125] For example, C_{18} modified magnetic microspheres were used in the profiling of proteomic targets.[124] The C_{18} group adsorbs a fraction of the materials through weak van der Waals interactions and

maintains the interactions during the washing procedures. For analysis, the retained molecules are removed from the particle by treatment with non-polar solvents, and the MALDI matrix is mixed with the isolated sample.

Silica nanoparticles have been used in a number of analyte detection schemes. However, applications for mass spectrometry analysis have not been widely investigated. This work explores the selective extraction and concentration of target molecules for high sample throughput. Additionally, an atmospheric pressure liquid MALDI was used as a medium the direct analysis of the functionalized nanoparticles to minimize sample loss and analysis time. Liquid matrices do not require the use of low pressure sample chambers and avoid the problems of inhomogeneous matrices, as seen with solid-based MALDI. Atmospheric pressure sampling provides an alternative approach to allow for rapid and reproducible sample analysis.[126] The focus is on the aptamer conjugated magnetic nanoparticles for selective peptide extraction, but C_{18} functionalized silica was investigated as well. Aptamers have been composed of single-stranded nucleic acids that bind to target molecules. These aptamers form a complex three-dimensional structure, enabling the aptamers to selectivity recognize a wide range of molecules with high affinities.

Experimental

Materials and Methods

Peptide standards (Sigma-Aldrich Corp., St. Louis, MO, USA), angiotensin I, angiotensin II, bradykinin, bradykinin fragment 1-7, and L-vasopressin were prepared as stock solutions of 500 pmoles/μL using either acetonitrile (ACN), for C_{18} nanoparticle extractions, or water, for aptamer nanoparticle extractions. D-vasopressin (Genomechanix, Gainesville, FL, USA) was synthesized using conventional fluorenylmethoxycarbonyl chemistry, and dissolved in water for analysis. Biotinylated DNA was also purchased from Genomechanix (Gainesville, FL USA).

Non-extraction analysis was conducted by spotting 0.5 μL of matrix onto 0.5 μL of analyte stock solutions.

Nanoparticle Synthesis

Silica C_{18} functionalized nanoparticles

The silica C_{18} functionalized nanoparticles were prepared using a previously reported synthesis procedure.[76,127] Briefly; the nanoparticles were prepared using a water-in-oil microemulsion (W/O) with a water-to-surfactant molar ratio of 10:1. The synthesis produced uniform silica nanoparticles (60 ± 5 nm in diameter) as shown in Figure 4-1 A. Twenty hours into the synthesis, 40 μL of octadecyltrimethoxysilane (Sigma-Aldrich Corp., St. Louis, MO, USA) and 10 μL of ~30% ammonium hydroxide (Fisher Scientific, Fair Lawn, NJ, USA) were added to the microemulsion. The mixture was stirred for an additional 4 hours to yield a C_{18} outer coating of the silica core nanoparticles. Prior to peptide extraction, the nanoparticles were washed with ethanol, acetone, and water three times each, and redispersed in acetonitrile. The final concentration of the nanoparticle suspension was approximated at ~6 mg/mL.

Magnetic aptamer nanoparticles

The iron oxide core magnetic nanoparticles were prepared using the Stöber method.[66] The magnetite core was formed by precipitating iron oxide through mixing ammonia hydroxide (2.5%) and iron chloride at 350 RPM using a mechanical stirrer (10 minutes). The iron chloride solution contained ferric chloride hexahydrate (0.5 M), ferrous chloride tetrahydrate (0.25 M), and HCl (0.33 M).[128] After three washes with water and once with ethanol, an ethanol solution containing ~1.2 % ammonium hydroxide was added to the iron oxide nanoparticles, yielding a final concentration of ~7.5 mg/mL.

Tetraethoxyorthosilicate (200 μL) was added to create the silica coating for the magnetite core particles. The mixture was sonicated for 90 minutes to complete the hydrolysis process, and the nanoparticles were washed three times with ethanol to remove excess reactants.

Aptamers were immobilized onto the particle surface through avidin-biotin linkage (5'–biotin-TCACGTGCAT GATAGACGGC GAAGCCGTCG AGTTGCTGTG TGCCGATGCA CGTA).[129] For avidin coating, a 0.1 mg/mL silica coated magnetic nanoparticles solution and a 5 mg/mL avidin solution were sonicated in the presence of the particles for 5 minutes and incubated at 4° C for 14 hours. The particles were magnetically separated and washed three times with 10 mM phosphate buffered saline (PBS) pH 7.4. The particles were redispersed at 1.2 mg/mL in 10 mM PBS and stabilized by cross-linking the coated nanoparticles with 1% glutaraldehyde (1 hour at 25º C). After another separation, the particles were washed three times with 1M Tris-HCl buffer. For aptamer attachment, the particles were dispersed at 0.2 mg/mL in 20 mM Tris-HCl, 5 mM $MgCl_2$, pH 8.0. Biotin labeled DNA was added to the solution at a concentration of 0.2 $x10^{-6}$ M. The reaction was incubated at 4° C for 12 hours. Three final washings of the particles were performed using 20 mM Tris-HCl, 5 mM $MgCl_2$ at pH 8.0. The nanoparticles were made to a final concentration of 0.2 mg/mL and stored at 4° C before use in the same buffer.

Matrix and Analyte Preparation

The liquid matrix was a UV absorbing formulation developed for use with APMALDI.[126] The matrix was prepared by mixing α-cyano-4-hydroxycinnamic acid (CHCA) (Sigma-Aldrich Corp., St. Louis, MO, USA) with a liquid support containing a solvent liquid, equal parts ethanol and water (Fisher Scientific, Fair Lawn, NJ, USA), and a viscous component, diethanolamine

(DEA) (Sigma-Aldrich Corp., St. Louis, MO, USA). The matrix was sonicated and vortexed to ensure dissolution.

Instrumentation

The mass spectrometer used was an orthogonal acceleration time-of-flight mass spectrometer (TOFMS) (LECO Corporation, St. Joseph, MI, USA). Ions are sampled through an atmospheric pressure interface using a heated curtain gas configuration with 5 L/min of 100° C nitrogen. Briefly, the source uses a 337 nm nitrogen laser (VSL-337-ND-S, Spectra-Physics, Mountain View, CA, USA), focused by a fused silica lens to ~ 250 μm, to irradiate the sample on a stainless steel target 2 mm in diameter. Laser pulses were ~ 20 μJ as measured using a pyroelectic detector (J4-09-030, Molectron Detector, Inc., Santa Clara, CA, USA). The target (2 kV) was positioned on-axis ~1.5 mm from and ~1 mm below the MS orifice (400 V) using a motorized xyz translational stage (8302/IPico Driver, New Focus, San Jose, CA, USA).

During analysis, the laser was pulsed (20 Hz) asynchronously with the MS repeller pulse (5 kHz). The spectrometer data acquisition system is based upon a time-to-digital converter (TDC) multichannel plate (MCP) assembly. The data system is designed to producing 100 spectra per second; however, for typical analysis, spectra were exported and stored in an external computer at a rate of ~ 4 spectra per second. The spectra shown are an accumulation of summed spectra for 1-5 minutes.

Fluorescence measurements for the extracted fluorescein labeled angiotensin II were made using a TECAN Safire microplate reader (Research Triangle Park, NC). Imaging of the C_{18} nanoparticles was conducted on an inverted Olympus microscope, 100X magnification, (Olympus, Melville, NY) using an intensified IPentamax III CCD (Roper Scientific, Trenton,

NJ). Transmission electron micrographs (TEM) of nanoparticles were taken using a Hitachi H-7000 transmission electron microscope.

Extraction Procedures

Two procedures were used for peptide extractions: a centrifugation technique was applied for the silica C_{18} particles, while the magnetic particles required only a magnetic separation. For the C_{18} functionalized particles, 90 μL of nanoparticle solution (~4 x 10^{-8} M) was incubated with 10 μL of stock analyte solution (~ 1:1000 particle-to-analyte ratio) for 10 minutes. The mixture was centrifuged for 5 minutes at 14000 RPM. After centrifugation, the supernatant was removed leaving ~1 μL of silica particles. The particles were washed to remove interferences and unabsorbed analyte. The wash solutions, 99 μL of acetonitrile or water, were added and the mixture was vortexed ~5 seconds. The wash solution used was dependent upon the desired result, analyte removal or retention. The procedure was repeated when additional washing steps were used. For nanoparticle extraction analysis, the silica particles remaining in the centrifuge tube after supernatant removal were applied directly to the MALDI target surface.

The aptamer functionalized magnetic nanoparticles allowed rapid separation using a simple magnetic extraction method. First, a buffer exchange was conducted using 50 μL of aptamer conjugated nanoparticles (~1 x 10^{-8} M). The particles were magnetically extracted and washed with 5 mM phosphate buffer and then 3 mM $MgCl_2$, pH 6.0. The buffer used was based upon the reported protocol for aptamer chiral separation of L and D vasopressin.[130,131] The resulting nanoparticle suspension was used in analyte extractions. For extraction, 10 μL of 50 pmol/μL analyte solution was incubated with 10 μg (50 μL) of the aptamer conjugated nanoparticles for 10 minutes (~ 1:100 particle-to-analyte ratio). A magnet directed the particles to the bottom of the vial for removal of the supernatant. The remaining particles, ~1 μL, were mixed with 5 μL

of water and 5 μL of liquid matrix. Analysis was conducted by spotting 0.5 μL of the aptamer particle/matrix mixture on the MALDI target.

Results and Discussion

Nonspecific Nanoparticle Applications

A study of C_{18} modified silica nanoparticles were investigated for the nonselective extraction of peptide molecules investigated by Turney et al.[65] The analyte bound silica-based nanoparticles were removed from solution by centrifugation. In the initial investigation, the particles were characterized by fluorescent labeled peptide molecules to demonstrate that the peptides adhered to the nanoparticle surface. These molecules not only adsorbed to the particle surface by hydrophobic interactions, but they were retained by the particles throughout the various wash steps. However, the FITC dye molecule labeled to the peptide may have contributed to the retention of the analytes to the hydrophobic nanoparticles. Further investigations involved using mass spectroscopic detection and unlabeled targets. The C_{18} functionalized nanoparticles performed with the same principles as reversed-phase chromatography where the investigated peptides were retained by the nanoparticles through nonpolar washes and then released with a polar solvent. Additionally, varying lengths of peptides were examined, where the smallest ones were removed from the particles first followed by the largest ones. The C_{18} nanoparticles were used directly in the liquid atmospheric pressure MALDI to reduce the chance for sample loss. Where with vacuum based systems, require removal of the analytes prior to analysis. However, this approach provides a low resolution separation for the studied peptides.

Selective Nanoparticle Applications

The C_{18} functionalized nanoparticles utilize hydrophobic interactions for the collection and isolation of target molecules. However, the wash procedure uses centrifugation as the means to

obtain the samples, which is time a consuming process. The DNA aptamer conjugated magnetic nanoparticles offer the possibility of a rapid-selective extraction of analytes from complex samples. These recognition molecules have nanomolar and picomolar dissociation constants for the best binding aptamers, which make them very attractive for numerous scientific and biotechnological devices. Aptamers have been used for investigating cellular protein function and protein-ligand interactions.[92,133,134] Common selective analyte extractions are achieved by using antibody-antigen interactions, where antibodies provide selectivity through conformational binding sites with high K_d.[133] However, limitations exist for antibody conjugated systems, such as diminished detection limits, extensive characterization are needed, and lengthy-complex procedures are required for obtaining these molecules.[135] Aptamers have several advantages compared to antibodies. Since aptamers can be constructed of single stranded DNA or RNA molecules, they are simple and less costly to synthesize with increased shelf lives. Modifications of aptamers are easily performed with site labeling because of the well understood-controllable oligonucleotide chemistry compared to engineering antibodies The aptamer used in this study was selected for D-vasopressin (H-Cys[1]-Tyr-Phe-Gln-Asn-Cys[6]-Pro-Arg-Gly-NH_2), which has a binding efficiency of ~ 1000 times that of L-vasopressin.[130,131]

The silica coated magnetic nanoparticles serve as the solid support for conjugation of the aptamer to extract targets. The magnetic property of the nanoparticles reduces the complexity of the separation protocol required for isolating the target molecules. Placing the particles directly into the liquid matrix allows a rapid analysis procedure that limits analyte loss allowing lower abundance samples to be detected.

The D-vasopressin aptamer provides high selectivity, but this aptamer has a large dissociation constant (K_D ~ 1μM), which allows for release of the analyte from the particles[131].

The aptamer was investigated previously when attached to a surface, and it retained its binding functionality with little or no reduction in its binding ability.[130] The selectivity of the nanoparticle bound aptamer was examined by conducting two control experiments. The first control used D-vasopressin aptamer conjugated magnetic particles, and they were treated with two control peptides, which were angiotensin II (ASP-ARG-VAL-TYR-ILE-HIS-PRO-PHE) and bradykinin fragment 1-7 (ARG-PRO-PRO-GLY-PHE-SER-PRO). These aptamer nanoparticles indicated no sufficient binding of either peptide and no mass spectrometry signal was produced after extraction. The second selectivity control demonstrated whether the vasopressin analytes nonspecifically bound to a random aptamer conjugated nanoparticles, where individual aliquots of L-vasopressin and D-vasopressin were incubated with an adenosine aptamer conjugated magnetic nanoparticles. This experiment demonstrated that the vasopressin molecules were not nonselectively extracted by aptamer conjugated nanoparticles as evidence of the lack of mass spectrometry signal.

The K_D values of the D-vasopressin aptamer for D-vasopressin compared to L-vasopressin were at a ratio of 1000:1[130]. This ratio provides an additional and interesting control for the D-vasopressin aptamer nanoparticles. The extraction of L-vasopressin should produce a limited mass spectrometry signal, and extraction of D-vasopressin should be more efficient indicated by an increased mass spectroscopy signal. Figure 4-1 shows the mass spectra for L- and D-vasopressin before and after treatment with the D-vasopressin aptamer conjugated nanoparticles. Figure 4-1 A displays the L-vasopressin molecular ion and sodium adducts before extraction the top spectrum. The bottom spectrum in Figure 4-1 A indicates the nanoparticle extraction for L-vasopressin. The limited signal intensity that was obtained confirmed lower binding of the aptamer modified nanoparticles for L-vasopressin. Figure 4-1 B provides the molecular ion and

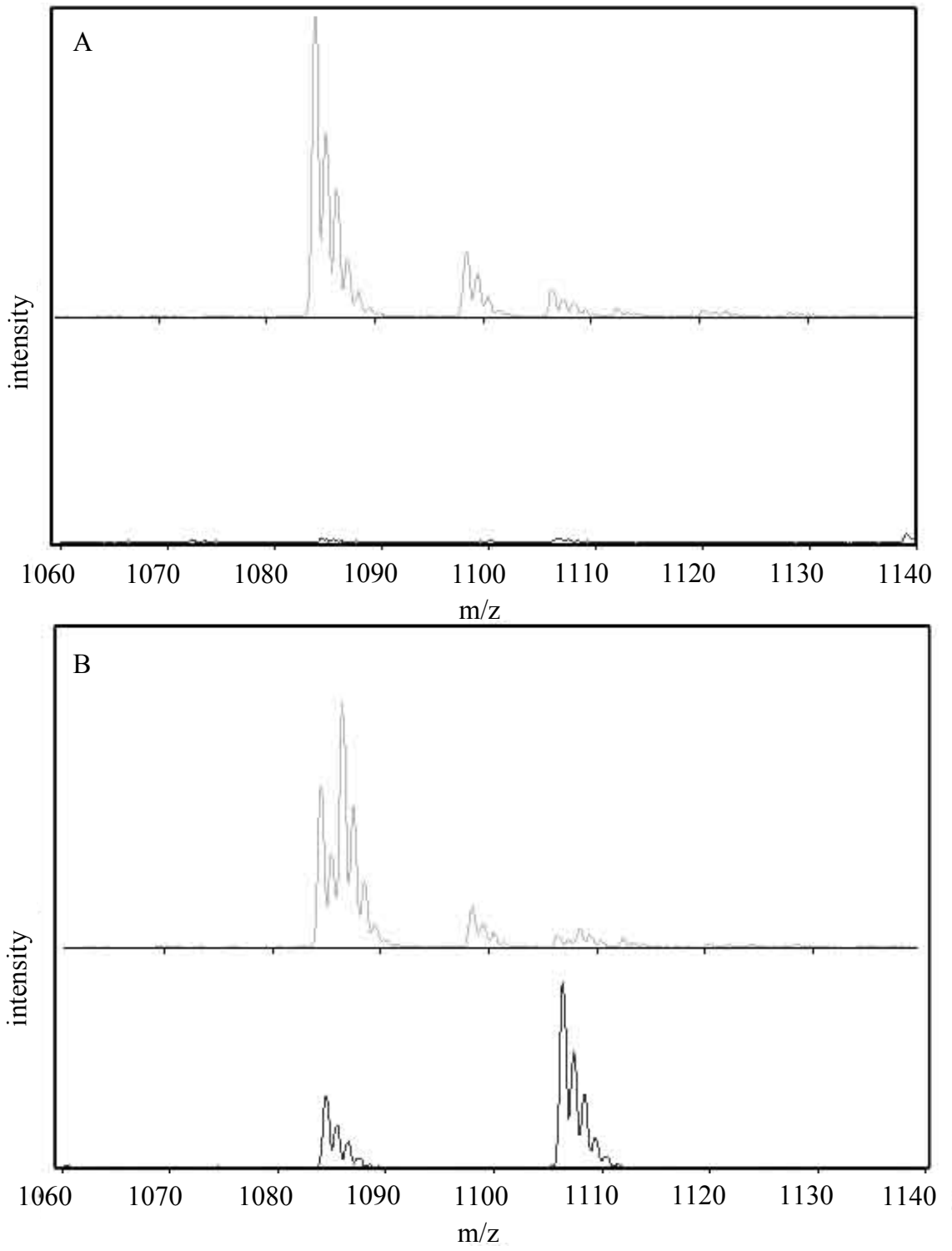

Figure 4-1. The mass spectra of the L- and D- vasopressin before and after extraction are shown. A) L-vasopressin before extraction the top spectrum and after extraction the bottom spectrum. B) D-vasopressin before extraction the top spectrum and after extraction the bottom spectrum.

sodium adducts for D-vasopressin prior to extraction the top spectrum. The bottom spectrum in Figure 4-1 B shows the extraction for D-vasopressin treated with the aptamer conjugated nanoparticles. The mass spectrometry intensities for the extracted samples are estimated to be an approximate ratio of ~ 1000:1 D-vasopressin to L-vasopressin, which is consistent with the reported K_D values for the aptamer. Additionally Figure 4-1 B, the before extraction and after extraction spectra indicated that the aptamer binds and extracts only the disulfide bridge containing peptide. For this experiment, the original sample solution contained both the oxidized and reduced forms of D-vasopressin, and after treatment and extraction of the sample with the nanoparticles the only oxidized peptide remained. This leads to the fact that the aptamer binds the tertiary structure of the target peptide and not the primary structure. Combining the selectivity of the aptamer conjugated magnetic nanoparticles with AP liquid MALDI analysis provides rapid analysis using by using magnetic extraction.

Conclusion

The use of nanoparticles has provided the development of a rapid analyte extraction technique for MS analysis. These silica-based nanoparticles act as a powerful scavenging agent for peptide molecules. The use of these functionalized particles with the liquid matrix allows for a rapid analysis procedure that limits analyte loss by direct insertion of the analyte bound nanoparticles. The C_{18} particles retained their chromatographic properties as evident through non-polar and polar washing procedures, and provided the extraction capability for a variety of peptide molecules.

The magnetic nanoparticles provided a simplified separation procedure through the use of magnetic extraction. These particles were functionalized with aptamers for a more selective analyte-nanoparticle interaction. The magnetic nanoparticles have the capability for wider

applications for the analysis of low abundance analytes. The aptamer conjugated nanoparticles allowed for the selective extraction of D-vasopressin, and the extraction of L-vasopressin was observed to the efficiency of the 1000:1 dissociation constant ratio for D-vasopressin to L-vasopressin.

CHAPTER 5
ANTIBODY-CONJUGATED MAGNETIC NANOPARTICLES FOR PROTEIN MICROARRAYS

Introduction

Biosensors have been development for target screening in clinical, environmental, water and food samples. The essential components of these systems are the recognition elements for selective identification of target analytes, which are typically antibodies. Antibodies have demonstrated high binding affinities with extraordinary selectivity for target molecules in complex sample matrices and at low target concentrations. The Array Biosensor developed at the Naval Research Laboratory (NRL) have been successfully used in increasingly more complex sample matrices for the detection of a variety of materials, such as protein toxins, organic molecules, biomarkers, viruses, and bacteria.[136-138] The two-dimensional nature of the sensing surface facilitates simultaneous analysis of multiple samples for multiple analytes. The immunoassays developed to date are rapid (15-25 min) and simple to perform, with little-if any sample pretreatment prior to analysis.

Much of the recent work in assay development with the NRL Array Biosensor has been concerned with the rapid detection of food-borne contaminants.[139-147] Limits-of-detection (LODs) obtained with the NRL Array Biosensor typically fall short of those for the desired analyte application or LODs obtained by the more complex-time consuming standard methodologies. However, the LODs for the NRL system are comparable to ELISAs and a number of other rapid biosensor-based technologies. One way to improve the current LODs obtained by the NRL Array Biosensor would be to include a target pre-concentration step prior to the immunoassay. In order to keep the detection method practical, these steps must minimally increase the overall assay time or demands on the operator.

One such preconcentration technique is immunomagnetic separation (IMS), this process is commonly used prior to detection. Magnetic particles have become increasingly popular for automated separations.[142,143] Commercially available magnetic particles are typically 1-2 μms in diameter and come with a variety of chemically active surfaces that can be used to functionalize the particle as desired. These magnetic particles have been used in immunoassays as solid supports for target biomolecule capture and concentration from complex sample matrices, such as clinical, environmental, and food samples. This process was performed to improve the sensitivity of the resulting assay. Target binding to the antibody coated magnetic particles is usually performed in solution, and the sample is concentrated, and the target measured using a method independent of the magnetic particles while generally still bound to the magnetic particles.

Methods commonly used for the quantification of particle treated samples are performed independently of the magnetic particles. These analysis techniques include culture followed by flow cytometry analysis,[150] PCR coupled with hybridization studies,[151] or enzyme-linked immunosorbent assays (ELISAs). For fluorescence-based measurements, quantification of the resulting fluorescent immunomagnetic-target complex is achieved using simple solution-based fluorescence microplate reader [152-154] or flow cytometry.[150,155-157] In the highlighted studies, the target remains bound to the magnetic particle during analysis, and additional steps are required to include fluorescently labeled primary or secondary antibodies for detection. The magnetic particles have also been measured using fluorescence microscopy,[158,159] and spotted onto protein binding membranes with capillary blotting techniques and the fluorescence from the resulting membrane were measured using a near IR sensitive photon counting system.[160] Magnetic beads were coupled with ELISAs and detection of the target obtained by optical or electrochemical

methods.[161-163] In one study, immunomagnetic separation coupled with PCR and ELISA detection gave LODs at 20 cfu/ml for Mycobacterium in milk.[161]

In less common applications, researchers have used the properties of the magnetic particles themselves to determine the presence of the bound target. For example, giant magnetoresistive (GMR) sensors were used to quantify DNA hybridization,[166] while an electromagnet has been used to read immunoassay sensor chips.[164] Additionally, a superconducting quantum interference device (SQUID) was developed to monitor biotin-avidin binding by measuring the magnetic moments.[165]

Advances in microfluidics and integrated technologies have resulted in the use of magnetic particles coupled with planar surfaces.[161,164,166,167] Magnetically-assisted transport evanescent field fluoroimmunoassay (MATEFFs) demonstrated that magnetic beads functionalized with a fluorescence sandwich immunoassay complex could be transported into the region of an evanescent field for detection using an external magnetic field.[168] A number of methods for interacting antibody-labeled magnetic particles with protein microarrays have been investigated, where magnetic brushing, magnetic scanning, and a push/pull method were used. In these methods, a magnet was used below the substrate to concentrate the beads to the surface and a magnet above the substrate to remove weakly bound or non-specifically bound magnetic particles.[169]

To date, there have been few studies investigating the direct interaction of magnetic particles with protein microarrays. This may be in part due to the relatively large size of the commercial magnetic particles used in most studies. The binding of large antigen-antibody-magnetic particle complexes to an antibody immobilized on a sensor surface is subject to shearing in the flow conditions normally used in immunoassays. One way to address this

problem is to decrease the size of the magnetic particles used. Nano-sized magnetite particles enveloped in lipid membranes, have been used in a number of studies.[170-172] Modifiable iron oxide-based magnetic nanoparticles have also been synthesized with a well defined size and monodispersity.[75,173-175]

Magnetic nanoparticles are starting to be used in ELISAs,[163] but to date have not been coupled with protein microarrays. The work presented here represents a proof-of-concept approach for exploiting magnetic nanoparticles (MNPs) for sensitive multiplexed immunoassays. Unlike the previously mentioned MATEFFs, this technique does not use the magnetic nanoparticles (MNPs) as the delivery method for localization of the target to the evanescent field sensing surface, but instead uses target recognition by surface-bound antibodies to localize the particles for signal generation in microarrays. These MNPs were coated with fluorescent labeled antibodies for signal generation. The ultimate goal is to use these magnetic nanoparticles to preconcentrate target analytes to allow simplification for subsequent detection with the aim of improving assay sensitivity without sacrificing ease of operation. For initial optimization and proof-of-concept, a simple direct-binding assay system was studied. MNPs were functionalized with target chicken IgG fluorescently labeled with Alexafluor 647 (Alex647-chick-MNPs), and the resulting particles were passed over sensor surfaces patterned with rabbit-anti-chick IgG. Assay performance was optimized by evaluating the MNPs surface composition, chick IgG conjugation conditions, the extraction time for concentration experiments and increased MNP concentration after extraction. Detection signals were generated directly by binding of the fluorescent MNPs to the slide surface.

Experimental

Materials and Methods

Unless otherwise specified, chemicals were of reagent grade and used as received. All materials, such as tetraethoxyorthosilicate (TEOS) and 2-(N-morpholino)ethane sulphonic acid (MES), were purchased from Sigma-Aldrich (St. Louis, MO) unless otherwise noted. Poly(dimethyl)siloxane (PDMS), used for making the assay flow cells, was obtained from Nusil Silicone Technology (Carpinteria, CA). Borosilicate glass slides from Daigger & Co. Inc. (Vernon Hills, IL) were used as slides in all the assays described. The 3-mercaptopropyl trimethoxy silane (MTS) and N-(γ-maleimidobutyryloxy) succinimide ester (GMBS) were purchased from Fluka Chemical Co. (St. Louis, MO). Carboxyethylsilanetriol sodium salt (Carboxy-silane) was purchased from Gelest, Inc. (Morrisville, PA). 1-Ethyl-3-[3-dimethylaminopropyl] carbodiimide hydrochloride (EDC), N-hydroxysuccinimide (NHS) and NeutrAvidin were purchased from Pierce Biotechnology, Inc. (Rockford, IL). Ammonium hydroxide was obtained from Fisher, Inc. The biotin-SP-conjugated rabbit anti-chicken IgY (Rb-anti-chick IgG) and chicken IgY (chick IgG) were purchased from Jackson ImmunoResearch (West Grove, PA). Fluorescent labeling of the chick IgG was achieved using succinimide ester-functionalized AlexaFluor647 (Alexa647), purchased from Molecular Probes (Eugene, OR).

Magnetic Nanoparticle (MNP) Synthesis

Iron oxide nanoparticles were synthesized by coprecipitating iron salts. Using a mechanical stirrer, ammonia hydroxide (2.5%) and iron chloride were mixed at 350 RPM for ten minutes, as described previously.[176] Briefly, the iron salt solution contained ferric chloride hexahydrate (0.5 M), ferrous chloride tetrahydrate (0.25 M), and HCl (0.33 M). The iron oxide nanoparticles were washed with water three times and ethanol once. The MNPs were dispersed

in an ethanol solution that contained ~1.2% ammonium hydroxide at a final concentration of ~7.5 mg/mL.

The magnetite core particles were coated with silica by adding 200 μL TEOS. The hydrolysis process was completed by sonicating for 90 minutes. Another aliquot of TEOS (10 μL) was added and sonication was continued for an additional 90 minutes. This additional TEOS step was used to post-coat the nanoparticles. The sample was again washed with ethanol three times. An 80 μL aliquot of the carboxy-silane was added to 1 mL of 10 mg/mL silica-coated MNPs in 10 mM PBS, pH 7.4 and continuously mixed for four hours. Finally, the particles were washed three times with 10 mM PBS and stored at room temperature until used.

Dye Labeling of Chick IgG

AlexaFluor labeling of the chick IgG prior to attachment to the MNPs was carried out according to the procedure of Anderson et al.[178] Labeled antibodies were separated from unincorporated dye using size exclusion chromatography (BioGel P10). Protein-to-dye ratios were determined using UV-Visible spectroscopy.

Optimized IgG Protocol

A 250 μL solution of 4 mg/mL carboxyl-modified MNPs were washed three times with 250 μL aliquots of a 0.5 mM MES, pH 5.0 buffer. The protein, chick IgG, modification was carried out by adding 50 μL of a 20 mg/mL EDC solution to the washed particles and incubated for fifteen minutes. Next, 100μg of Alexa647-chick IgG with a 1-to-5 molar equivalent of a 5000 Da amine-PEG (polyethylene glycol) was added to the activated carboxyl particles. The solution was incubated for two hours with vortexing every 15-to-30 minutes. The MNPs were magnetically extracted and washed three times with 500 μL aliquots of 10 mM PBS buffer. After the third wash, the Alex647-chick-MNP complex was resuspended in 500 μL of 30 mM

hydroxylamine with 1% BSA in 10 mM PBS pH 7.4 buffer and incubated for thirty minutes. Finally the Alex647-chick-MNPs were washed three times and resuspended in 500 μL aliquots of 10 mM PBS with 0.05% Tween 20 and 0.1% BSA at pH 7.4. The final concentration of the MNPs was 2 mg/mL, and the samples were stored at 4 ˚C until used.

Slide Preparation, MNP Extraction, and Immunoassay

Microscope slides, used as waveguides, were cleaned by immersion in a 10% (w/v) KOH in 2-propanol for 30 min at room temperature, followed by rinsing with deionized water and drying with a nitrogen stream. The slides were immediately immersed in a toluene solution containing 2% MTS for 1 h under nitrogen. The silanized slides were then rinsed with toluene, dried with nitrogen and immediately immersed in 1 mM GMBS in absolute ethanol for 30 min at room temperature. The slides were rinsed with water and incubated in 25 μg/mL NeutrAvidin in PBS overnight at 4 ˚C before being washed in PBS and either used immediately for patterning or stored in PBS at 4 ˚C until required.

Patterning of the biotinylated Rb-anti-chick IgG (10 μg/mL) in PBS + 0.05 % Tween (PBST) was carried out using a 6-channel patterning PDMS flow cell clamped onto the NeutrAvidin functionalized slide surface and injecting the biotinylated capture antibody into 4 or 5 of the channels.[178] Biotinylated goat anti-mouse IgG (10 μg/mL in PBST) was introduced into the remaining channels for use as a negative control (C). The slides were then incubated overnight at 4 ˚C. After the flow cell channels were rinsed with 1 mL PBST, the slide was removed from the PDMS patterning template and placed in PBS blocking solution containing 1% casein. After ~1 h, the slides were rinsed with Milli-Q water and assembled in a 6- or 12-channel assay PDMS flow cell, with the flow channels orientated perpendicular to the stripes of immobilized biotinylated antibodies. Each channel was hooked up to an ISMATEC® multi-

channel pump (Cole-Parmer Instruments Company, Vernon Hills, IL) at one end (outlet) and syringe barrels (1 mL) were then attached at the opposite end (inlet), ready for the immunoassay.

The Alex647-chick-MNPs were first sonicated and vortexed briefly to resuspend the sample. The Alex647-chick-MNPs where then either directly diluted in 1mL of the PBS/0.1 % casein/0.05% deoxycholic acid (DOC) buffer for direct immunoassays or extraction studies. A typical extraction procedure involved diluting 200 μL of the stock Alex647-chick-MNPs in 10 mL PBS/0.1% casein/0.05% DOC. The samples were prepared for the assay as follows: 1mL of the diluted sample was kept for the assay and referred to as "As is". The "As is Ex" sample involved taking 1 mL of the diluted sample and extracting the MNPs using the Epindorf magnet. The liquid was removed and the Alex647-chick-MNPs resuspended in 1 mL of PBS/0.1% Casein/0.05% DOC (x 0 concentration). For the extracted and concentrated sample, referred to as "Ex", 6 x 1 mL of the diluted sample was extracted using the Epindorf magnet, the liquid was removed and the Alex647-chick-MNPs in each Epindorf resuspended in 0.2 mL of PBS/0.1% Casein/0.05% DOC before the contents of the 6 Epindorf tubes were combined (x5 concentration). This procedure was carried out the day before, and the samples stored at 4 °C, or the day of the flow cell surface assay. The samples were sonicated for either 1 min or 5 min (5 min was found to be optimal), prior to use.

The MNPs labeled with Alexa647-chick IgG, prepared as described above, were applied to each channel (0.8 mL) at a flow rate of 0.1 mL/min. The channels were then washed with 1 mL at 0.25 mL/min. The PDMS flow cell was removed, and the slide was washed with Milli-Q water, dried with nitrogen and imaged on the Array Biosensor.

Immunoassay Array Imaging and Analysis

The slides were imaged using a Peltier-cooled CCD camera, as previously been described.[179] Briefly, evanescent wave excitation of the surface-bound fluorescent species was achieved using a 635 nm, 12 mW diode laser (Lasermax, Rochester, NY). Light was launched into the end of the slide at an appropriate angle through a 1 cm focal length lens equipped with a line generator. The fluorescence emission was monitored at right angles to the planar surface. A two-dimensional graded index of refraction (GRIN) lens array (Nippon Sheetglass, Summerset, NJ) was used to image the fluorescent pattern onto the Peltier-cooled CCD camera (Spectra Source, Teleris, Westlake Village, CA).[84] Long-pass (Schott 0G-0665, Schott Glass, Duryea, PA) and band-pass filters (Corion S40-670-S, Franklin, MA) were mounted on the device scaffolding to eliminate excitation and scattered light prior to CCD imaging.

Data was acquired in the form of digital image files in Flexible Image Transport System (FITS) format. To analyze the images, a custom software application was written in LabWindows/CVI (National Instruments). The program creates a mask consisting of data squares (enclosing the areas where the capture antibody is patterned) and background rectangles which are located on either side of each data square. The average background value is subtracted from the average data square value, and net intensity value is calculated and imported into a Microsoft Excel file for data analysis.

Results and Discussion

The NRL Array Biosensor has demonstrated the rapid detection of a number of food-borne contaminants including bacterial cells, mycotoxins and bacterial protein toxins.[139-147] In an effort to improve the limits-of-detection (LODs) while maintaining a rapid assay time, immunomagnetic concentration of the targets with simultaneous fluorescent labeling for biosensor analysis was investigated. For initial optimization and proof-of-concept, the direct-

binding assay between Alex647-chick IgG functionalized MNPs and Rb-anti-chick IgG modified surfaces was studied.

Initial investigations with micron-sized magnetic particles demonstrated successful binding under static conditions with buffer containing casein (1%) and deoxycholic acid (DOC; 0.05%). However, the direct binding assay performed poorly under flow conditions and resulted in low signal intensities in the regions of the slide patterned with Rb-anti-chick IgG. This poor assay performance was probably due to the large diameter of the magnetic beads and the shear force they experience at the surface under flow conditions. To address this problem using magnetic microparticles, MNPs synthesized in-house were investigated. Silica coated iron oxide nanoparticles, were functionalized with carboxy-silane, and chick IgG was conjugated to the particles via EDC coupling chemistry. These particles were found to be ~65 nm in diameter. To generate a signal in the evanescent field of the NRL Array Biosensor, the chick IgG attached to the MNPs was labeled with Alexafluor 647 dye. The ratios were kept between 2-4 dyes molecules per chick IgG determined by UV-visible spectroscopy. This was done to ensure that free lysines were available for coupling to the MNP surface.

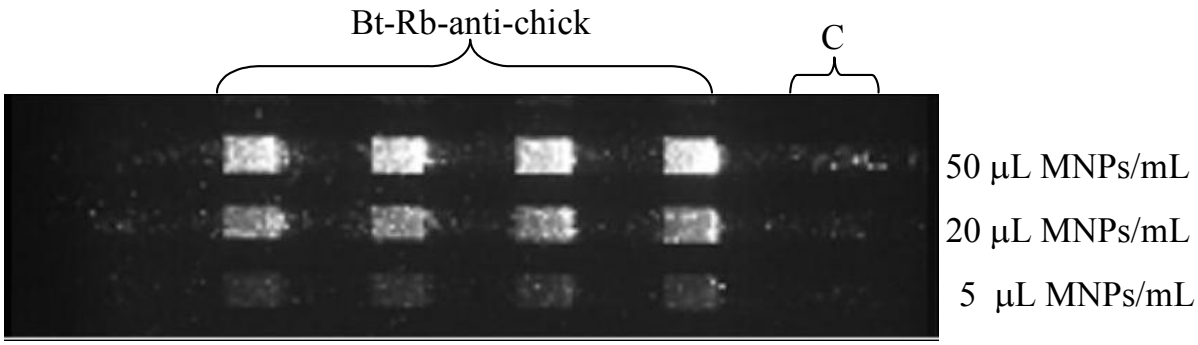

Figure 5-1. The fluorescence image of the immunoassay treated with Chick-MNP.

The EDC activated MNPs were initially exposed to a total of 350 μg Alexa647-chick IgG purified, and then 50, 20 or 5 μL of the stock was diluted in 1 mL of the running buffer (PBS/0.1

% casein/0.1% DOC) for assay studies. A Neutravidin slide was patterned with Rb-anti-chick IgG and blocked with a 1 % casein solution. The assay pattern was formed using a PDMS flow cell. The slide was then exposed to the purified-diluted Alex647-chick-MNPs at a flow rate of 0.1 mL/min. After washing with buffer, the flow cell was removed and the slide imaged on the NRL Array Biosensor. The CCD image of these initial assays is shown in Figure 5-1. Strong signals are found in the Rb-anti-chick IgG functionalized regions of the slide, which decrease in intensity with decreased concentration of the stock Alex647-chick-MNPs. No signal is observed in the control lane (C), demonstrating the specificity of the interaction. These experiments illustrate that these chick-MNPs work well under flow conditions. However, the non-uniform-speckled fluorescence signal observed in Figure 5-1 suggests that aggregation of the MNPs a still problem.

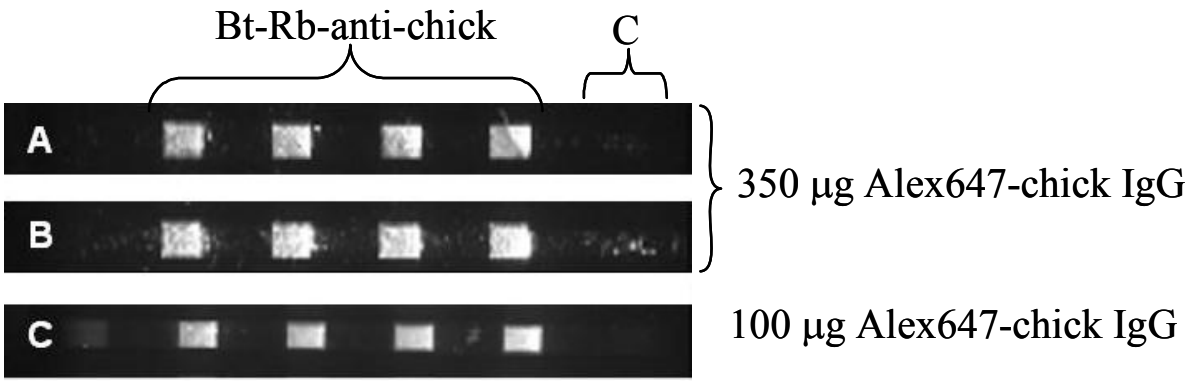

Figure 5-2. Fluorescence images of the immunoassay treated with Alex647-chick-MNPs run under various parameters. A) Magnetic nanoparticles exposed to 350 μg Alex647-chick IgG; assay buffer PBS/0.1 % Casein/0.1% Tween-20. B) Magnetic nanoparticles exposed to 350 μg Alex647-chick IgG; assay buffer PBS/0.1 % Casein/0.1% DOC. C) Magnetic nanoparticles exposed to 100 μg Alex647-chick IgG; assay buffer PBS/0.1 % Casein/0.05% DOC.

To address aggregation, a number of parameters were investigated including, changing the assay buffer conditions, the amount of Alexa647-chick IgG the MNPs were exposed to, and the density of carboxy-groups present on the surface of the MNPs (Figures 5-2 and 5-3). Chick-

MNPs made using 350 μg Alex647-chick IgG were diluted 50 μL/1 mL in PBS/0.1% casein containing either 0.1% Tween (Figure 5-2 A) or 0.1% DOC (Figure 5-2 B), and passed over a rabbit-anti-chick IgG patterned slide. Changing the surfactant does not eliminate the speckled fluorescence signal observed in the CCD images.

However, when the amount of Alexa647-chick IgG exposed to the EDC activated MNPs was reduced from 350 μg to 100 μg (Figure 5-2 A versus 5-2 C), the resulting fluorescence signal is much more uniform in intensity within individual data squares, suggesting less aggregation of the chick-MNPs. The percentage of carboxy-groups (COOH) present on the surface of the MNPs was also investigated. The silica coated MNPs surface was exposed to silane solutions containing 100, 75, 50 or 25 % COOH groups with the remainder of the solution consisting of silane containing the EDC-unreactive $–PO_2^-$ group. Either 350 μg or 100 μg of Alex647-chick IgG was exposed to the MNPs in the presence of EDC. The purified Alex647-chick-MNPs were then diluted 150 μL in 1 mL PBS/0.1% casein/0.05% DOC, and 0.8 mL of this solution were passed over an antibody-functionalized surface at a flow rate of 0.1 mL/min. The resultant bar graph (Figure 5-3) shows the relative intensity of the purified chick-MNPs, fabricated using 350 μg (black) or 100 μg (gray) of Alex647-chick IgG captured by the surface as a function of their solution exposed COOH groups.

As seen in the figure as the % COOH decreases, so does the final intensity reached in the Rb-anti-chick IgG functionalized squares. However in the case of the MNPs exposed to 350 μg of the Alex647-chick IgG, the decreased COOH concentration did not decrease the speckled nature of the fluorescence signal observed in the images, which suggests the aggregation was still present. As observed previously, only reduction of the exposed Alex647-chick IgG amount from 350 μg to 100 μg seemed to improve the uniformity of the fluorescence signal.

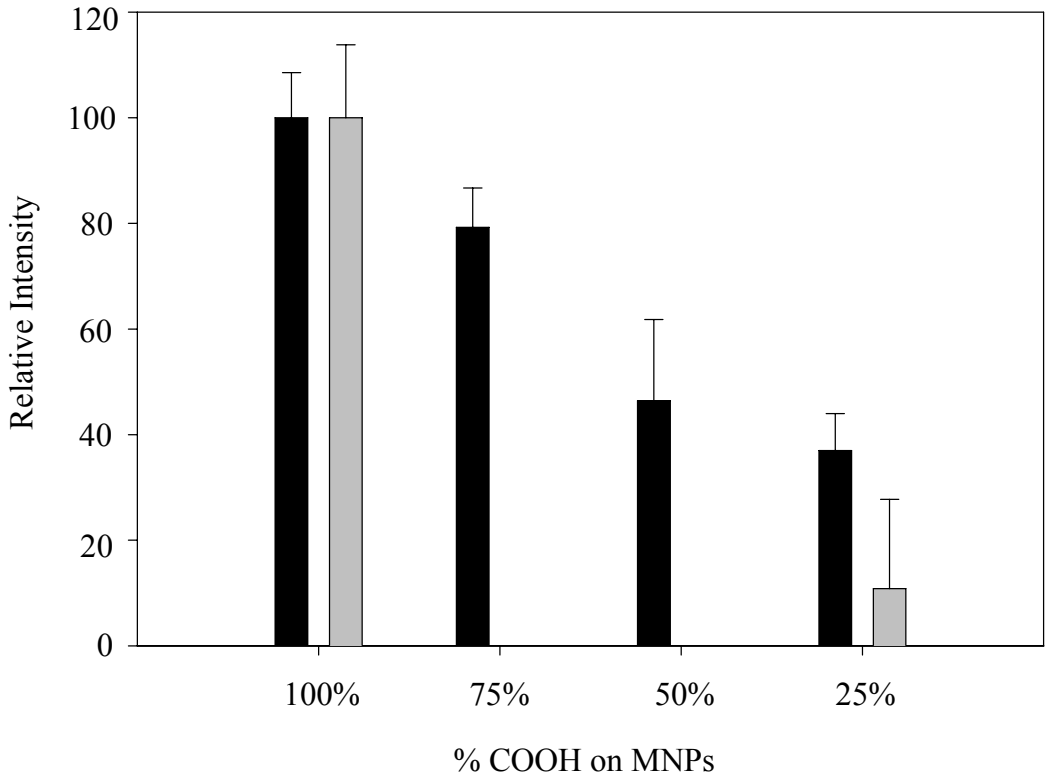

Figure 5-3. The fluorescence data showing the effect of the % COOH terminated silane used to modify the surface of the MNPs. Fluorescent signals are measured as the net intensity in the CCD image and normalized relative to 100% COOH Alex647-chick-MNPs. Error bars represent the standard deviation in net intensity values obtained from a minimum of 4 squares.

The effect of the EDC exposure method used to attach 100 μg of Alex647-chick IgG on the surface of 100% COOH MNPs was also investigated. In this study, the EDC was not removed from the MNP solution prior to the addition of the Alex647-chick IgG (referred to as method a). Since the protein chick-IgG contains both -COOH and -NH_2 groups, it is likely that multilayers of Alex647-chick IgG are formed on the MNP surface. To investigate the effect of the EDC method on the amount of Alex647-chick IgG attached to the surface of the MNPs, five different procedures were investigated and summarized in Table 5-1.

Table 5-1. EDC protocols investigated for MNP modification with Alex647-chick IgG.

EDC exposure method	EDC MNP activation procedure prior to Alex647-chick IgG addition
EDC a	EDC/ resuspend in IgG solution.
EDC b	EDC/ collect magnet/ resuspend in IgG solution.
EDC c	EDC/ collect magnet/ PBS or MES wash/ collect magnet/ resuspend in IgG solution.
EDC d	EDC + NHS/ collect magnet/ PBS wash/ collect magnet/ resuspend in IgG solution.
EDC e	EDC [x5]/ collect magnet/ MES wash/ collect magnet/ resuspend in IgG solution.

The purified Alex647-chick-MNPs were then diluted 100 μL in 1 mL PBS/0.1% casein/0.05% DOC and 0.8 mL of this solution passed over a Rb-anti-chick IgG functionalized surface at a flow rate of 0.1 mL/min. The resulting bar graph (Figure 5-4) shows the relative intensity of the Alex647-chick-MNPs prepared using the various EDC methods "a-e" captured by the rabbit-anti-chick IgG functionalized surface. The net intensities obtained from the images were normalized to the EDC a procedure, which produced the brightest fluorescence intensity on the slide surface. Slides 1 (black) and 2 (light gray) were washed with PBS for EDC-c, whereas Slide 3 (dark Gray) used an MES wash. As expected, the EDC-a procedure resulted in the brightest signals obtained from the Rb-anti-chick IgG functionalized regions. The EDC-b procedure included removal of the EDC prior to addition of the Alex647-chick IgG, and resulted in a significant decrease in the overall intensity of the MNPs. A further reduction in signal was observed in EDC-c, where the MNPs were washed with PBS to IgG exposure (compare the black bars EDC a-c). The EDC reactive intermediate was found to be more stable using a wash step at lower pH (MES 5.0-5.5 versus PBS pH 7.4) by comparing the EDC-c (black and dark gray bars) by the higher relative intensity observed from the CCD intensity.

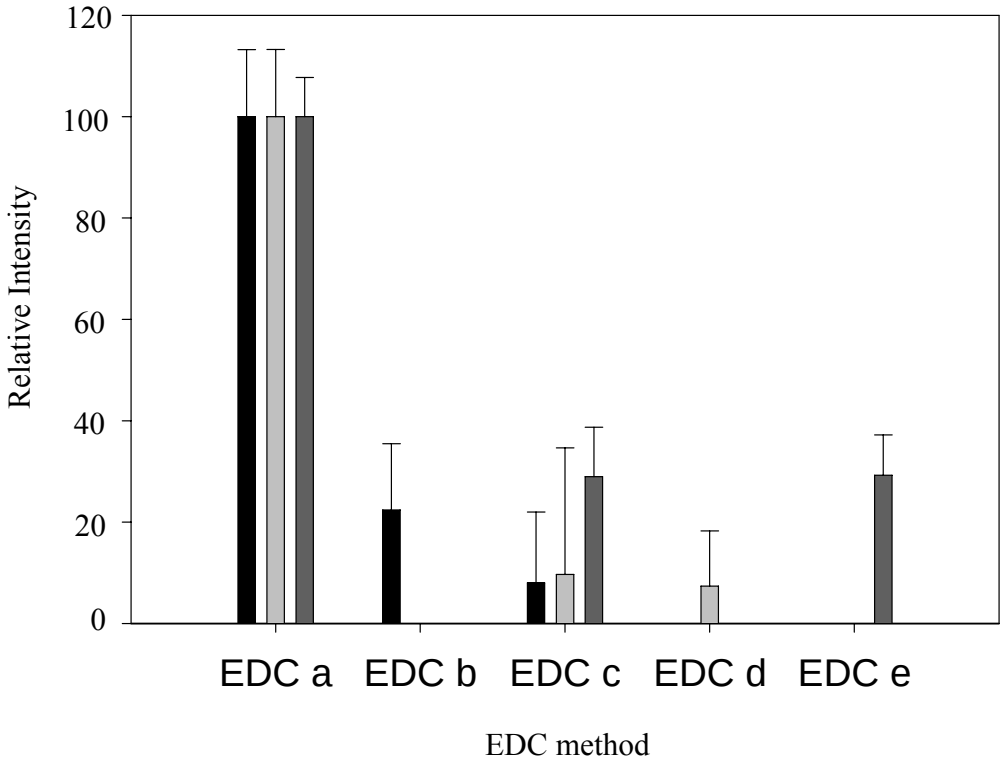

Figure 5-4. The fluorescence data obtained to determine the effect of the EDC exposure methods a-e.

Neither the addition of NHS EDC-d (light gray bar), which is reported to stabilize the reactive EDC intermediate or an excess of EDC as in method EDC-e (dark gray bar) seemed to increase the intensity of the signal obtained relative to procedure EDC-c. Solution UV-Visible absorption experiments also confirmed that more IgG was removed from the reaction solution when EDC-a versus EDC-c was used (data not shown). While EDC-a probably results in multilayers of Alexa647-chick IgG on the surface of the MNP, it also produces the brightest fluorescence signals. Therefore EDC-a, along with the addition of 100 μg Alexa647-chick IgG to the EDC activated MNPs was chosen as the optimized protocol.

The next step was to investigate the extraction and concentration procedures of the Alex647-Chick-MNPs to determine their performance in the direct immunoassays. Alex647-Chick-MNPs were diluted 150 μL in 10 mL PBS/0.1% casein/0.05% DOC. The Alex647-

Chick-MNPs were extracted from 1 mL of sample for 3, 7, 15, or 30 min using an Epindorf magnet, which can hold up to 6 x 1.5 mL Epindorf tubes. The liquid was then removed and the Alex647-chick-MNPs resuspended in 0.5 mL of PBS/0.1% casein/0.05% DOC, which is a potential concentration factor of 2. The extracted Alex647-Chick-MNPs and a portion of the pre-extraction sample (both 0.5 mL) were passed over an antibody patterned surface at a flow rate of 0.1 mL/min. The resulting bar graph (Figure 5-5) shows the relative signal intensity of the Alex647-chick-MNPs obtained from the CCD image as a function of the extraction time. These intensities were normalized to the pre-extraction sample. Relative signal intensity versus extraction time suggests that 15 min extractions were optimal for the extraction procedure.

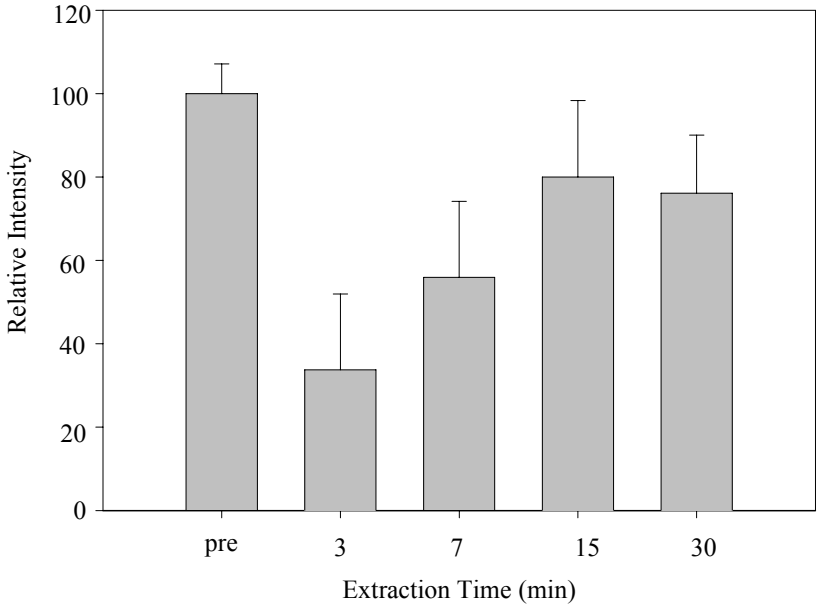

Figure 5-5. The effect of the extraction time used to collect the Chick-MNPs on the final signal intensity obtained from the CCD image. The resulting bar graph shows the relative intensity, normalized to the pre-extracted sample, of the Chick-MNPs captured by the Rb-anti-chicken IgG functionalized surface as a function of their extraction time.

However, Figure 5-5 demonstrates that although the Alex647-Chick-MNPs were concentrated by factor of two, this did not translate to an increased intensity from the CCD array biosensor image for the concentrated samples. In fact, the data suggests that the intensities are

slightly lower than the original sample (PRE). Sonication of the concentrated Alex647-chick-MNPs for 5 min versus the original 1 min gave a signal intensity improved up to a factor of ~2, which suggests that the drop in signal that is observed when the samples are extracted may be due to aggregation. Aggregation of the Alex647-chick-MNPs leads to larger particles, which may not be as effectively captured by the surface under the shear force of the flow conditions.

A number of extraction experiments were performed using the optimized Alex647-chick-MNPs with 5 min sonication prior to analysis by the immunoassay. Alex647-chick IgG (100 μg) was attached to the surface of 100% COOH modified MNPs using the EDC a method (no wash). The purified Alex647-chick-MNPs (200 μL) were then diluted into 10 mL PBS/0.1% casein/0.05% DOC. The samples were prepared for the assay as follows. The "As is" samples were simply 1 mL of the diluted sample kept for the assays. For the "Ex" samples, 6 x 1 mL of the diluted sample was extracted using the Epindorf magnet for 15 min. The liquid was removed and the Alex647-Chick-MNPs in each Epindorf tube were resuspended in 0.2 mL of PBS/0.1% casein/0.05% DOC. The contents of the 6 Epindorf tubes were combined to give a 1 mL sample with a potential concentration factor of 5. After sonication for 5 min, 50 μl was diluted in 950 μl of milli Q water for both the "As is" and "Ex" samples for UV-Visible and fluorescence spectroscopy measurements.

Table 5-2, summarizes the relative ratio of the "Ex" versus the "As is" samples for solution and surface characterization for an average of five separately prepared batches of these Alex647-chick-MNPs. The UV-Visible measurements at 400 nm demonstrates an increase in the amount of MNPs in solution following extraction, the solution fluorescence at 650 nm illustrates a respective increase in concentration of Alexa647-chick-MNPs in solution, and the intensity taken from the CCD images from the rabbit-anti-chicken IgG functionalized regions following the

immunoassay demonstrated the effectiveness of capture of the extracted Alex647-Chick-MNPs. As shown in Table 5-2, both the solution absorbance and the fluorescence data show an increase in intensity following extraction. This demonstrates that the MNPs were collected and concentrated using the magnet.

Table 5-2. The solution and surface measurements used to characterize the Alex647-chick-MNP samples pre and post extraction.

Chick-MNP sample	# of batches	Solution absorbance	Solution fluorescence emission	Surface fluorescence
MNP	5	3.0 ± 0.3	2.3 ± 0.3	1.2 ± 0.4
MNP overnight	2	2.9 ± 0.6	2.1 ± 0.6	1.6 ± 0.5
5A:1P PEG A	1	3.0	1.6	0.9
1A:1P PEG A	3	4.0 ± 0.4	2.4 ± 0.4	1.3 ± 0.4
1A:5P PEG A	2	4.5 ± 0.5	2.6 ± 0.4	1.5 ± 0.1
1A:10P PEG A	1	4.3	1.9	0.6
5A:1P PEG B	1	2.8	1.4	0.6
1A:1P PEG B	1	3.6	2.4	1.0
1A:5P PEG B	1	3.7	2.0	0.9

However, this did not translate to an increase in CCD fluorescence signal generated from the immunoassay captured Alex647-Chick-MNPs. This is likely a result of MNP aggregation that leads to larger particles which may not be as effectively captured by the surface. Note that this observation was also noted for samples prepared using the EDC-c method. Therefore, the potential for multilayers of chicken IgG on the surface of the MNPs causing these observations can be eliminated as the possible reason.

To determine if this lower than expected increase in CCD fluorescence signal was a result of the extraction or the concentration of the MNPs, an extra control was included in the immunoassay called the “As is Ex” sample. Here, 1 mL of the diluted sample was extracted using the Epindorf magnet, the liquid was removed, and the Alex647-chick-MNPs resuspended

in 1 mL of PBS/0.1% Casein/0.05% DOC. This means the sample was extracted, but not concentrated. While the absorbance measurements suggested that the concentration of the chick-MNPs in the solutions "As is" and "As is Ex" were the same, both the solution fluorescence and surface intensity taken from the CCD image suggest a drop in the fluorescence for the chick-MNPs following extraction. This is seen by the lower half of Figure 5-6 of the CCD image. This suggests that the extraction process itself is affecting the fluorescence from the MNPs in some manner. Aggregation of the Alex647-chick-MNPs may produce particles that are too large to remain bound to the surface due to the shear force that occurs at the surface under the flow conditions of the assay, which may explain the decrease in signal from the surface.

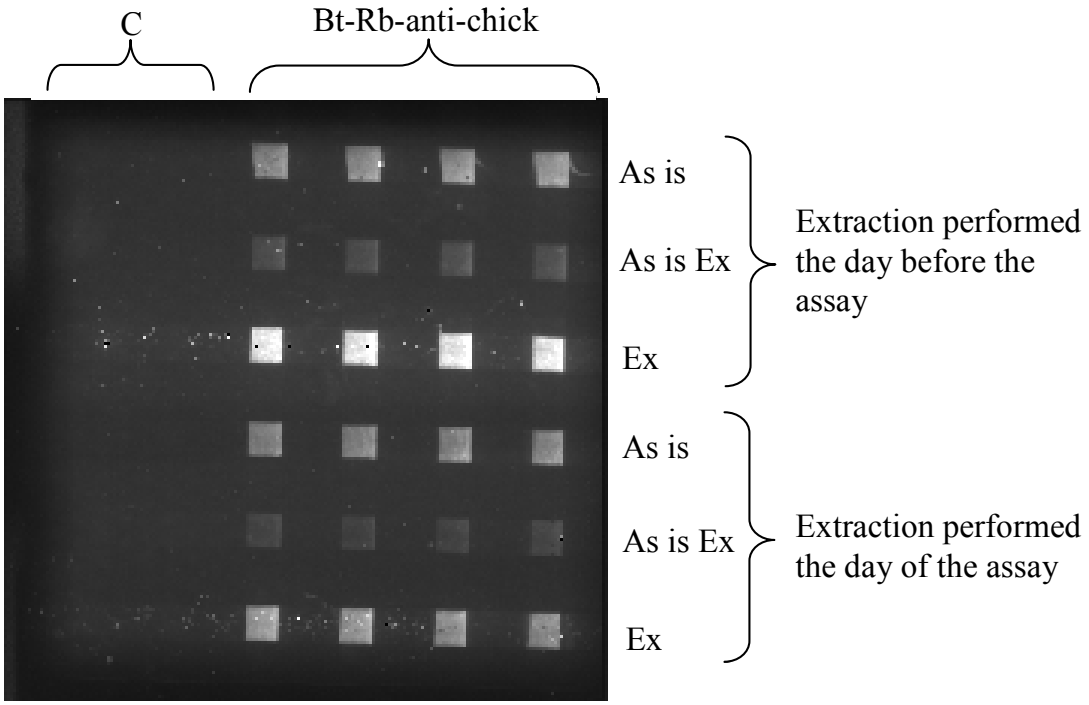

Figure 5-6. Fluorescence image displaying the effect of the time from extraction procedure to time the assay was preformed.

Additionally after extraction, the samples were allowed to sit overnight in the fridge before the analysis on the immunoassay. A significant increase of nearly double the fluorescent signal obtained from the CCD image of the surface was observed. The MNP overnight samples are

displayed in Figure 5-6 and Table 5-2. This would suggest that if MNP aggregation was the cause of these lower signal intensities that it is at least partially reversible.

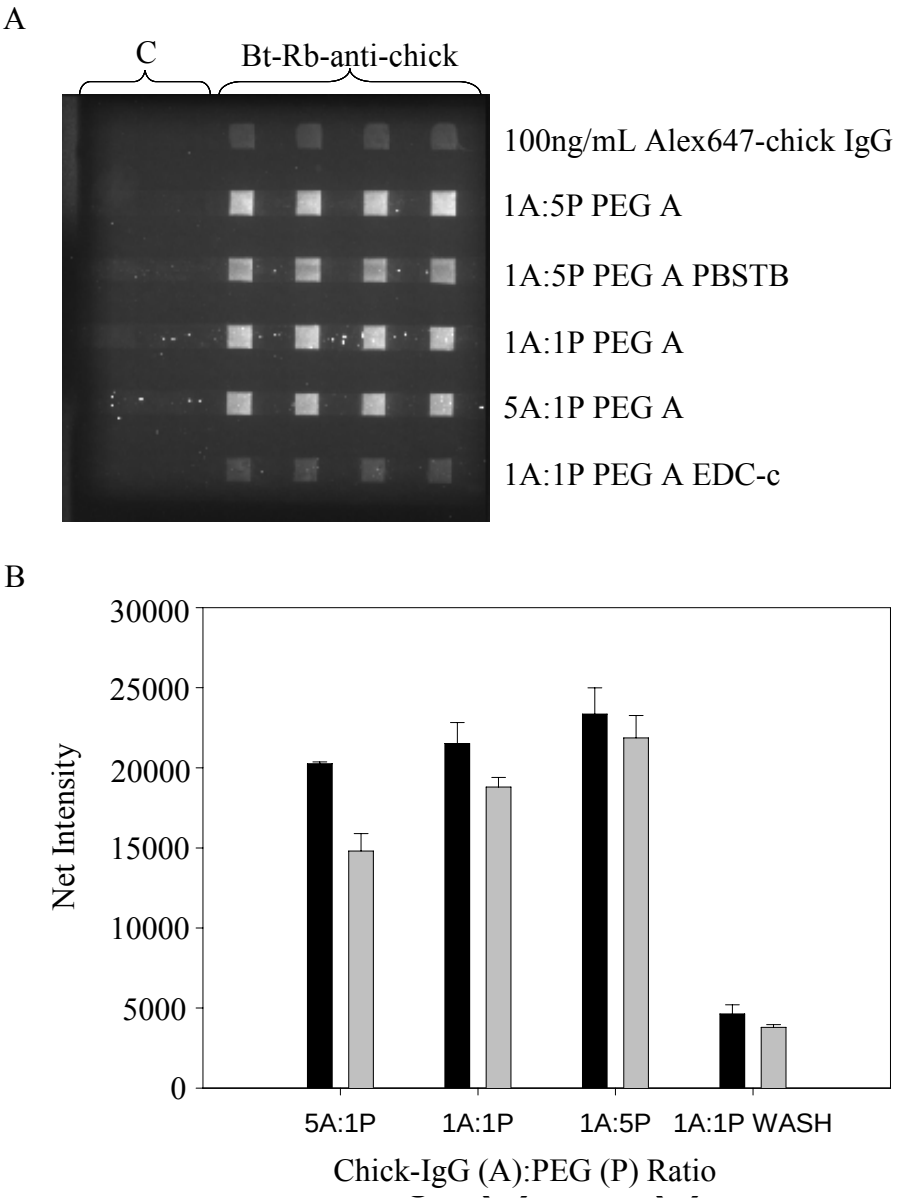

Figure 5-7. The fluorescence data obtained for the magnetic nanoparticles (MNPs) modified with Alex647-chick IgG and PEG molecules. A) The resulting fluorescence image for the different Alex647-chick IgG/PEG (MW 5000) modified MNPs. B) A bar graph of the net intensities taken from the fluorescence image of the different Alex647-chick IgG-MNPs, where the 5000 MW PEG samples are black and the 10,000 MW PEG B samples are gray.

The main issue with extracting and leaving samples overnight is that it is not conducive to the rapid analysis time expected for many applications. Furthermore, investigations involved the addition of PEG to the surface of the Alex647-chick-MNPs to determine if this would help prevent aggregation. Carboxy MNPs activated using either the EDC-a (no wash) or EDC-c (MES wash) protocols were simultaneously exposed to Alex647-chick IgG (100 μg), and either amine-PEG A (5,000 MW) or amine-PEG B (10,000 MW) at different mole ratios. Purified Alex647-chick-MNPs-PEG were then diluted 50 μL in 1 mL PBS/0.1% casein/0.05% DOC. The samples (0.8 mL) were passed over an antibody patterned surface at a flow rate of 0.1 mL/min. The resulting image for the different Alex647-chick IgG-PEG A or PEG B (PEG B image not displayed) modified MNPs are shown in Figure 5-7 A. The bar graph (Figure 5-7 B) plots the net intensities taken from the CCD image for the different Alex647-chick-MNPs modified with either PEG A (black) or PEG B (Gray) molecules. As illustrated in Figure 5-7 B, the smaller PEG A modified Alex647-Chick-MNPs produces slightly stronger fluorescent signals from the CCD image than the corresponding ratio of PEG B modified Alex647-Chick-MNPs. For both PEG molecules, the fluorescence intensity increases slightly with increasing PEG ratios.

Data from the extraction experiments are summarized in Table 5-2 for both the solution and surface characterization. The extraction experiments with Alex647-chick-MNPs modified with the smaller of the amine-PEG molecules (PEG A = 5,000 MW) showed promising data. The Alex647-chick-MNPs modified with PEG A at a ratio of 1 chick IgG:5 PEG A molecules provided a similar enhancement in CCD fluorescent signal in less time than the regular Alex647-Chick-MNPs extracted and left overnight.

Conclusion

The use of MNPs for target preconcentration and signal generation in biosensor assays performed under flow conditions was demonstrated in a direct binding assay format. The

optimal conditions for synthesizing the MNPs were determined by exploring the surface composition, antibody immobilization procedures, and various blocking buffers. In addition to investigating the MNP synthesis, the best extraction time and method for introducing the concentrated MNPs to the biosensor were ascertained. However, the magnetic concentration process had an adverse effect on the modified MNPs, and further study into nanoparticle surface treatment was performed by adding PEG polymers along with the antibody during the immobilization step.

Using MNPs in conjunction with sensing, under flow has not been previously demonstrated. MNPs were essential to this work mainly due to their small size, which reduced the shearing effect of the fluid flow on the surface bound particles compared to standard magnetic particles. By including the MNPs in the assay instead of removing the bound target or requiring the addition of a secondary fluorescent species minimized the number of steps in the assay and reduces the chance of losing the target analyte. Furthermore, little time is added to the overall assay protocol and the target is concentrated prior to performing the analysis. The next step will be to demonstrate sandwich assays where the analyte is pulled out of solution by MNPs coated with fluorescent antibodies and concentrated prior to biosensor analysis.

CHAPTER 6
APTAMER-CONJUGATED SILICA NANOPARTICLES FOR CANCER CELL EXTRACTION AND DETECTION

Introduction

The need for accurate-sensitive diagnosis and understanding of human diseases at the molecular level has been limited by the lack of probes available to recognize the distinct molecular features of diseases. Diseases like cancer originate due to mutations and alterations at the genetic level. These changes cause the infected cells to behave differently at the molecular level, which can facilitate the effective treatment programs implemented by clinicians. Determining the molecular characteristics of cancers, particularly knowing the characteristic biomarkers associated with a specific cancer can be of great benefit. These differences contain significant potential for aiding the understanding of diseases based on the biological processes and mechanisms, which are vital for disease diagnosis, prevention, and treatment. The detection of leukemia uses standard analysis methods for bone marrow and peripheral blood cytochemicals by karyotyping,[180] immunophenotyping,[181] microarrays,[182] and amplification mutated genes by PCR.[183]

Immunophenotypic analyses uses antibody recognition elements commonly labeled with fluorescent dye molecules to differentiate disease cells from healthy cells by profiling with a panel of antibodies. The major limitations of this method are the lack of sensitivity and it is subject to false positive results. In addition, antibody integrity is continually in question due to the lifetime of the sources needed to obtain a reliable antibody.

PCR based methods are highly sensitive analysis techniques for cellular recognition by amplifying low copy numbers of critical gene mutations.[183-185] This technique requires complex-lengthy sample preparation procedures for analysis to be performed. In addition, PCR is limited by inconsistent sensitivities. These limitations result in false-negative results especially in

samples with low-level signals even after amplification.[183] Therefore, a need to develop new technologies for rapid-simple cell detection is of great interest.

Aptamer-conjugated nanoparticles (ACNPs) were used for the rapid extraction and detection of acute leukemia cells using high-affinity DNA aptamers for recognition. Aptamers form complex three-dimensional structures creating hydrophobic, hydrophilic, and electrostatic interactions for distinct target binding recognition. These recognition molecules were selected using intact cultured tumor cells through the process of cell-SELEX.[186] The aptamer oligonucleotides used here were selective for CCRF-CEM acute leukemia (CEM), Burkitt's lymphoma (Ramos), and non-Hodgkin's B cell lymphoma (Toledo). The sequences were attached to magnetic nanoparticles (MNPs) and fluorescent nanoparticles (FNPs) to act as the solid platform to collect and detect the respective intact cancer cells from simple buffer and biologically complex samples.

Combining the selectivity of aptamers with the power of MNP based separation has produced a selective and sensitive method for collecting, enriching, and subsequently detecting targets. In this work, the aptamers were attached to three spectrally different FNPs to provide enhanced signaling. Fluorophore doped silica nanoparticles (NPs) have been used to increase signals and ease for bioconjugation compared to single dye molecules.[73,187,188] Using the functional groups on the particle surface has proven useful for oligonucleotide detection,[73,189] protein, and antigen detection.[189-192] Each NP contains thousands of dye molecules, and provide increased signal for every cell binding event through the aptamer recognition.

Aptamer-conjugated MNP based cell sorting was employed in this work for the selective isolation of target cells. However, magnetic based cell collection has been used for the enrichment of a number of different cell types from a variety of species.[193-198] These methods

used micrometer-sized magnetic particles, where the magnetic particles studied here were 65 nm silica coated MNPs. The small size of these particles provide surface area to volume ratios, which provide enhanced extraction capabilities compared to the microspheres.[74] Magnetic extraction reduces the need for complex presample clean-up by removing FNP aggregates and any material not associated with the magnetic nanoparticles.

Fluorescence based imaging, flow cytometry, and a microplate reader spectrometer were used to detect the extracted cell samples by the ACNP technique. Using FNPs and the three aptamers, allowed for the demonstration of this method for both inorganic and organic dye-doped silica NPs, and the multiple extraction of three different related cell lines from the same sample. This method demonstrates the ability to reproducibly extract target cells from complex mixtures and biological fluids establishing a foundation for the relevance of this method for clinical applications.

Experimental

Materials and Methods

All materials were purchased from Sigma-Aldrich (St. Louis, MO) unless otherwise noted. Fetal bovine serum (FBS) was obtained from Invitrogen (Carlsbad, CA). Whole blood samples were obtained from Research Blood Components, LLC (Brighton, MA). Fluo-4 was purchased from Molecular Probes (Eugene, OR). Carboxylethylsilanetriol sodium salt was purchased from Gelest, Inc. (Morrisville, PA). 1-Ethyl-3-[3-dimethylaminopropyl] carbodiimide Hydrochloride (EDC) was purchased from Pierce Biotechnology, Inc.(Rockford, IL) and ammonium hydroxide was obtained from Fisher Scientific (Fair Lawn, NJ). Cy5-NHS was purchased from Amersham Biosciences and Tetramethyl rhodamine succinimidyl ester (TMR SE) (mixed isomers) was purchased from Molecular Probes. Deoxyribonucleotides, 5`-amino-modifiers, and biotin phosphoramidite were purchased from Glen Research (Sterling, Va).

Fluorescent Nanoparticle Synthesis

Rubpy dye-doped nanoparticles (NPs) were synthesized by the reverse microemulsion method.[176] Briefly the NPs were synthesized by adding 1.77 mL Triton X-100, 7.5 mL cyclohexane, 1.6 mL n-hexanol to a 20 mL glass vial with continuous magnetic stirring. Next 400 μL of H_2O and 80 μL of 0.1M tris(2,2' –bipyridyl) dichlororuthenium (II) hexahydrate (Rubpy) dye (MW=748.63) were added. Followed by the addition of 100 μL tetraethyl orthosilicate (TEOS) the materials stirred for thirty minutes of stirring. To initiate silica polymerization, 60μL NH_4OH was added. After 18 hours, a post-coating of carboxyl modified silica was performed by adding 50 μL TEOS and 50 μL carboxylethylsilanetriol sodium salt. This polymerization was allowed to proceed for 18 hours. The particles were centrifuged, sonicated, and vortexed four times with 10 mL aliquots of fresh 95% ethanol, followed by a wash with a 10 mL aliquot of H_2O. Each wash step was performed from the addition of fresh ethanol or H_2O with sonication and vortexing to the next centrifugation step typically within 3-5 minutes. The DNA modification was carried out by adding 1.2 mg EDC, 0.5 nmoles DNA, and 2 mg of particles to 1.5 mL of 10 mM MES buffer (pH= 5.5). The solution was vortexed for three and a half hours. Particles were washed by centrifuging at 14000 rpm and dispersing in 200 μL of 0.1 M Phosphate Buffered Saline (PBS) (pH=7.2) three times. Rubpy NPs were stored at 4º C and dispersed in cell media buffer at a final concentration of ~10 mg/mL.

Tetramethylrhodamine (TMR SE) and Cy5 doped NPs were synthesized according to the following: TMR SE and Cy5-NHS were each dissolved in DMSO at a concentration of 5 mg/mL and 3-Aminopropyltriethoxysilane (APTS) was added at a molar ratio of 1.2:1 APTS:dye. The APTS was allowed to conjugate to the amine reactive dye for 24 hours in the dark with shaking prior to synthesis of the particles. Glass reaction vessels and Teflon coated

magnetic stir rods were washed with 1M NaOH solution for 30 minutes, rinsed with DI water and ethanol, and allowed to dry. This wash step was performed to clean the glass vessel and stir rods and smooth the inside surface of the glass vessel which prevents unwanted seeding and NP formation. After conjugation, 4.19 mL of ethanol was mixed with 239 μL of ammonium hydroxide solution in the reaction vessel. 36 μL of TMR-APTS conjugate or 54 μL of Cy5-APTS conjugate were added to the reaction vessels, yielding 3.44×10^{-7} moles of dye per reaction (A ratio of 2300 moles of silica per mole of dye). 177 μL of TEOS was added rapidly to the reaction mixture and the vessels were sealed. The reaction was allowed to proceed for 48 hours in the dark before the particles were recovered by centrifugation at 14000 rpm. The particles were washed three times with phosphate buffer to remove any dye molecules that are weakly bound. The synthesis method was found to reproducibly produce a number average particle size of 50 nm ± 5 nm with a mono-modal distribution when measured with a Honeywell UPA 150 dynamic light scattering instrument.

To modify with carboxy groups with these NPs, a 2mg solution of NPs were diluted in 200 μL of 10 mM PBS, pH 7.4, and 40 μL of the carboxyl silane were continuously mixed for four hours. The NPs were washed three times and resuspended in 200 μL aliquots of 10 mM PBS by centrifuging at 14,000 RPM for fifteen minutes and stored at room temperature until use. DNA modification was completed as described above.

Magnetic Nanoparticle Synthesis

Iron oxide core MNPs[65] were synthesized by coprecipitating iron salts. A mechanical stirrer was used to mix ammonia hydroxide (2.5%) with an iron chloride solution at 350 RPM for ten minutes. The iron chloride solution contained ferric chloride hexahydrate (0.5 M), ferrous chloride tetrahydrate (0.25 M), and HCl (0.33 M). The iron oxide NPs were washed three times

with 5 mL aliquots of H_2O and once with a 5 mL aliquot of ethanol. Each wash was performed by decanting the supernatant, adding fresh wash solution, and redispersing in the fresh solution typically within 3-5 minutes. Next the iron oxide NPs were dispersed in an ethanol solution containing ~1.2% ammonium hydroxide at a final concentration of ~7.5 mg/mL.

The magnetite core particles were coated with silica by adding tetraethoxyorthosilicate (200 μL), and the mixture sonicated for 90 minutes to complete the hydrolysis process. An additional aliquot of TEOS (10 μL) was added and again sonicated for 90 minutes to add a post-coating to the NPs. The sample was washed three times with ethanol to remove excess reactants.

A solution of 0.1 mg/mL silica coated magnetic nanoparticles (MNPs) solution in 10 mM PBS, pH 7.4, and a 5 mg/mL avidin solution in 10 mM PBS, pH 7.4 were vortexed for 5-10 minutes to initiate an avidin coating. The resulting sample was incubated at 4° C for 12-14 hours. Next the particles were washed three times and dispersed at 1.2 mg/mL with 100 mM PBS. The avidin coating was stabilized by cross-linking the coated NPs with 1% glutaraldehyde (1 hour at 25º C). Again the particles were magnetically separated, washed three times, and dispersed in 1M Tris-HCl buffer. The samples was incubated in the 1M Tris-HCl buffer (3 hours at 4º C), followed by three additional washes with 20 mM Tris-HCl, 5 mM $MgCl_2$, pH 8.0 at a concentration of ~0.2 mg/mL.

Finally, the DNA was attached to the particles by adding biotinylated DNA (3 pmol) to a solution of 500 μL at 0.2 mg/mL in 20 mM Tris-HCl, 5 mM $MgCl_2$, pH 8.0 avidin coated MNPs. The attachment was performed at 4° C for 12 hours, and three final washes were performed using 20 mM Tris-HCl, 5 mM $MgCl_2$ at pH 8.0. The MNPs were stored at 4° C and used at a final concentration of ~0.5 mg/mL.

Magnetic Extraction

Two different magnetic extraction procedures were used, and each were performed by adding the specified amounts of MNPs to each sample as described in the experimental sections for the respective extraction procedures. For the initial studies, aptamer conjugated magnetic nanoparticles were then incubated with the target cells for 5 minutes unless specified otherwise. After the incubation period a magnetic field was applied to the side of the sample container. After a minute the non-magnetic materials were removed with a pasteur pipette and then fresh buffer was added and the magnetic field was removed. The materials were mixed in the buffer and previous steps were repeated for a total of three times to remove anything nonspecifically bound to the magnetic nanoparticles. For later extraction studies, the aptamer-conjugated MNPs were incubated with the cell samples for 15 min, a magnetic field was introduced to the sample container, and after 2-5 minutes the nonmagnetic materials were decanted using a pasteur pipette. To complete the wash process, the magnetic field was removed and the samples were redispersed in 200 μL fresh media buffer and this process was repeated three times.

Cells

CCRF-CEM cells (CCL-119 T-cell, human acute lymphoblastic leukemia), Ramos cells (CRL-1596, B-cell, human Burkitt's lymphoma), and Toledo cells (CRL-2631, non-Hodgkin's B cell lymphoma) were obtained from ATCC (American Type Culture Association). The cells were cultured in RPMI medium supplemented with 10% fetal bovine serum (FBS) and 100 IU/mL penicillin-Streptomycin. The cell density was determined using a hemocytometer, and this was performed prior to any experiments. After which, approximately one million cells dispersed in RPMI cell media buffer were centrifuged at 920 rpm for five minutes and redispersed in cell media three times, and were then redispersed in 1 mL cell media buffer. During all experiments, the cells were kept in an ice bath at 4° C.

DNA Aptamer Synthesis

The following aptamers have been selected for the CCRF-CEM, Ramos, and Toledo cells respectively, 5'-TTT AAA ATA CCA GCT TAT TCA ATT AGT CAC ACT TAG AGT TCT AGC TGC TGC GCC GCC GGG AAA ATA CTG TAC GGA TAG ATA GTA AGT GCA ATC T-3', 5'-AAC ACC GGG AGG ATA GTT CGG TGG CTG TTC AGG GTC TCC TCC CGG TG-3', and 5'- ATA CCA GCT TAT TCA ATT ATC GTG GGT CAC AGC AGC GGT TGT GAG GAA GAA AGG CGG ATA ACA GAT AAT AAG ATA GTA AGT GCA ATC T-3'. Both the amine and biotinylated versions of the aptamer sequencers were synthesized in-house. An ABI3400 DNA/RNA synthesizer (Applied Biosystems, Foster City, CA) was used for the synthesis of all DNA sequences. A ProStar HPLC (Varian, Walnut Creek, CA) with a C_{18} column (Econosil, 5u, 250×4.6 mm) from Alltech (Deerfield, IL) was used to purify all fabricated DNA. A Cary Bio-300 UV spectrometer (Varian, Walnut Creek, CA) was used to measure absorbances to quantify the manufactured sequences. All oligonucleotides were synthesized by solid-state phosphoramidite chemistry at a 1 μmol scale. The completed sequences were then deprotected in concentrated ammonia hydroxide at 65 ºC overnight and further purified twice with reverse phase high-pressure liquid chromatography (HPLC) on a C-18 column.

Sample Assays

To determine the extraction and detection capabilities in an artificial complex sample, equal amounts of CEM and Ramos cells were mixed and tested using the assay. Approximately 10^5 cells of each type were mixed, followed by magnetic and fluorescent nanoparticle incubation for five minutes. Magnetic extraction procedures were performed three times to remove

unbound cells. A 2 μL aliquot of the redispersed extracted sample was then imaged by confocal microscopy.

To show applicability in real biological samples, whole blood was spiked with 10^5 CEM cells. Fluorescent and magnetic nanoparticles were then incubated for five minutes with spiked and unspiked blood samples, followed by three magnetic extractions. Confocal imaging was then used to characterize cell extractions.

Collection efficiency was measured from pure cell samples and spiked blood samples. For efficiency studies, cell samples subjected to nanoparticle incubation and magnetic extractions were compared to samples not subjected to any separations by magnetic extraction. For pure cell analyses, 5 - 30μg of magnetic nanoparticles were individually incubated in 5μg increments with approximately 10^5 cells initially, and subjected to magnetic extractions after five minute incubation. The efficiency of cell extraction from the spiked blood sample was determined by incubating magnetic nanoparticles (30μg) with 500 μL whole blood spiked with 10^5 CEM cells. Cells were counted by flow cytometry for pure samples, and by imaging for blood samples. Various magnetic nanoparticle concentrations were used to determine maximum collection efficiency and optimal separation efficiency.

Cell Imaging

Fluorescence imaging was conducted with a confocal microscope setup consisting of an Olympus IX-81 inverted microscope with an Olympus Fluoview 500 confocal scanning system and three lasers, a tunable Argon Ion laser (458nm, 488nm, 514nm), a green HeNe laser (543nm), and a red HeNe laser (633nm) with three separate photomultiplier tubes (PMT) for detection. The cellular images were taken with a 10x objective. The Rubpy NPs were excited with 488nm line of the Argon ion laser and emission was detected using a 610nm long pass

filter. The TMR NPs were excited with the 543nm laser line and were detected with a 560-600nm band pass filter. The Cy5 NPs were excited with the 633nm laser line and the emission was detected with a 660nm long pass filter.

Flow Cytometry

Fluorescence measurements were also made using a FACScan cytometer (Becton Dickinson Immunocytometry Systems, San Jose, CA). To support imaging data, Rubpy fluorescence of pure samples initially containing 10^5 cells were measured by counting 30000 events. Cell experiments were performed exactly as stated for imaging experiments, except all solutions were diluted to a final volume of 200 μL. Cell sorting allowed for accurate quantitative analysis of cell samples, as well as a platform for collection efficiency determination.

Microplate Reader

All plate reader experiments were conducted with a Tecan Safire microplate reader with 384 well Corning small volume plates. The excitation and emission wavelength used were the same as those in the fluorescent imaging. For each experiment 20μL of the extracted cell solution was placed in the well and the fluorescence of the sample was measured immediately.

Magnetic Extraction and Labeling

To establish the extraction and detection capabilities of the method, equal amounts of cells in media were tested using the two NP approach. When using the CEM cells as the target the Ramos and Toledo cell types were used as the control (nontarget) cells, when the Ramos cells were used as the target the CEM and Toledo cell types were used as the control cells, and finally when using the Toledo cells as the target the CEM and Ramos cell types were used for the control experiments.

The extraction of the multiple individual cell types (CEM, Ramos, and Toledo) using their respective aptamer conjugated NPs was performed by the following procedure. Approximately

10^5 of each cell type were obtained in individual test tubes. To the cell samples, 5 μL of the MNP solution was added, and the mixture was incubated for 15 min. After incubation, the cells were washed by magnetic extraction with 200 μL of fresh cell media three times, and resuspended in 200 μL of the media buffer. The wash was performed by removal of the supernatant, addition of fresh buffer, and the sample resuspended in the fresh buffer typically with in 3-5 minutes. To complete the stepwise process, 2 μL of FNPs were added and incubated for 5 min. The concentration of MNPs to FNPs in the samples was 2:1. Again the sample was washed three times with 200 μL of cell media as described previously, and then dispersed in 20 μL of media for imaging and microplate reader analysis. The FNPs used to label the Ramos cells were doped with cy5, and the fluorescent dye doped in the NPs for Toledo and CEM cells were Rubpy and TMR, respectively. All pure cell samples contained 1.0×10^5-5.0×10^5 cells before NP incubation. The multiple cell type extraction procedure will be described in a later section.

For determining the detection limit, the extraction was performed by first determining the number of cells in 1 μL of stock cell solution. The total number of cells was counted. This process was repeated five times, the determined values were averaged, and extrapolated to obtain the number of cells per microliter. The cell samples were diluted to 200 μL with cell media accordingly. Next, cell samples were subjected to MNP incubations for 15 minutes followed by magnetic extraction and washing as described previously, and FNP incubations for 5 minutes with magnetic extraction and washing as described above. All cell samples were treated with MNPs and FNPs at a ratio of 2:1 using the stepwise format, and extracted samples were analyzed by the microplate reader.

Results and Discussion

Aptamer-Conjugated Nanoparticle Characterization

Collection efficiency

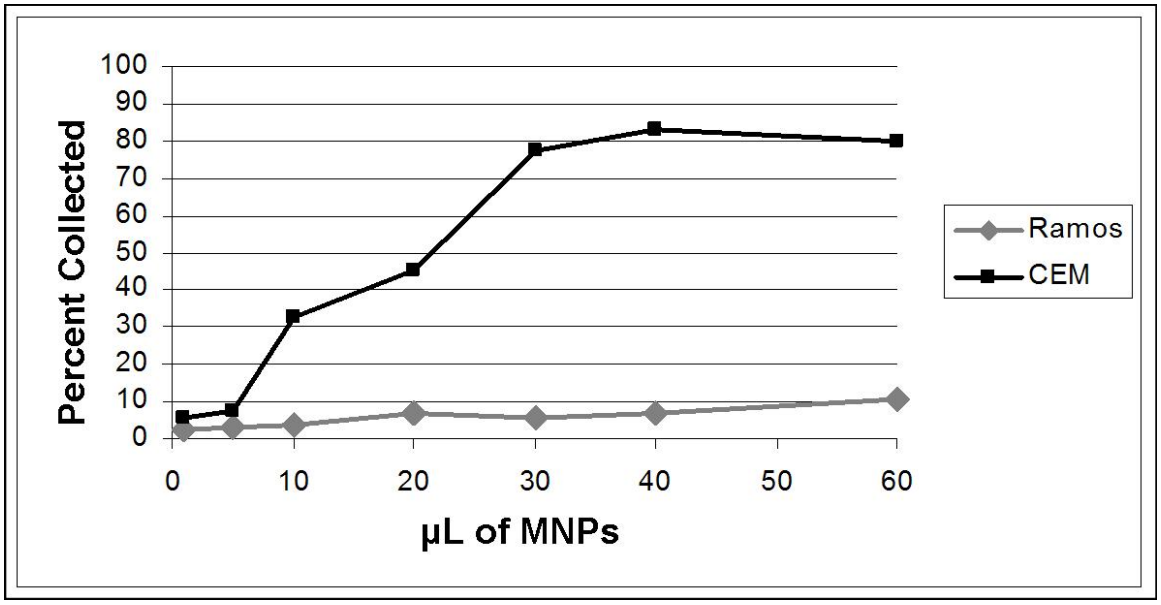

Figure 6-1. The flow cytometry determination of magnetic nanoparticle collection and separation efficiencies for target (CEM) and control (Ramos) cells.

The collection efficiency was obtained by incubating increasing amounts of magnetic nanoparticles (MNPs) with the CEM and Ramos cells. The samples were extracted and counted using the flow cytometry by the counting of signal events. A 200 µL aliquot of the target and control cell samples were counted before extraction, and these values were used as the reference cell amounts in each 200 µL volume. The collection efficiency was calculated by dividing the number of cells collected by the reference cell number. Figure 6-1 displays the collection efficiency of target (CEM) cells and control (Ramos) cells. The collection efficiencies for target cells increased from 30-80% and plateau at around 80%. The collection efficiencies for the control cells were no higher than 5% for the maximum amount of MNPs added. This data indicates that the CEM cells are preferably extracted with little nonselective extraction of the

control cells. The 10μL magnetic nanoparticle sample had the highest separation efficiency with minimal nonselectivity for that sample. Therefore, this amount of MNPs was used for the remainder of these experiments unless otherwise noted.

Dye and nanoparticle fluorescent intensity comparison

The increased fluorescent signals of the aptamer-conjugated Rubpy doped nanoparticles were compared to individual Rubpy dye molecules linked to the DNA aptamer. Equal concentrations of magnetic and Rubpy nanoparticles (0.5 nM) were incubated with the CEM cells, then washed by magnetic extraction with 500 μL media buffer three times, and redispersed in 20 μL buffer for imaging and 200 μL buffer for flow cytometric analysis. Figure 6-2 A and

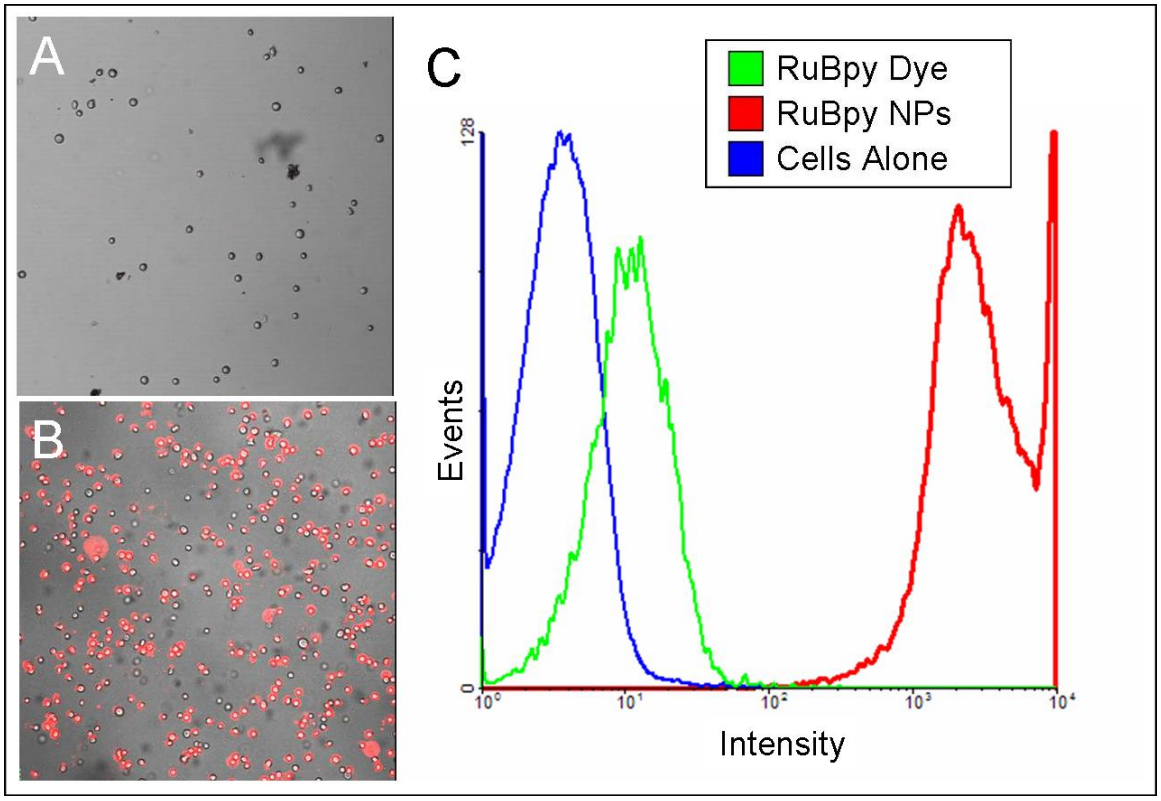

Figure 6-2. Fluorescence images and flow cytometry data of Rubpy dye and Rubpy doped nanoparticle treated cells. A) Magnetic nanoparticle extracted cells treated with 40 μM Rubpy dye-aptamer conjugates. B) Magnetic nanoparticle extracted cells treated with 0.5 nM Rubpy nanoparticle-aptamer conjugates. C) Flow cytometry comparison of dye labeled cells to nanoparticle labeled cells extracted using magnetic nanoparticles.

Figure 6-2 B show the extracted cell samples extractions labeled with fluorescent nanoparticles and with Rubpy dye, respectively. An observable signal difference was seen in the confocal images. The flow cytometry data (Figure 6-2 C) confirmed the Rubpy nanoparticles provided increased fluorescence. Figure 6-2 C indicated over a 100-fold signal difference produced by the Rubpy nanoparticle labeled cells. This figure also shows the nanoparticle labeled cells in an apparent bimodal distribution. These experiments illustrated the advantage of using the fluorescent nanoparticles compared to the individual fluorophores.

Nanoparticle selectivity

CEM and Ramos cell solutions were treated with the two particle procedure and the samples analyzed by fluorescence imaging and flow cytometric. Fluorescent and magnetic nanoparticles were added to the cell solutions at a 20:1 ratio, respectively. After five minutes, the cells were magnetically extracted and washed as described, and the samples suspended in 20 μL buffer for imaging and 200 μL buffer for flow cytometric analyses. The cell samples contained 1.0×10^5 - 5.0×10^5 cells before nanoparticle treatment. These experiments were repeated 10 times. Figure 6-3 contains 2 μL aliquots of target cells (A), and control cells (B) after five minute incubation.

This experiment demonstrates a notable difference in the amount of cells collected and the fluorescent signal obtained for these samples. The magnetic collection approach removed few control cells while a large number of target cells were extracted. In addition, the extracted control cells were labeled with only a few FNPs producing little or no fluorescent signal. The target CEM cells that were extracted had intense fluorescent signals that made them easily distinguishable from the control cells. The flow cytometry data confirmed the results obtained

by confocal imaging Figure 6-3 C. There were little cells counted in the control samples compared to the target samples. Additionally, a large signal was observed for the CEM cells.

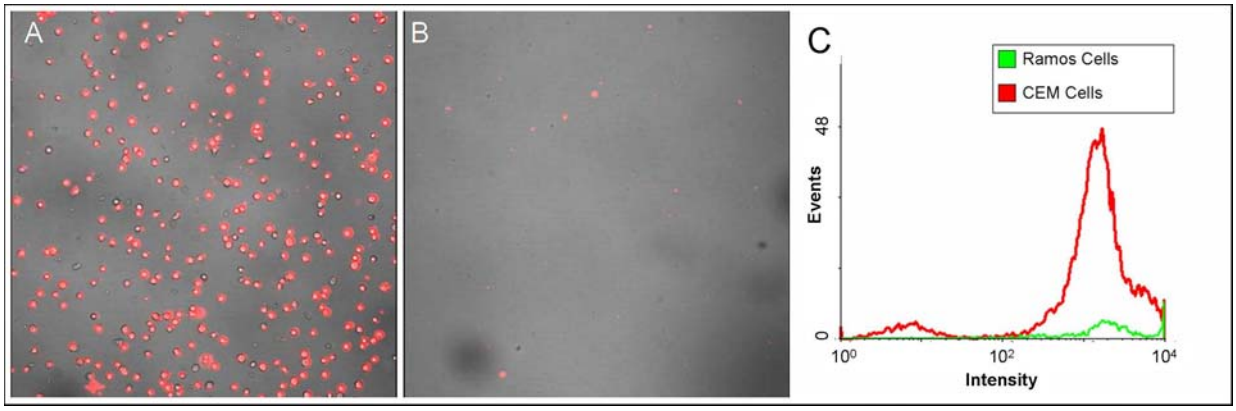

Figure 6-3. Fluorescence images and flow cytometry data of target (CEM) and control (Ramos) cells extracted using aptamer conjugated-magnetic nanoparticles and labeled with aptamer conjugated- Rubpy nanoparticles. A) Fluorescence image of CEM cells extracted using magnetic nanoparticles and labeled with Rubpy nanoparticles. B) Fluorescence image of Ramos cells treated with the aptamer conjugated-nanoparticles. C) Flow cytometry comparison of the CEM and Ramos cells treated with the aptamer-conjugated nanoparticles.

Single cell type extractions

To expand the concept of the two particle-based magnetic collection and detection technique to include three different leukemia cell lines by using three different aptamer molecules for three different cell lines. CEM, Ramos, and Toledo cell samples were extracted using ACNPs followed by fluorescent imaging and analysis by the microplate reader. Each pure cell sample extraction was repeated 10 times. As was mention in the methods section, the control cells used for the CEM experiments were the Ramos and Toledo cell types, for Ramos were the CEM and Toledo, and for the Toledo were the CEM and Ramos. Figure 6-4 shows representative confocal images of 2 μL aliquots of the CEM target cells (left) and Ramos nontarget cells (right) using CEM ACNPs (red) (A), Toledo target cells (left) and CEM nontarget cells (right) using Toledo ACNPs (green) (B), and Ramos target cells (left) and CEM nontarget

cells (right) using Ramos ACNPs (blue) (C) after NP incubations and magnetic washes. The figure indicates Ramos, CEM, and CEM as the respective controls for those experiments. The

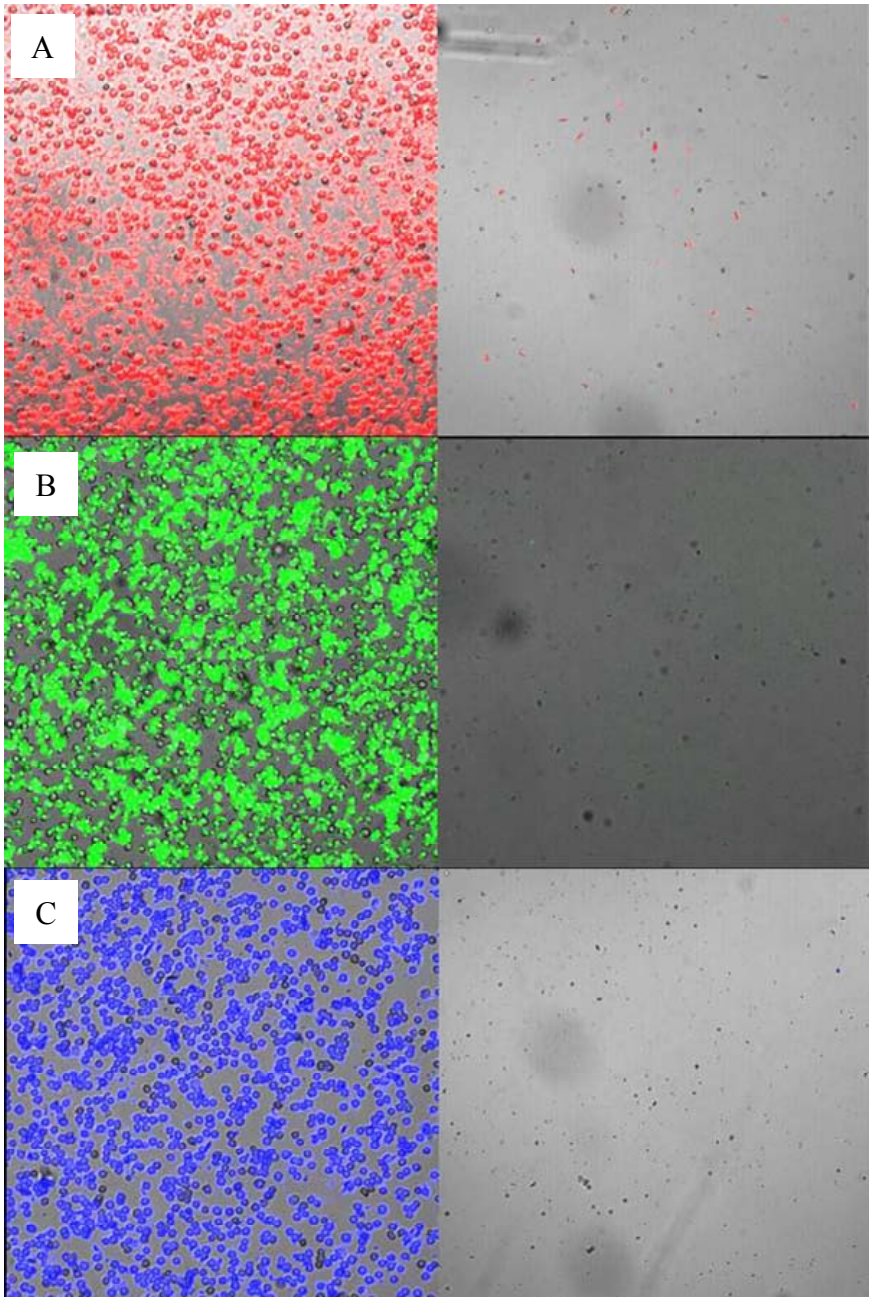

Figure 6-4. Fluorescence images of pure cell samples in buffer after magnetic extraction. A) Fluorescence image of CEM nanoparticle treated samples with target cells on the left and Ramos nontarget cells on the right. B) Fluorescence image of Toledo nanoparticle treated samples with target cells on the left and CEM nontarget cells on the right. C) Fluorescence image of Ramos nanoparticle treated samples with target cells on the left and CEM nontarget cells on the right.

other control cell type experiments were performed and resulted in the same responses as the one presented (data not shown). In addition, some fluorescence spots were observed in the images. However when the samples were analyzed with the microplate reader and compared to sample blanks treated with the MNPs and FNPs, the levels of fluorescence signal were the same (images not shown). Table 6-1 provides the fluorescence data obtained from the microplate reader. The first column represents the cell sample that was analyzed, the second column represents the signal produced by the CEM NPs, the third column represents the signal produced by the Toledo NPs, and the fourth column represents the signal produced by the Ramos NPs. The rows in the table display the cell samples that were investigated using the ACNPs.

Table 6-1. The microplate reader data for the evaluation of single cell type extraction experiments.

Sample cells	CEM NP signal	Toledo NP signal	Ramos NP signal
Ramos	945	965	7,574
CEM	48,967	1,056	314
Toledo	1,075	36,728	438

Based on the fluorescence images a significant difference is evident in both the amount of cells extracted and fluorescent signal present between the target and control cells in all samples. However, some control cells that were inadvertently collected and even labeled with some FNPs, but no significant signal was indicated by the microplate reader data for those samples producing signals in the same realm as sample blanks (images not shown). On the contrary, the target cells subjected to this procedure had very intense fluorescent signals that made them easily discernible from the control cells. A closer look at the characterization of expanding the ACNP technique to multiple cell types the microplate reader data (Table 6-1) demonstrated that when using 100,000

cells in each of the pure cell samples at a collection efficiency of 85%, all target cell samples produced signals in upwards of 24-fold enhancements above the background and as high as 50-fold. The target samples indicated in Table 6-1 for this experiment were the CEM cells (row 2) for the CEM NPs (column 1), the Toledo cells (row 3) for the Toledo NPs (column 2), and the Ramos cells (column 3) for the Ramos NPs (column 3). The control samples for these experiments were represented in the remainder of the table for each of the NPs and cell types. The signals for the control samples at the conditions mentioned above and the collection efficiency for the MNP amounts used in these experiments for the control cells determined to be no greater than 5%, resulted in fluorescence signals at the same level as a buffer blank sample treated with the ACNPs. This data indicates that the MNPs were both selective for the target cells by discriminating against the control cells and reproducible in all sample types investigated.

Detection Limit

The limit of detection (LOD) was determined using pure cell samples, and the extractions were performed as described previously. The limit of detection threshold was taken to be three standard deviations above the blank, and because of this any residual fluorescence in the blank was accounted for. The LOD was performed using CEM target cells. Each of the samples was then analyzed with NPs using the previously mentioned protocols with the fluorescence intensity being determined on the microplate reader following completion of the ACNP technique. The detection limit was computed by plotting the fluorescence intensity versus the cell number present in the sample. Consequently, the plotted data produced a linear response as seen in Figure 6-5 A, and Figure 6-5 B displays the data zoomed in on the lower sample concentrations. From this plot the detection limit was determined to be approximately 250 cells with a dynamic range covering more than two orders of magnitude. This indicates that the ACNP system has the ability to sensitively detect low amounts of intact targets cells from a given sample, and that a

wide range of cell concentrations can be analyzed by this method with little to no sample preparation depending on the amount of ACNPs used.

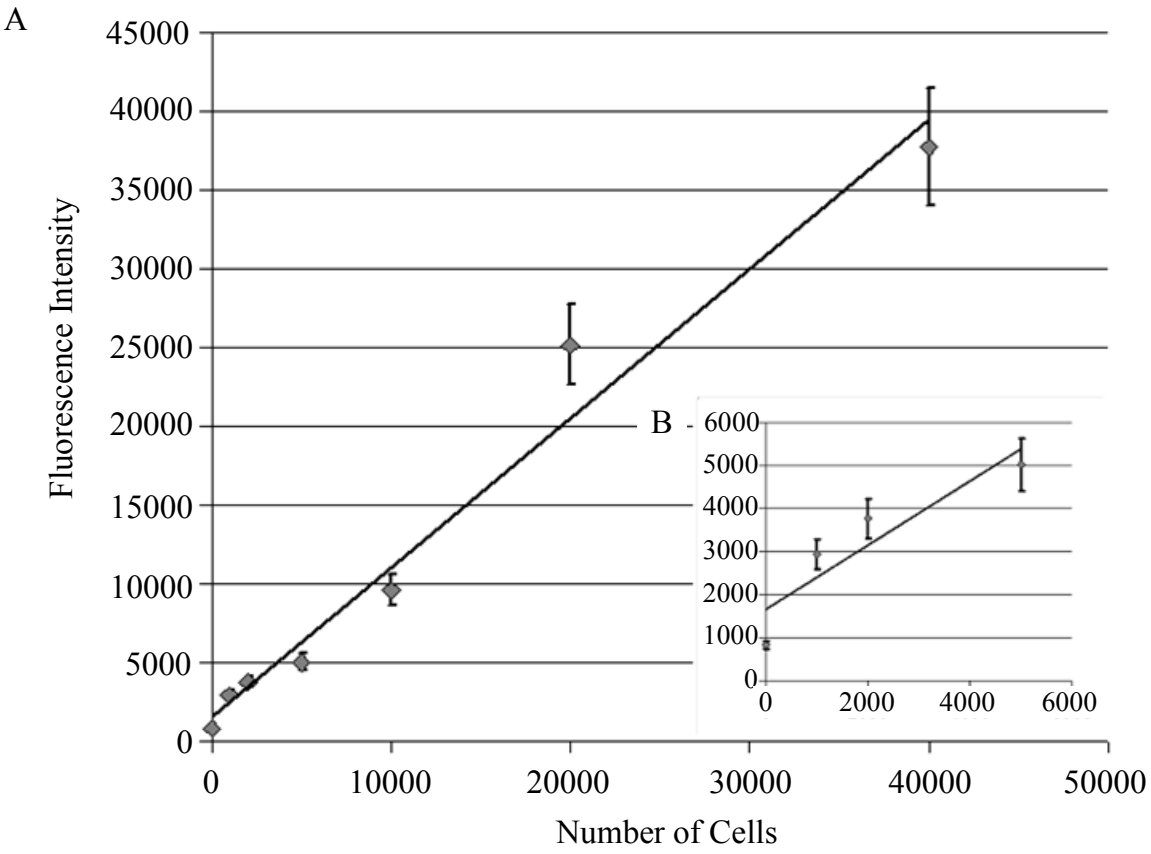

Figure 6-5. The limit of detection experiments for the stepwise addition of the magnetic and fluorescent nanoparticles using the microplate reader for detection. A) The full calibration curve obtained using the two nanoparticle approach. B) An inset displaying a zoomed image of the lower concentration range.

Complex Sample Extractions

Single type cell mixed sample extraction

Complex samples were tested to determine extraction and detection capabilities of the two particle approach in complex matrices. Figure 6-6 shows the results from a mixed cell sample extraction, where equal numbers of CEM and Ramos cells were mixed together. The two cell types were differentiated by treating the Ramos cells with Fluo-4, which is a fluorescent calcium

ion indicator. Fluo-4 labeled control cells were mixed with the unlabeled CEM cells, and the data is shown in Figure 6-6 A. The mixed cell sample was treated with the magnetic and fluorescent nanoparticles simultaneously, and the sample incubated at 4 ºC for five minutes. A magnetic field was applied to remove the unbound cells from the sample, where 2 μL aliquots of the extracted sample was analyzed by monitor the Fluo-4 and Rubpy fluorescence by confocal imaging, as seen in Figure 6-6 B and C respectively. The image indicated that the magnetic nanoparticles were able to collect the CEM cells, and the fluorescence signal from the Rubpy nanoparticles made them easily distinguishable from the control samples. This experiment was

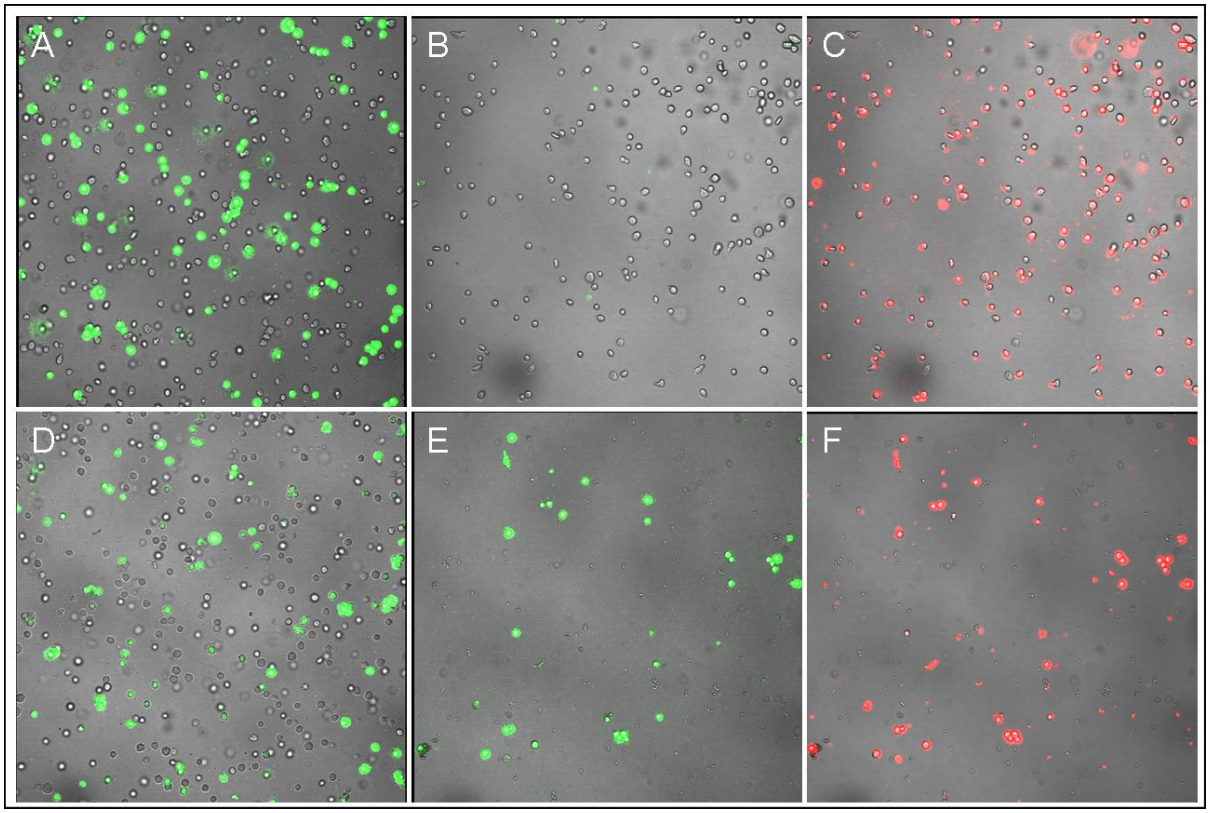

Figure 6-6. The confocal images for single cell mixed extraction samples. A) The confocal image of a 1:1 ratio of target cells (CEM) mixed with Fluo-4 stained control cells (Ramos). B) Confocal image analyzing for the Fluo-4 signal after extraction. C) Rubpy signal obtained after extraction of the CEM target cells. D) Confocal images of a 1:1 ratio of Fluo-4 stained target cells mixed with control cells. E) Confocal image analyzing the Fluo-4 signal after extraction. F) Rubpy signal obtained after extraction of the CEM cells.

repeated by labeling the CEM cells with the Fluo-4 dye (Figure 6-6 D). The cells were separated by the magnetic nanoparticles as seen in Figure 6-6 E, and all the extracted cells exhibited the Fluo-4 signal. In Figure 6-6 F shows the simultaneous labeling of the extracted cells by the Rubpy nanoparticles. The Fluo-4 fluorescence confirms that only the CEM cells were collected and imaged. The lack of Fluo-4 signal in Figure 6-6 B, along with the presence of the Fluo-4 signal in Figure 6-6 E prove that the target cells were extracted using this method from 1:1 cell mixtures. These samples were repeated 5 times producing similar results.

Multiple cell type extraction method

Determining the multiple extraction and detection capability of the ACNP was performed by creating artificial complex samples of CEM, Ramos, and Toledo cells. Figure 6-7 displays the schematic diagram of the multiple cell extraction procedure that was employed. The samples with one, two, and three cell types were analyzed using the ACNPs. The samples were prepared by obtaining approximately 10^5 cells of each type for the respective sample type. The stepwise extraction protocol was performed by adding the specified amounts of MNPs for Ramos cells, followed by CEM aptamer-conjugated MNPs, and finally with Toledo specific MNPs. Each set of MNPs were incubated with the cell samples separately for 15 minutes. After the Ramos MNPs were incubated with the cell samples, magnetic extraction was performed, and the supernatant kept to be treated with the CEM specific MNPs. The remainder of the magnetic extractions was carried out as described in the magnetic extraction section. The sample was redispersed in 200 μL cell media, followed by addition of the Ramos aptamer-conjugated FNPs with 5 minute incubation, and magnetic extraction procedure performed. Similarly, the respective CEM and Toledo aptamer-conjugated FNPs were subsequently introduced to their samples. After the final wash, the cell sample was dispersed in 20 μL media buffer. The

samples were analyzed by confocal imaging with 2 μL aliquots and plate reader spectrometer with 20 μL aliquots.

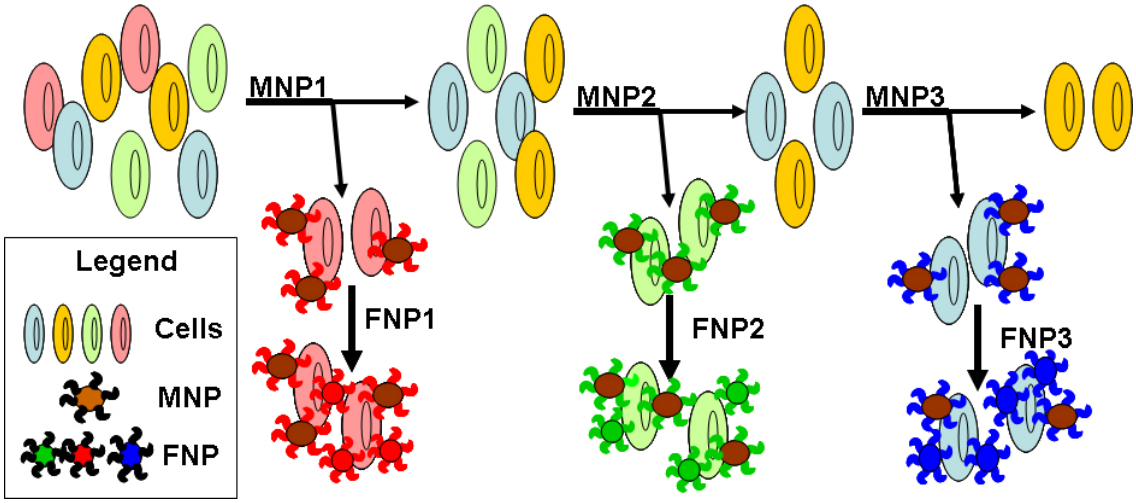

Figure 6-7. The schematic diagram used for the extraction of multiple cells.

Multiple cell type mixed cell extractions-buffer samples

The power of the multiple extraction procedure needed to be evaluated using complex sample mixtures. Figure 6-8 A, B, and C demonstrates the results from artificial complex samples by mixing equal amounts of the appropriate cell types for the three different multiple extraction samples diluted in cell media buffer, where CEM, Ramos, and Toledo cells were mixed and the ACNP process applied as described above. A total of 100,000 cells in all samples was used, cell and buffer volumes were adjusted accordingly. To exhibit that the MNPs indeed have the ability to selectively differentiate the cells from one another in a multiple cell mixture format, single, double, and triple cell mixed samples were evaluated. Figure 6-8 A illustrates the selective nature of the technique by performing the ACNP steps with a single cell sample, Ramos cells. The single cell sample was first treated with CEM ACNPs followed by Toledo ACNPs, and finally Ramos ACNPs. The samples were incubated at 4º C with the MNPs and FNPs as expressed in the previous section. Based on the fluorescence images, this method was able to

selectively collect the Ramos cells (blue) only when the Ramos ACNP were introduced to the cell sample Figure 6-8 A. The Toledo and Ramos cells were used in single cell sample

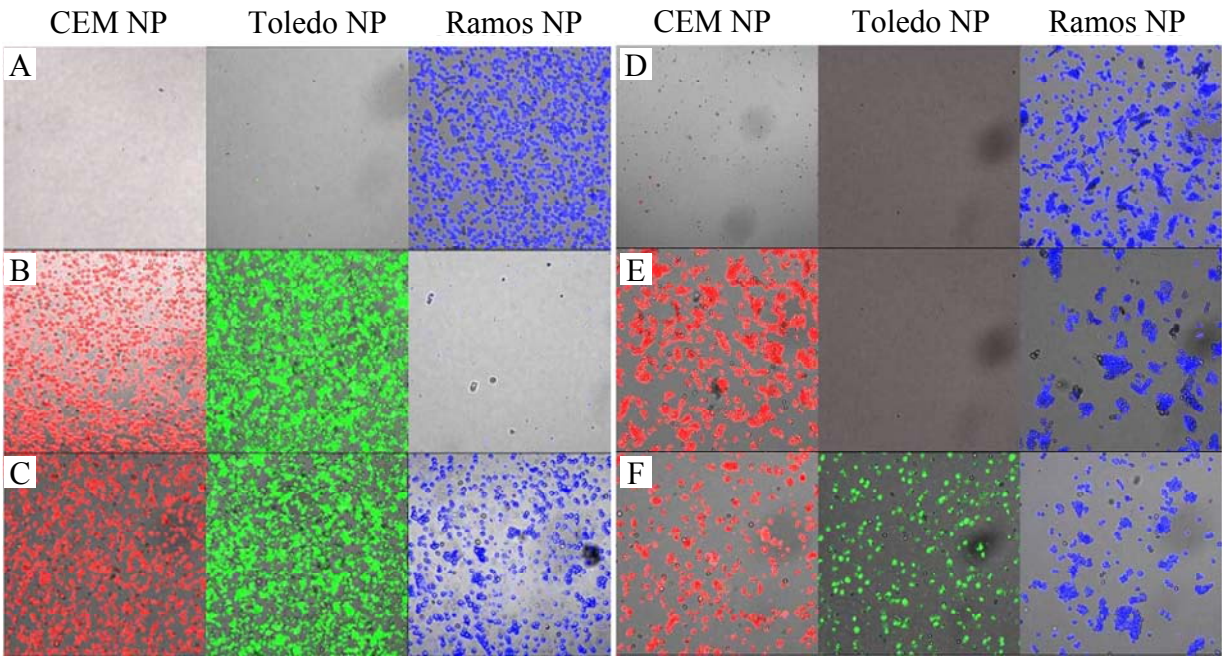

Figure 6-8. The confocal images of buffer and serum extracted mixed cell samples using the multiple extraction procedure. A) Confocal image of sample containing only Ramos cells in buffer. B) Confocal image of sample containing CEM and Toledo cells in buffer. C) Confocal image of sample containing CEM, Toledo, and Ramos cells in buffer. D) Images of samples containing only Ramos cells in serum. E) Images of samples containing CEM and Ramos cells in serum. F) Images of samples containing CEM, Toledo, and Ramos cells in serum.

extractions as well (image not shown). This method was further tested by performing the ACNP steps with a mixture of two different cell types, CEM and Toledo. Figure 6-8 B displays the selective nature of this technique for the cells indicated. The fluorescence images again demonstrate selective isolation of the CEM (red) and Toledo (green) cells. Other CEM, Toledo, and Ramos two cell type mixed samples were performed as well (image not shown). The final test was to perform this technique with a mixture of all three cell types in the same sample using the CEM, Toledo, and Ramos cells at the same time. Figure 6-8 C reveals the selective nature of the method for each of the cells indicated. Fluorescence images again depict the selective

isolation of the CEM, Toledo, and Ramos cells, Figure 6-8 C left (red), middle (green), and right (blue) images respectively.

Table 6-2. The microplate reader data obtained from buffer extracted cells by the multiple cell type extraction procedure.

Sample cells	CEM NP signal	Toledo NP signal	Ramos NP signal
Ramos	1,281	1,040	7,862
CEM	44,972	920	375
Toledo	1,025	34,972	320
CEM, Ramos	46,874	2,367	7,385
CEM, Toledo	43,890	37,896	414
CEM, Toledo, Ramos	42,145	32,945	7,524

Microplate reader data was in complete agreement with the confocal image data and presented in Table 6-2. The first column represents the cell samples that were analyzed, the second column represents the signal produced by the CEM NPs, the third column represents the signal produced by the Toledo NPs, and the fourth column represents the signal produced by the Ramos NPs. The rows in the table display the cell samples that were investigated using the ACNPs. With 100,000 total cells present in all samples, samples containing target cells produced signals in upwards of 24-fold enhancements above the background and as high as 47-fold with the exception of the Toledo nontarget sample, sample 4. The signals for the control samples at the conditions mentioned above resulted in fluorescence signals at the same level as a buffer blank sample treated with the ACNPs with the exception of the Toledo nontarget sample in sample 4. Standard deviations determined for all these samples were determined to be 8-12%.

This data indicates that the MNPs were both selective for the target cells by discriminating against the control cells and reproducible in all sample types investigated. However, the Toledo nontarget sample in sample 4 produced a background signal above the background observed for other Toledo nontarget samples. The Toledo aptamer is less selective then the other aptamers that were used, which would explain the higher background produced in this particular sample.

Multiple cell type mixed extractions-serum samples

To show applicability of the stepwise process in real biological samples, fetal bovine serum (FBS) was used. FBS was spiked with each of the respective cell types for the corresponding one cell, two cell, and three cell extraction experiments (500 μL). The process was performed as described above. Confocal imaging and fluorescence microplate reader were used to characterize cell extractions. Figure 6-8 D, E, and F illustrate the results of the FBS spiked complex samples by mixing equal amounts of the indicated cells at a total cell concentration of approximately 100,000 cells. Figure 6-8 D, E, and 4F present the selective nature of the technique for the single, double, and triple mixed cell type samples. The samples were treated with CEM ACNPs followed by Toledo ACNPs, and finally Ramos ACNPs. For the single cell sample experiment, the sample was first treated with CEM ACNPs followed by Toledo ACNPs, and finally Ramos ACNPs. The samples were incubated at 4 ºC with the MNPs and FNPs as expressed previously. Figure 6-8 D fluorescence image shows the sample contains Ramos cells extracted and labeled only after being treated with Ramos ACNP (blue). Extractions with the CEM and Toledo cell types were completed as well (images not shown). Figure 6-8 E left image (red) and right image (blue) show the CEM cells and Ramos cells extracted when treated with CEM and Ramos ACNP for the two cell type extraction experiment. Other two cell type extractions with the CEM, Toledo, and Ramos cell types were performed as

well (images not shown). Figure6-8 F left (red), middle (green), and right (blue) images show the extraction of all three cells treated with all the ACNP.

The fluorescence imaging data was confirmed by collecting fluorescence data using the microplate reader, Table 6-3. The table layout was the same as in the previous table: first column was cell samples, second column was the CEM NP signals, third column was Toledo NP signals, and fourth column was the Ramos NP signal. The rows in the table display the cells mixed to make the samples that were analyzed. The standard deviations determined to be 8-12% for all samples measured in the FBS. With 100,000 total cells present in each sample dispersed in FBS, the signal enhancements determined above the background ranged from 10 to about 24. In all cases, the signals for all target samples were lower than those for the cell media buffer, and the background signals were all higher. The Toledo samples produced the lowest enhancement of all the extracted samples, which produced the highest background signal of the three ACNPs pairs. The fluorescence images and microplate reader data demonstrated that the MNPs were both selective for the target cells by discriminating against the control cells and reproducible even in spiked FBS samples. The performance of the Toledo aptamer with nontarget samples was again evident in FBS compared to the other aptamers, which would be further evidence pointing to the lower selectivity of this aptamer compared to the others.

Table 6-3. The microplate reader data obtained from serum extracted cells by the multiple cell type extraction procedure.

Sample cells	CEM NP signal	Toledo NP signal	Ramos NP signal
Ramos	1,845	3,241	6,776
CEM, Ramos	43,835	3,554	6,980
CEM, Toledo	40,767	31,240	452
CEM, Toledo, Ramos	42,973	33,112	7,078

Whole blood sample assays

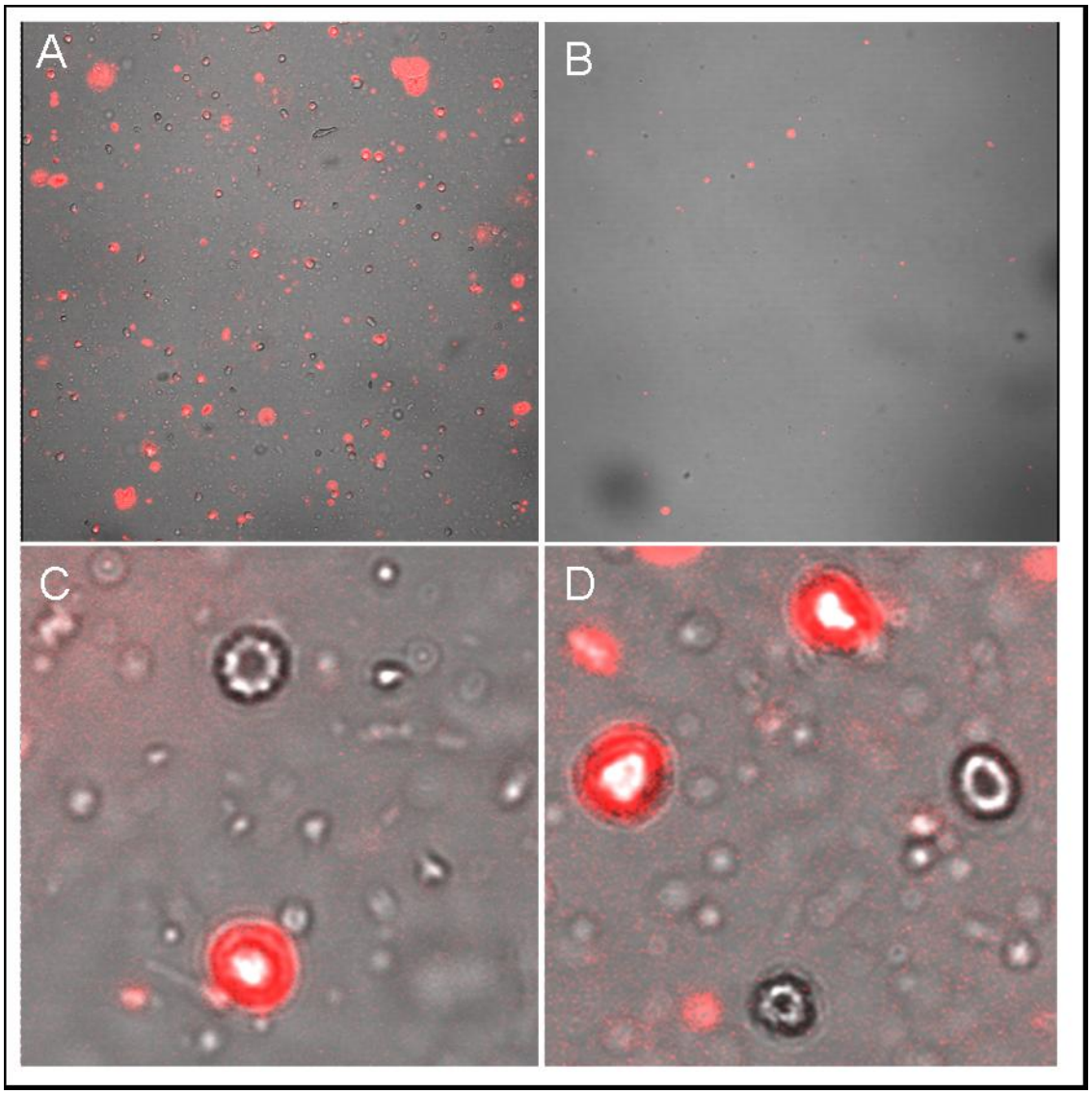

Figure 6-9. The confocal images of the cells extracted from whole blood. A) Confocal image of cells extracted from target cell spiked whole blood. B) Image of aptamer conjugated-nanoparticle treated unspiked whole blood samples. C) and D) Magnified images of extracted cells from whole blood spiked samples.

For further determination of complex biological solution extraction, spiked whole blood samples were investigated. The aptamer sequence used was stable in serum for up to 2 hours based on performed control experiments. The target cells were spiked into whole blood samples (500 μL). This sample was compared to unspiked samples. Figure 6-9 indicated the

nonselective extraction of red blood cells from all samples. However, there was no fluorescence signal observed by the presence of the FNPS on the nontarget cells. For the spiked whole blood samples, 40% of the spiked target cells were recovered. This was estimated after accounting for washing and dilution, which is comparable to extraction efficiencies reported by immunomagnetic separation.[194, 196] These experiments were repeated five times and similar results were obtained for each sample.

Conclusions

ACNPs were demonstrated to selectively extract and detect multiple intact target cells from complex samples with limited sample preparation. The inherent advantages of the ACNP include the aptamer-conjugated FNPs produce high signal intensity and signal stability, and aptamer-conjugated MNPs allow for the selective extract of analytes. Magnetic extraction allows for the easy of sample clean-up by removing excess FNPs and other unbound fluorescent materials resulting in a lower background. Employing magnetic extractions to such a system provides a separation and scavenging capability that is unlike any other method available in that the MNPs can be introduced to the sample of interest, locate the target, and remove the bound substance from the remainder of the sample. This isolation step can also be used to enrich or concentrate the sample after removal of the unwanted sample components with provided ease of washing due to the ability to manipulate the bound samples with a magnetic field. The MNPs have also demonstrated high collection efficiencies for biological species. The detection limit studies resulted in a wide ranged linear response with a good detection limit. The ACNP detection process has been performed relatively quickly in as little as 30 minutes in complex samples of FBS and whole blood containing target cells, as opposed to the hours needed for immunophenotyping or PCR-based methods. Therefore, the ACNP procedure has been used as a rapid detection method for cancer detection. Nanoparticle bound aptamers retain their binding

properties with the intact cells. Using the two nanoparticles add an additional level of selectivity, where only cells that are magnetically extracted and are bound with FNPs are recognized as target cells.

LIST OF REFERENCES

(1) Niemeyer, C. M. *Angew. Chem. Int. Ed. Engl.* **2001,** *40,* 4128-4158.

(2) Nicewarner-Pena, S. R.; Freeman, R. G.; Reiss, B. D. *Science* **2001,** *294,* 137-141.

(3) Hirschfeld, T.; Callis, J. B.; Kowalski, B. R. *Science* **1984,** *226,* 312-318.

(4) Swager, T. M. *Acc. Chem. Res.* **1998,** *31,* 201-207.

(5) Gao, X. H.; Nie, S. M. *Trends Biotechnol.* **2003,** *21,* 371-373.

(6) More, M. I.; Herrick, J. B.; Silva, M. C.; Ghiorse, W. C.; Madsen, E. L. *Applied and Environmental Microbiology* **1994,** *60,* 1572-1580.

(7) Nelson, D. L.; Cox, M. M. *Lehniger Principles of Biochemistry;* Worth Publishers: New York, NY; **2000**.

(8) Rosenthal, D.; Hu, F.; Pacheco, F.; Landuyt, J.; Barnes, C.; Portnoy, J. *Ann. Allergy Asthma Immunol.* **1998,** *80,* 471-475.

(9) Hughes, T. R., Mao, M. Jones, A. R.; Burchard, J.; Marton, M. J.; Shannon, K. W.; Leftkowitz, S. M.; Ziman, M.; Schelter, J. M.; Meyer, M. R.; Kobayashi, S.; Davies, C.; Dai, H.; He, Y. D.; Stephaniants, S. B.; Cavet, G.; Walker, W. L.; West, A.; Coffey, E.; Shoemaker, D. D.; Stoughton, R. *Nature Biotechnol.* **2001,** *19,* 342-347.

(10) Saiki, R. K.; Gelfand, D. H.; Stoffel, S.; Scharf, S. J.; Higuchi, R.; Horn, G. T.; Mullis K. B.; Erlich, H. A. Science 1998, 239, 487-491.

(11) Erlich, H. A.; Arnheim, N. *Annu. Rev. Genet.* **1992,** *26,* 479-506.

(12) Valasek, M. A.; Repa, J. J. *Advan. Physiol. Edu.* **2005,** *29,* 151-159.

(13) Higuchi, R.; Dollinger, G.; Walsh, P. S.; Griffith, R. Biotechnology, 1992, 11, 413-417

(14) Pasquali, C.; Fialka, I.; Huber, L. A. *Electrophoresis* **1997,** *18,* 2573-2581.

(15) O'Ferrell, P. H. *J. Biol. Chem.* **1975,** *250,* 4007-4021.

(16) Gjertsen, B. T.; Oyan, A. M.; Marzolf, B.; Hovland, R.; Gausdal, G.; Doskeland, S.-O.; Dimitrov, K.; Golden, A.; Kalland, K.-H.; Hood, L.; Bruserud, O. *Journal of Hematotherapy and Stem Cell Research* **2002,** *11,* 469-481.

(17) Shevchenko, A.; Wilm, M.; Vorm, O.; Mann, M. *Anal. Chem.* **1996,** *68,* 850-858.

(18) Gygi, S. P.; Corthals, G. L.; Zhang, Y.; Rochon, Y.; Aebersold, R. *Proc. Natl. Acad. Sci. USA* **2000,** *97,* 9390-9395.

(19) Thomas, P. A. *Diagnostic Cytopathology* **2006,** *10,* 303.

(20) Bruserud, O.; Gjertsen, B. T.; Foss, B. Huang, T.-S. *Stem Cells* **2001,** *19,* 1-11.

(21) Seraydarian, K.; Mommaerts, W. F. H. M. *The Journal of Cell Biology* **1965,** *26,* 641-656.

(22) Qadir, M.; Barcos, M.; Stewart, C. C.; Sait, S. N. J.; Ford, L. A.; Baer, M. R. *Cytometry Part B* **2006,** *70B,* 329-334.

(23) Shutter, J.; Atkins, K. A.; Ghartey, K.; Herzog, T. *J. Int. J. Gynecol. Cancer* **2007,** *17,* 311-315.

(24) O'Donnell, M. R.; Appelbaum, F. R.; Baer, M. R.; Byrd, J. C.; Coutre, S. E.; Damon, L. E.; Erba, H. P.; Estey, E.; Foran, J.; Lancet, J.; Maness, L. J.; Maslak, P. G.; Millenson, M.; Moore, J. O.; Przepiorka, D.; Shami, P.; Smith, B. D.; Stone, R. M.; Tallman, M. S. *J. Natl. Compr. Canc. Netw.* **2006,** *4,* 16-36.

(25) Leatherdale, C. A.; Woo, W. K.; Mikulec, F. V.; Bawendi, M. G. *J. Phys. Chem. B* **2002,** *106,* 7619-7622.

(26) Michalet, X.; Pinaud, F. F.; Bentolila, L. A.; Tsay, J. M.; Doose, S.; Li, J. J.; Sundaresan, G.; Wu, A. M.; Gambhir, S. S.; Weiss, S. *Science* **2005,** *307,* 538-544.

(27) Michalet, X. *Single Mol.* **2001,** *2,* 261.

(28) Ho, Y. P.; Kung, M. C.; Yang, S.; Wang, T. H. *Nano Lett.* **2005,** *5,* 1693-1697.

(29) Zhang, C. Y.; Yeh, H. C.; Kuroki, M. T.; Wang, T. H. *Nature Materials* **2005,** *4,* 826-831.

(30) Dahan, M. *Science* **2003,** *302,* 442.

(31) Pinaud, F.; King, D.; Moore, H.-P.; Weiss, S. *J. Am. Chem. Soc.* **2004,** *126,* 6115.

(32) Lagerholm, B. C.; Wang, M.; Ernst, L. A.; Ly, D. H.; Liu, H.; Bruchez, M. P.; Waggoner, A. S. *Nano Letters,* **2004,** *4 (10),* 2019-2022.

(33) Mattheakis, L. C.; Dias, J. M.; Choi, Y. J.; Gong, J.; Bruchez, M. P.; Liu, J.; Wang, E. *Anal. Biochem.* **2004,** *327 (2),* 200-208.

(34) Kloepfer, J. A.; *Appl. Environ. Microbiol.* **2003,** *69,* 4205.

(35) Ornberg, R. L.; Liu, H.; Harper, T. F. *Nature Methods* **2005,** *2,* 79-81.

(36) Lidke, D. S.*Nature Biotechnol.* **2004,** *22,* 198.

(37) Sugunan, A; Thanachayanont, C.; Dutta, J.; Hilborn, J. G. *Science and Technology of Advanced Materials* **2005,** *6,* 335-340.

(38) Jain, P. K.; Lee, K. S.; El-Sayed, I. H.; El-Sayed, M. A. *J. Phys. Chem. B* **2006,** *110,* 7238-7248.

(39) Merkin, C. *J. Am. Chem. Soc.* **1998,** *120,* 12674-12675.

(40) Mirkin, C. *Clinica Chimica Acta* **2006,** *363,* 120.

(41) Tsai, C.-S.; Yu, T.-B.; Chen, C.-T. *Chem. Commun.* **2005,** 4273-4275.

(42) Isola, N. R.; Stokes, D. L.; Vo-Dinh, T. *Anal. Chem.* **1998,** *70,* 1352-1356.

(43) Jeanmarie, D. L.; Van Duyne, R. P. *J. Electroanal. Chem.* **1977,** *84,* 1.

(44) Albrecht, M. G.; Creighton, J. A. *J. Am. Chem. Soc.* **1977,** *99,* 5215.

(45) Petry, R.; Schmitt, M.; Popp, J. *Chemphyschem.* **2003,** *4,* 14-30.

(46) Ni, J.; Lipert, R. J.; Dawson, G. B.; Porter M. D. *Anal. Chem.* **1999,** *71,* 4903-4908.

(47) Graham, D.; Mallinder, B. J.; Whitcombe, D.; Watson, N. D.; Smith, W. E. *Anal. Chem.* **2002,** *74,* 1069-1074.

(48) Kneipp, K; Kneipp, H.; Itzkan, I.; Dasari, R. R.; Feld, M. S. *Chem. Rev.* **1999,** *99,* 2957-2975.

(49) Gearheart, L. A.; Ploehn, H. J.; Murphy, C. J. *J. Phys. Chem B.* **2001,** *105,* 12609-12615.

(50) Graham, D.; Mallinder, B. J.; Smith, W. E. *Angew. Chem. Int. Ed.* **2000,** *39,* 1061-1063.

(51) Doering, W. E.; Nie, S. *Anal. Chem.* **2003,** *75,* 6171-6176.

(52) Foultier, B.; Moreno-Hagelsieb, L.; Flandre, D.; Remacle, J. *IEE Proc.-Nanobiotechnol.* **2005,** *152,* 3-12.

(53) Goya, G. F.; Berquo, T. S.; Fonseca, F. C. *Journal of Applied Physics* **2003**, *94,* 3520.

(54) Patrick J. Leamy 2003. Dissertation.

(55) Liu, X. L.; Xing, J.; Guan, Y.; Shan, G.; Liu, H. *Colloids and Surfaces A* **2004**, *238,* 127-131.

(56) Hou, Y.; Yu, J.; Gao, S. *Journal of Material Chemistry* **2003**, *13,* 1983.

(57) Bartolozzi, C.; Lencioni R.; Donati, F.; Cioni, D. *European Radiology,* **1999,** *9,* 1496-1512.

(58) Schutt, W.; Gruttner, C.; Hafeli, U.; Zborowski, M.; Teller, J.; Putzar, H.; Schumichen, C. *Hybridoma,* **1997,** *16,* 109-117.

(59) Driscoll, C. F.; Morris, R. M.; Senyei, A. E.; Widder, K. J.; Heller, G. S. *Microvascular Research,* **1984,** *27,* 353-369.

(60) Anzai, Y.; Blackwell, K. E.; Hirschowitz, S. L.; Rogers, J. W.; Sato, Y.; Yuh, W. T. C.; Runge, V. M.; Morris, M. R.; McLachlan, S. J.; Lufkin, R. B. *Radiology,* **1994,** *192,* 709-715.

(61) Gorwin, S. C.; Peterson, C.; Hoh, C.; Bittner C. *Journal of Magnetism and Magnetic Materials,* **1999,** *194,* 132-139.

(62) van Blaaderen, A.; Imhof, A.; Hage, W.; Vrij, A. *Langmuir* **1992,** *8,* 1514-1517.

(63) van Blaaderen, A.; Vrij, A. *Langmuir* **1992,** *8,* 2921-2931.

(64) Verhaegh, A. M. N.; van Blaaderen, A. *Langmuir* **1994,** *10,* 1427-1438.

(65) Turney, K.; Drake, T. J.; Smith, J. E.; Tan, W; Harrison, W. W. *Rapid Communications in Mass Spectrometry* **2004,** *18,* 2367.

(66) Stöber, W.; Fink, A.; Bohn, E. J. *Colloid Interface Sci.* **1968,** *26,* 62-69.

(67) Lindberg, R.; Sjöblom, J.; Sundholm, G. *Colloids Surfaces A.* **1995,** *99,* 79.

(68) Osseo-Asare, K.; Arriagada, F. J. *Colloids Surfaces* **1990,** *50,* 321.

(69) Yamauchi, H.; Ishikawa, T.; Kondo, S. *Colloids Surfaces* **1989,** *37,* 71.

(70) Santra, S.; Zhang, P.; Wang, K.; Tapec, R.; Tan, W. *Anal. Chem.* **2001,** *73,* 4988-4993.

(71) Santra, S.; Wang, K.; Tapec, R.; Tan, W. *J. Biomed. Opt.* **2001,** *6,* 160.

(72) Tapec, R.; Zhao, X.; Tan, W. *Journal of Nanoscience and Nanotechnology* **2002,** *2,* 405.

(73) Zhao, X.; Tapec, R.; Tan, W. *Journal of American Chemical Society* **2003,** *125,* 11474-11475.

(74) Zhao, X.; Tapec-Dytioco, R.; Wang, K.; Tan, W. *Anal. Chem.* **2003,** *75,* 3476-3483.

(75) Santra, S.; Tapec, R.; Theodoropoulou, N.; Dobson, J.; Hebard, A.; Tan, W. *Langmuir* **2001,** *17,* 2900-2906.

(76) Qhobosheane, M.; Santra, S.; Zhang, P.; Tan, W. *Analyst* **2001,** *126,* 1274-1278.

(77) Hilliard, L. R.; Zhao, X. J.; Tan, W. H. *Anal. Chim, Acta* **2002,** *470,* 51-56.

(78) Deng, G.; Markowitz, M. A.; Kust, P. R.; Gaber B. P. *Mater. Sci. Eng.: C* **2000,** *11,* 165-172.

(79) Zheng, M.; Davidson, F.; Huang, X. Y. *J. Am. Chem. Soc.* **2003,** *125,* 7790-7791.

(80) Farokhazd, O. C.; Jon, S.; Khademhosseini, A.; Tran, A. T.-NT.; LaVan, D. A.; Langer, R. *Cancer Res.* **2004,** *64,* 7668-7672.

(81) Santra, S.; Yang, H.; Stanley, J. T.; Holloway, P. H.; Tan, W. H.; Moudgil, B. M.; Mericle, R. A. *Chem. Commun.* **2004,** *24,* 2810-2811.

(82) Santra, S.; Xu, J. S.; Wang, K. M.; Tan, W. H. *J. Nanosci. Nanotechnol.* **2004,** *4,* 590-599.

(83) Gerion, D.; Pinard, F.; William, S, C.; Parak, W. J.; Zanchet, D.; Weiss, S.; Alivisatos, A. P. *J Phys. Chem. B* **2001,** *105,* 8861-8871.

(84) Golden, J. P.; Taitt, C. R.; Shriver-Lake, L. C.; Shubin, Y. S.; Ligler, F. S. *Talanta,* **2005,** *65,* 1078-1085.

(85) Wang, L; Wang, K.; Santra, S.; Zhao, X; Hilliard, L. R.; Smith, J. E.; Wu, Y.; Tan, T. *Anal. Chem.* **2006,** *78,* 647-654.

(86) Costa, A. R. C.; Leite, A. P. C.; Galembeck, F. *J. Phys. Chem. B* **2003,** *107,* 4747-4755.

(87) Kneuer, C.; Sameti, M.; Bakowsky, U.; Schiestel, T.; Schirra, H.; Schmidt, H.; Lehr, C. M.; *Bioconjugate Chem.* **2000,** *11,* 926-932.

(88) van Blaaderen, A.; Vrij, A. *J. Colloid Interface Sci.* **1993,** *156,* 1-18.

(89) Jain, T. K.; Roy, I.; De, T. K.; Maitra, A. N. *J. Am. Chem. Soc.* **1998,** *120,* 11092.

(90) Gold, L. *JBC* **1995,** *270,* 13581-13584.

(91) Famulok, M. Mayer, G. *Current Topics in Microbiology and Immunology* **1999,** *243,* 123-136.

(92) Brody, E. N.; Gold, L. *Rev. Mol. Biotechnol.* **2000,** *74,* 5-13.

(93) Conrad, R.; Keranen, L. M.; Ellington, A. D.; Newton, A. C. *J. Biol. Chem.* **1994,** *269,* 32051-32054.

(94) Hirao, I.; Spingola, M.; Peabody, D.; Ellington, A. D. *Mol. Divers* **1998,** *4,* 75-89.

(95) Macaya, R. F.; Schultze, P.; Smith, F. W.; Roe, J. A.; Feigon, J. *Proc. Natl. Acad. Sci. USA* **1993,** *90,* 3745-3749.

(96) Kelly, J. A.; Feigon, J.; Yeates, T. O. *J. Mol. Biol.* **1996,** *256,* 417-422.

(97) Gold, L.; Polisky, B.; Uhlenbeck, O.; Yarus, M. *Annu. Rev. Biochem.* **1995,** *64,* 763-797.

(98) White, R. R.; Sullenger, B. A.; Rusconi, C. P. *J. Clin. Invest.* **2000,** *106,* 929-934.

(99) Bock, L. C.; Griffin, L. C.; Latham, J. A.; Vermaas, E. H., Toole, J. J. *Nature,* **1992,** *355,* 564-566.

(100) Shangguan, D.; Li, Y.; Tang, Z.; Cao, Z. C.; Chen, H. W.; Mallikaratchy, P.; Sefah, K.; Yang, C. J.; Tan, W. *PNAS* **2006,** *103,* 11838-11843.

(101) Li, J. W.; Fang, X. H.; Tan, W. H. *Biochemical and Biophysical Research Communications* **2002,** *292,* 31-40.

(102) Dresco, P. A.; Zaitsev, V. S.; Gambino, R. J.; Chu, B. *Langmuir* **1999,** *15,* 1945.

(103) Fach, P.; Gibert, M.; Griffais, R.; Guillou, J. P.; Popoff, M. R. *Applied and Environmental Microbiology* **1995,** *61,* 389-392.

(104) Birren, B.; Lai, E. *Pulsed-Field Electrophoresis;* Academic Press: San Diego, CA; 1990; Vol 1, No. 2.

(105) Behne, D.; Kuriakopoeulos, A.; Weiss-Nowak, C.; Kalckloesch, M.; Westpal, C.; Gessner, H. *Biol. Trace Elem. Res.* **1996,** *55,* 99-110.

(106) Levison, P. R.; Munford, C.; Streater, M.; Brandt-Nielsen, A.; Pathiramna, N. D.; Badger, S. E. *J. Chromatogr., A* **1997,** *760,* 151-158.

(107) Technical Bulletins. http://www.idtdna.com

(108) Chan, W. C. W; Nie, S. *Science* **1998,** *281,* 2016.

(109) Kolodny, L. A.; Williard, D. M.; Carillo, L. L.; Nelson, M. W.; Van Orden, A. *Anal. Chem.* **2001,** *73,* 1959-1966.

(110) Chela, Y. R.; Grossman, H. L.; Poon, Y.; Mcdermott, R.; Stevens, R.; Alper, M. D.; Clarke, J. *Proc. Natl. Acad. Sci. U.S.A.* **2000,** *26,* 14268-14272.

(111) Hawkins, T. L.; Mckernan, K. J.; Jacotot, L. B.; MacKenzie, B.; Richardson, P. M.; Lander, E. S. *Science* **1997,** *276,* 1887.

(112) Safarik, I.; Safarikova, M. *J. Chromatogr., B* **1999,** *722,* 33-35.

(113) Srinivas, V. S.; Arijit, B. *Colloids Surf. B* **1997,** *8,* 1999-2004.

(114) Doktycz, M. J.; Hurst, G. B.; Habibi-Goudarzi, S.; McLuckey, S. A.; Tang, K.; Chen, C. H.; Uziel, M.; Jacobson, K. B.; Woychik, R. P.; Buchanan, M. V. *Anal. Biochem.* **1995,** *230,* 205-214.

(115) Hurst, G. B.; Doktycz, M. J.; Vass, A. A.; Buchanan, M.V. *Rapid Commun. Mass Spectrom.* **1996,** *10,* 377-382.

(116) Krahmer, M. T.; Johnson, Y. A.; Walters, J. J.; Fox, K. F.; Fox, A.; Nagpal, M. *Anal. Chem.* **1999,** *71,* 2893-2900.

(117) Naito, Y.; Ishikawa, K.; Koga, Y.; Tsuneyoshi, T.; Terunuma, H. *Rapid Commun. Mass Spectrom.* **1995,** *9,* 1484-1486.

(118) Naito, Y.; Ishikawa, K.; Koga, Y.; Tsuneyoshi, T.; Terunuma, H.; Arakawa, R. *J. Am. Soc. Mass Spectrom.* **1997,** *8,* 737-742.

(119) Saiki, R. K.; Scharf, S.; Faloona, F.; Mullis, K. B.; Horn, G. T.; Erlich, H. A.; Arnheim, N. *Science* **1985,** *230,* 1350-1354.

(120) Buetow, K. H.; Edmonson, M.; MacDonald, R.; Clifford, R.; Yip, P.; Kelley, J.; Little, D. P.; Strausberg, R.; Koester, H.; Cantor, C. R.; Braun, A. Proc. Natl. Acad. Sci. USA **2001,** 581-584.

(121) Null, A. P.; George, L. T.; Muddiman, D. C. *J. Am. Soc. Mass Spectrom.* **2002,** *13,* 338-344.

(122) Lim, H.; Eng, J.; Yates, J. R. III; Tollaksen, S.; Giometti, C.; Holden, J.; Adams, M.; Reich, C.; Olsen, G.; Hays, L. *Journal of American Society of Mass Spectrometry* **2003,** 957-970.

(123) Petricoin, E.; Liotta L. *Current Opinion in Biotechnology* **2004,** *15*, 24-30.

(124) Villanueva, J.; Philip, J.; Entenberg, D.; Chaparr, C.; Tanwar, M.; Holland, E.; Tempst, P. *Analytical Chemistry* **2004,** *76*, 1560-1570.

(125) Yaneva, M.; Tempst, P. *Analytical Chemistry* **2003,** *75*, 6437-6448.

(126) Turney, K.; Harrison, W. *Rapid Communications in Mass Spectrometry* **2004,** *18*, 629-635.

(127) Schroedter, A.; Weller, H. *Angewandte Chemie, International Edition* **2002,** *41*, 3218-3221.

(128) Massart, R. Magnetic Fluids and Process for Obtaining Them. [4,329,241]. 1982. United States.

(129) Kleinjung, F.; Klussmann, S.; Erdmann, V. A.; Scheller, F. W.; Fuerste, J. P.; Bier, F. F. *Analytical Chemistry* **1998,** *70*, 328-331.

(130) Michaud, M.; Jourdan, E.; Villet, A.; Ravel, A.; Grosset, C.; Peyrin, E. *Journal of the American Chemical Society* **2003,** *125*, 8672-8679.

(131) Williams, K. P.; Liu, X. H.; Schumacher, T. N.; Lin, H. Y.; Ausiello, D. A.; Kim, P. S.; Bartel, D. P. *Proceedings of the National Academy of Sciences of the United States of America* **1997,** *94*, 11285-11290.

(132) Fang, X.; Mi, Y.; Li, J. J.; Beck, T.; Schuster, S.; Tan, W. *Cell Biochemistry and Biophysics* **2002,** *37*, 71-81.

(133) Rajendran, M.; Ellington, A. D. *Optical Biosensors* **2002,** 369-396.

(134) Neubert, H.; Jacoby, E. S.; Bansal, S. S.; Iies, R. K.; Cowan, D. A.; Kicman, A. T. *Analytical Chemistry* **2002,** *74*, 3677-3683.

(135) Jayasena, S. D. *Clinical Chemistry* **1999,** *45*, 1628-1650.

(136) Sapsford, K. E.; Shubin, Y. S.; Delehanty, J. B.; Golden, J. P.; Taitt, C. R.; Shriver-Lake, L. C.; Ligler, F. S. *J. Appl. Microbiol.* **2004,** *96*, 47-58.

(137) Taitt, C. R.; Anderson, G. P.; Ligler, F. S. *Biosens. Bioelectron.* **2005,** *20*, 2470-2487.

(138) Ligler, F. S.; Sapsford, K. E.; Golden, J. P.; Shriver-Lake, L. C.; Taitt, C. R.; Dyer, M. A.; Barone, S.; Myatt, C. J. *Anal. Sci.* **2007,** *in press*.

(139) Ngundi, M. M.; Shriver-Lake, L. C.; Moore, M. H.; Lassman, M. E.; Ligler, F. S.; Taitt C. R. *Anal. Chem.* **2005,** *77*, 148-154.

(140) Ngundi, M. M.; Qadri, S. A.; Wallace, E. V.; Moore, M. H.; Lassman, M. E.; Shriver-Lake, L. C.; Ligler, F. S.; Taitt C. R. *Environ. Sci. Technol.* **2005,** *40*, 2352-2356.

(141) Sapsford, K. E.; Rasooly, A.; Taitt, C. R.; Ligler, F. S. *Anal. Chem.* **2004,** *76*, 433-440.

(142) Sapsford, K. E.; Taitt, C. R.; Loo, N.; Ligler, F. S.; *Appl. Environ. Microbiol.* **2005,** *71,* 5590-5592.

(143) Sapsford, K. E.; Taitt, C. R.; Fertig, S.; Moore, M. H.; Lassman, M. E.; Maragos, C. A.; Shriver-Lake, L. C. *Biosens. Bioelectron.* **2006,** *21,* 2298-2305.

(144) Sapsford, K. E.; Ngundi, M. M.; Moore, M. H.; Lassman, M. E.; Shriver-Lake, L. C.; Taitt C. R.; Ligler, F. S. *Sens. Actuators B* **2006,** *113,* 599-607.

(145) Shriver-Lake, L. C.; Shubin, Y. S.; Ligler, F. S. *J. Food Protect.* **2003,** *66,* 1851-1856.

(146) Shriver-Lake, L. C.; Taitt, C. R.; Ligler, F. S.; *J. AOAC Internat.* **2004,** *87,* 1498-1502.

(147) Taitt, C. R.; Shubin, Y. S.; Angel, R.; Ligler, F. S.; *Appl. Environ. Microbiol.* **2004,** *70,* 152-158.

(148) Gijs, M. A. M. *Microfluidics and Nanofluidics* **2004,** *1,* 22-40.

(149) Magnani, M.; Galluzzi, L.; Bruce, I. J. *J. Nanosci. Nanotechnol.* **2006,** *6,* 2302-2311.

(150) Yitzhaki, S.; Zahavy, E.; Oron, C.; Fisher, M.; Keysary, A. *Anal. Chem.* **2006,** *78,* 6670-6673.

(151) Metzger-Boddien, C.; Khaschabi, D.; Schönbauer, M.; Boddien, S.; Schlederer, T.; Kehle, J. *Internat. J. Food Microbiol.* **2006,** *110,* 201-208.

(152) Yu, H. *Anal. Chim. Acta* **1998,** *376,* 77-81.

(153) DeCory, T. R.; Durst, R. A.; Zimmerman, S. J.; Garringer, L. A.; Paluca, G.; DeCory, H. H.; Montagna, R. A. *Appl. Environ. Microbiol.* **2005,** *71,* 1856-1864.

(154) Yang, L.; Li, Y. *The Analyst* **2006,** *131,* 394-401.

(155) Splettstoesser, W. D.; Grunow, R.; Rahalison, L.; Brooks, T. J.; Chanteau, S.; Neubauer, H. *Cytometry Part A* **2003,** *53A,* 88-96.

(156) Øren, A.; Husebø, C.; Iversen, A.-C.; Austgulen, R. *J. Immunol. Methods* **2005,** *303,* 1-10.

(157) Hibi, K.; Abe, A.; Ohashi, E.; Mitsubayashi, K.; Ushio, H.; Hayashi, T.; Ren, H.; Endo, H. *Anal. Chim. Acta* **2006,** *573-574,* 158-163.

(158) Yu, L. S. L.; Uknalis, J.; Tu, S.-I. *J. Immunol. Methods* **2001,** *256,* 11-18.

(159) Steingroewer, J.; Knaus, H.; Bley, T.; Boschke, E. *Eng. Life Sci.* **2005,** *5,* 267-272.

(160) Zhao, X.; Shippy, S. A. *Anal. Chem.* **2004,** *76,* 1871-1876.

(161) Gehring, A. G.; Crawford, C. G.; Mazenko, R. S.; Van Houten, L. J.; Brewster, J. D. *J. Immunol. Methods* **1996,** *195,* 15-25.

(162) Tudorache, M.; Co, M.; Lifgren, H.; Emnéus, J. *Anal. Chem.* **2005,** *77,* 7156-7162.

(163) Mao, C. L.; Zientek, K. D.; Colahan, P. T.; Kuo, M. Y.; Liu, C. H.; Lee, K. M.; Chou, C. C. *J. Pharmaceutical Biomed. Analysis* **2006,** *41,* 1332-1341.

(164) Aytur, T.; Foley, J.; Anwar, M.; Boser, B.; Harris, E.; Beatty, P. R. *J. Immunol. Methods* **2006,** *314,* 21-29.

(165) Horng, H. E.; Yang, S. Y.; Huang, Y. W.; Qiang, W. Q.; Hong, C.-Y.; Yang, H. C.; *IEEE Trans. Appl. Superconductivity* **2005,** *15,* 669-671.

(166) Edelstein, R. L.; Tamanaha, C. R.; Sheehan, P. E.; Miller, M. M.; Baselt, D. R.; Whitman, L. J.; Colton, R. J. *Biosens. Bioelectron.* **2000,** *14,* 805-813.

(167) Choi, J.-W.; Oh, K. W.; Thomas, J. H.; Heineman, W. R.; Halsall, H. B.; Nevin, J. H.; Helmicki, A. J.; Henderson, H. T.; Ahn, C. H. *Lab Chip* **2002,** *2,* 27-30.

(168) Wellman, A. D.; Sepaniak, M. J. *Anal. Chem.* **2006,** *78,* 4450-4456.

(169) Morozov, V. N.; Morozova, T. Y. *Anal. Chimi. Acta* **2006,** *564,* 40-52.

(170) Matsunaga, T.; Okamura, Y.; Tanaka, T. *J. Mater. Chem.* **2004**, *14,* 2099-2105.

(171) Yoshino, T.; Kato, F.; Takeyama, H.; Nakai, M.; Yakabe, Y.; Matsunaga, T. *Anal. Chim. Acta* **2005,** *532,* 105-111.

(172) Amemiya, Y.; Tanaka, T.; Yoza, B.; Matsunaga, T. *J. Biotechnol.* **2005,** *120,* 308-314.

(173) Lu, Y.; Yin, Y.; Mayers, B. T.; Xia, Y. *Nano Lett.* **2002,** *2,* 183-186.

(174) Smith, J. E.; Wang, L.; Tan, W. *Trends Anal. Chem.* **2006,** *25,* 848-855.

(175) Lattuada, M.; Hatton, T. A. *Langmuir* **2007,** *23,* 2158-2168.

(176) Herr, J. K.; Smith, J. E.; Medley, C. D.; Shangguan, D.; Tan, W. *Anal. Chem.* **2006,** *78,* 2918-2924.

(177) Anderson, G. P.; Merurkar, N. L. *J. Immunol. Methods* **2002,** *271,* 17-24.

(178) Golden, J. P.; Shriver-Lake, L. C.; Sapsford, K. E.; Ligler, F. S. *Methods.* **2005,** *37,* 65-72.

(179) Feldstein, M. J.; Golden, J. P.; Rowe, C. A.; MacCraith, B. D.; Ligler, F. S. *J. Biomed. Microdevices* **1999,** *1,* 139-153.

(180) Faderl, S.; Kantarjian, H. M.; Talpaz, M.; and Estrov, Z. *Blood* **1998,** *91,* 3995-4019.

(181) Paredes-Aguilera, R. *American Journal of Hematology* **2001,** *68,* 69-74.

(182) Belov, L.; de la Vega, O.; dos Remedios, C. G.; Mulligan, S. P.; and Christopherson, R.I. *Cancer Research* **2001,** *61,* 4483-4489.

(183) Ghossein, R.A.; Bhattacharya, S. *European Journal of Cancer* **2000,** *36,* 1681-1694.

(184) Iinuma, H.; Okimaga, K.; Adachi, M.; Suda, K.; Sekine, T.; Sakagawa, K.; Baba, Y.; Tamura, J.; Kumagai, H.; Ida, A. *Int. J. Cancer* **2000,** *89,* 337-344.

(185) Liu Y. J. A.; Grimwade, D. *Lancet* **2002,** *360,* 160-162.

(186) Daniels, D. A.; Chen, H.; Hicke, B. J.; Swiderek, K. M.; Gold, L. *PNAS* **2003,** *100,* 15416-15421.

(187) Bagwe, R.; Zhao, X.; Tan, W. *J. Dispersion Sci. and Tech* **2003,** *24,* 453-464.

(188) Zhao, X.; Bagwe, R.; Tan, W. *Advanced Materials* **2004,** *16,* 173.

(189) Lian, W.; Litherland, S.; Badrane, H.; Tan, W.; Wu, D.; Baker, H.; Gulig, P.; Lim, D.; Jin, S. *Anal. Biochem.* **2004,** *334,* 135-144.

(190) Yang, W.; Zhang, C. G.; Qu, H. Y.; Yang, H. H.; Xu, J. G. *Analytica Chimica Acta* **2004,** *503,* 163-169.

(191) Yang, H.; Qu, H.; Lin, P.; Li, S.; Ding, M.; Xu, J. *Analyst* **2003,** *128,* 462-466.

(192) Ye, Z.; Tan, M.; Wang, G.; Yuan, J. *Anal. Chem.* **2004,** *76,* 513-518.

(193) Griwatz, C.; Brandt, B.; Assmann, G.; Zänker, K. S. *J. Immun. Methods* **1995,** *183,* 251-265.

(194) Marelli-Berg, F. M.; Peek, E.; Lidington, E. A.; Stauss, H. J.; Lechler, R. I. *J. Immun. Methods* **2000,** *244,* 205-215.

(195) Porter, J.; Robinson, J.; Pickup, R.; Edwards, C. *J. Applied Microbiology* **1998,** *84,* 722-732.

(196) Stanciu, L. A.; Shute, J.; Holgate, S. T.; Djukanovic, R. *J. Immun. Methods* **1996,** *189,* 107-115.

(197) Hu, X. C.; Wang, Y.; Shi, D. R.; Loo, T. Y.; Chow, L. W. C. *Oncology* **2003,** *64,* 160-165.

(198) Benez, A.; Geiselhart, A.; Handgretinger, R.; Schiebel, U.; Fierlbeck, G. *J. Clin. Lab. Analysis* **1999,** *13,* 229-233.

BIOGRAPHICAL SKETCH

Joshua Elliot Smith was born in Clarion, PA on August 21, 1976 to John and Dorothy Smith. He was raised in Rimersburg, PA and graduated in 1995 from Union High School. He entered Clarion University of Pennsylvania (CUP) to study chemistry and mathematics. After Josh received his Bachelors of Science and Bachelors of Education in Chemistry and Mathematics from CUP in May 2002, he began his doctorate study under the supervision of Dr. Weihong Tan at the University of Florida in August that year. He earned his Doctorate of Philosophy in Analytical Chemistry in August 2007.